This is to certify that the
dissertation entitled

THEORETICAL, NUMERICAL AND EXPERIMENTAL STUDY ON
VENTURI VALVES FOR STEAM TURBINE INFLOW CONTROL

presented by

Donghui Zhang

has been accepted towards fulfillment
of the requirements for the

Ph.D. degree in Mechanical Engineering

Major Professor's Signature

12/10/2003

Date

DATE DUE	DATE DUE	DATE DUE

THEORETIC

VENTURI V

THEORETICAL, NUMERICAL AND EXPERIMENTAL STUDY ON VENTURI VALVES FOR STEAM TURBINE INFLOW CONTROL

By

Donghui Zhang

A DISSERTATION

Submitted to
Michigan State University
in partial fulfillment of the requirements
for the degree of

DOCTOR OF PHILOSOPHY

Department of Mechanical Engineering

2003

THEORETI
VENTURI

Because of the

have been widely

for about half a ce

reported. Improve

complicated natur

from being fully

error methods, w

The literature i

of fluid mechani

instability, unste

mathematic mod

A 2-D and 3-

large amplitudes

asymmetric flow

can finally break

shown to result

the plug balance

ABSTRACT

THEORETICAL, NUMERICAL AND EXPERIMENTAL STUDY ON VENTURI VALVES FOR STEAM TURBINE INFLOW CONTROL

by

Donghui Zhang

Because of the converging diverging configuration of the valve passage, venturi valves have been widely used in large turbines to regulate inlet flow as turbine governing valves for about half a century. From the 1960's, a number of valve failure incidents have been reported. Improvement to current designs was strongly demanded, but due to the complicated nature of the fluid structure interaction mechanisms, valve failure is still far from being fully understood. There are several improved designs obtained by trial and error methods, while the rules, or even a clear direction for improvement is non-existent.

The literature in this field is reviewed. Based on former research and basic knowledge of fluid mechanics and structure dynamics, the theoretical investigation of the flow instability, unsteady forces, and fluid-structure interaction mechanisms are performed and mathematic models are derived.

A 2-D and 3-D numerical investigation was performed here. The study confirmed that large amplitudes of hydraulic forces, moment and torque are caused by unexpected asymmetric flow patterns. All these excitations can result in severe valve vibration and can finally break the valve. Improved designs were simulated by using CFD tools and shown to result in symmetric flow patterns and a reduction in the intensity of excitation at the plug balanced position.

An experimental system was designed and built. The experimental data on a ½ scale valve were obtained. The study confirmed that asymmetric unstable flows are the root cause of valve problems, such as noise, vibration, and failure.

ACKNOWLEDGEMENTS

I would like to express my sincere gratitude to my advisor, Dr. Abraham Engeda for his guidance, support and encouragement throughout my graduate study. I would also like to thank Dr. Norbert Müller, Dr. Craig W. Somerton, Dr. Charles R. MacCluer and James Hardin for serving on my guidance committee and giving me valuable suggestions to my research. Particular thank goes to Ronald Aungier at Elliott Company for initiating this work and for fruitful discussions. Of course, I wish to express my gratitude to Elliott Turbomachinery Co. for supporting this project.

My deepest thanks go to my wife, Yuqing Chen for her endless love, understanding and continuous support that makes my life enjoyable.

I am also very thankful to Christopher Zielesch and Roy Bailiff for their help in building the experiment rig. Special thank goes to Dr. Yunbae Kim and Petter Menegay at Dresser-Rand Company for help in CFD and friendship. Michael J. Cave at Solar Turbines Company and James M. Sorokes at Dresser-Rand Company are specially acknowledged for giving me the chances for internship and for their encouragement.

I also appreciate the assistance and friendship from the students in the turbomachinery lab during my Ph.D. program at Michigan State Univeristy: Yinghui Dai, Muhammad M. Raheel, Faisal Mahroogi, Jaewook Song, Zeyad Alsuhaibani, Dr. Fahua Gu (former graduate now working at Concepts ETI), and the students in Dr. Müller's group.

TABLE OF CONTENTS

LIST OF FIGURES

Images in this dissertation are presented in color.

LIST OF TABLES

A

A,B,C,D,E

c

D

E

F

G

h

I, i, J, j

k

L

l

M,m

Mo

m

Opr

P

Pr

R

r

T

t

NOMENCLATURE

A	Area
A,B,C,D,E	Flow regions and patterns
c	Damping factor
D	Vertical force, Diameter of plug
E	Young's modulus or energy
F	Force
G	Shear modulus
h	Traveling of valve plug, cutting hight or enthalpy
I, i, J, j	Moment of inertia or node number
k	Stiffness or node number
L	Lateral force
l	Length or vertical displacement
M,m	Mass, Mach number
Mo	Moment around holding position
$\dot{m}$	Mass flow rate
Opr	Opening ratio=h/D
P	Pressure
Pr	Pressure ratio
R	Radius or gas constant
r	Radius
T	Temperature or torque
t	Time

U	
V	
v	
$\alpha,\beta,\psi,\omega,\theta$	
ρ	
ζ	
π	
η	
τ	
μ	
ε	
λ	
ω	

Subscript

0	
0,1...8	
01,1	
1/2	
ave	
eq	
G	
is	
L,a	

U	Tangential velocity
V	Velocity
v	Volume
$\alpha,\beta,\psi,\omega,\theta$	Angle
ρ	Density
ζ	Damping ratio
π	Pressure ratio or 3.14
η	Efficiency
τ	Shear stress
μ	Viscosity
ε	Seat throat and plug area ratio
λ	Plug stem and plug area ratio
ω	Natural frequency

Subscript

0	Plug natural position or maximum cross section
0,1,..8	Pressure sensor number or flow pattern number
01,1	Inlet total
1/2	Inlet/outlet chest
ave	Average quantity
eq	Equivalent
G	Gauge
is	Isentropic
L, α	Lateral

max	M
n	N
o	Or
plug	Val
r	Rat
s	Stat
seat	Valv
t	Total
z	Verti

max	Maximum value
n	Node number or natural
o	Original design
plug	Valve plug side
r	Ratio
s	Static
seat	Valve seat side
t	Total
z	Vertical

1.1Valves

Valves are w

vessels. Flow re

can be performe

automatically.

Valves can be

flow control valv

special purpose v

Flow-control v

on-off service, th

globe valve, pisto

diaphragm valve a

valves are manual

valves are operate

properties by a con

valves.

Reverse flow pre

automatic on-off va

Closure is designed

special designed me

CHAPTER 1

INTRODUCTION

1.1Valves

Valves are widely used fluid control elements in piping systems or on fluid contained vessels. Flow regulation and pressure control are two major functions of valves, which can be performed by adjusting closure member position either by manually or automatically.

Valves can be roughly divided into four main categories according to their functions: flow control valves, reverse flow prevent valves, pressure-control valves and other special purpose valves.

Flow-control valves are most commonly used valves to serve three major functions: on-off service, throttling and diverting. There are various types in this category, such as globe valve, piston valve, gate valve, plug valve, ball valve, butterfly valve, pinch valve, diaphragm valve and so on. They are either manual valves or control valves. Manual valves are manually operated or power-operated but manually controlled valves; Control valves are operated automatically on the signal obtained by timing or sensing fluid properties by a control unit. Generally all manual valves can be changed to control valves.

Reverse flow prevent valves are more commonly called check valves, which are automatic on-off valves that open with forward flow only to prevent reverse flow. Closure is designed to automatically be operated by its weight, by back-pressure, by special designed mechanism, such as spring or by a combination of forgoing.

Pressure-co

are most comm

protect system

There are sti

specific applica

so on.

1.1.1 Steam tur

As a large flu

steam turbine va

there are large n

intercept valve, s

and by pass valv

emergency servi

1.1.2 Turbine in

As shown in F

boiler into the tu

steam flow rate t

control valve mu

temperature and

from the close to

inevitable and ca

important to turb

Pressure-control valves are more commonly specified as pressure relief valves, which are most commonly used valves in this category. Pressure relief valves are designed to protect system against excessive pressure.

There are still a lot of valves called special purpose valves, which are designed for specific applications, such as flush bottom valves, sampling valves, solenoid valves and so on.

1.1.1 Steam turbine valves

As a large fluid system, steam turbine has various types of valves. The major duty of steam turbine valves is to regulate the steam flow to or from or through the turbine, so there are large number of flow control valves, such as inlet control valve, reheat turbine intercept valve, steam seal regulator make-up valve, astern valve, and all kinds of throttle and by pass valves. There are also check valves like reheat-stop valve, safety valves for emergency service and special purpose valves.

1.1.2 Turbine inlet control valve

As shown in Fig. 1.1, turbine inlet control valve is used to regulate steam flow from boiler into the turbine. In response of desired frequency and load, the valve controls steam flow rate through the turbine, which produces the right amount of power output. A control valve must be able to operate at high temperature and pressure with possible large temperature and pressure drop, be free from instability or chatter of the control system from the close to wide open state. Flow pressure drop when passing through a valve is inevitable and can cause poor thermal efficiency. A higher thermal efficiency is very important to turbine, so it is important for valve to be able to control flow with minimum

pressure drop.

carefully cons

www.

Venturi valve

regulate the flow

turbine. The valv

The closure head

from the fully clo

seat is essentially

is mounted on the

like two converg

pointing to the v

pressure loss.

As turbines beca

volume flow rate.

pressure drop. In general, structure, control and thermodynamic concerns must be carefully considered when design a turbine control valve.

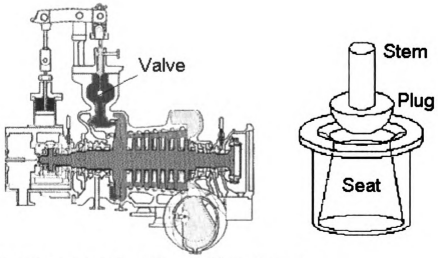

www.mtc.ac.jp/cadets_e/hassane/st-turbine.html

Fig. 1.1 Turbine and steam inlet control valve

Venturi valves are widely used in modern turbines as turbine governor valves to regulate the flow entering the turbine. Fig.1.1 shows a typical single venturi valve in a turbine. The valve has a moving component, closure, a stationary seat, and valve chest. The closure head, called the plug, is operated by a controller through the closure stem from the fully closed to the fully open position in response to desired turbine output. The seat is essentially a converging-diverging nozzle with a very short converging section and is mounted on the bottom of the valve chest. The cross-section of the valve passage looks like two converging-diverging nozzles formed by one side of the plug and of the seat, pointing to the valve center. This design is believed to be able to minimize the total pressure loss.

As turbines became larger, the larger venturi valve should be used to handle greater volume flow rate. It is very difficult to overcome the critical hydraulic force for control

and maintain t

at partial load

instead of one

All valves are

turbine is not r

clearance D > (

opened first, N

previous valve

Fig.

and maintain the performance. For modern large turbines, to improve turbine efficiency at partial load and reduce the lifting force required, multiple smaller valves are used instead of one large valve. These valves are operated in sequence, as shown in Fig. 1.2. All valves are in the closed position with the initial clearances (A through D) when the turbine is not running. The valve opening is controlled by the liftbar. Because the clearance D > C > B > A, when the liftbar is lifted by the liftrod, the No. 1 valve is opened first, No.2 second, No. 3 third, and No. 4 last. Each valve starts to open as the previous valve is almost fully open. Thus there is overlap.

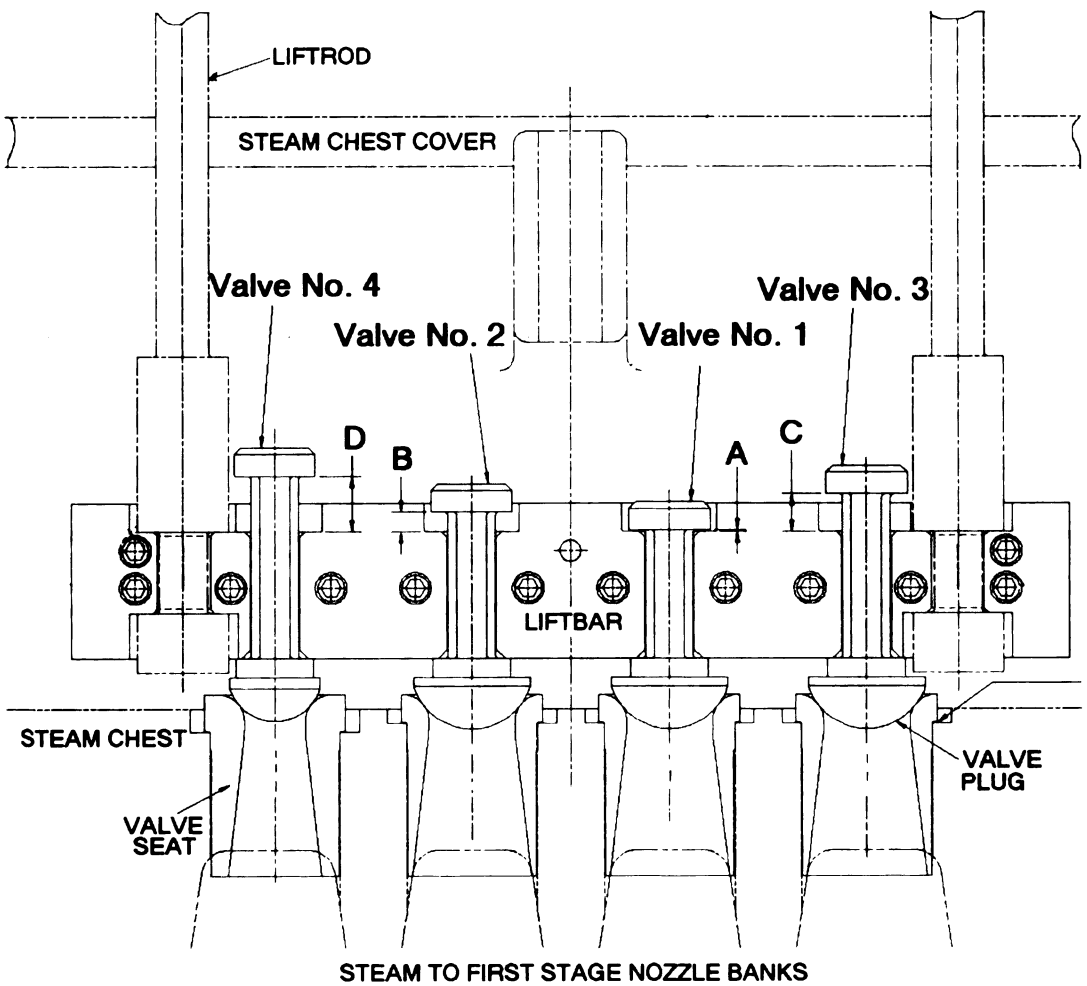

Fig. 1.2. Cross section of multiple venturi valves (after J. Hardin)

1.2 Demands o

Normally, th

thermal power p

fully open valve

situation, the hig

forces due to th

surface cause sev

in a very short tir

material fatigue.

Since the 19

increasing turbin

of the flow throu

research area. Th

problems. First, in

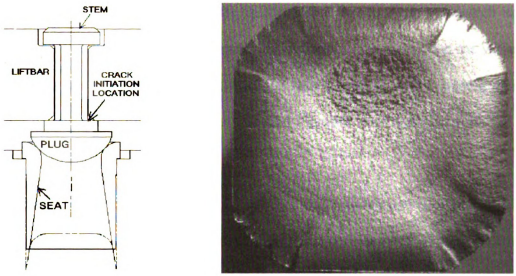

Fig. 1.3 The Venturi valve and its failure (after J. Hardin)

1.2 Demands on The Study of Turbine Steam Control Valves

Normally, the inlet valves are operated under very severe conditions. For example, in thermal power plants, the steam inlet temperature, pressure, and pressure drop through a fully open valve can reach as high as 1000°F, 4,000Psi and 200Psi respectively. In such a situation, the high speed flow can be very asymmetric and unstable. Thus, hydraulic forces due to the strong asymmetric and unstable pressure distribution along the plug surface cause severe problems, such as vibration and noise. The valve plug can be broken in a very short time due to the large amplitude of forces, or in long-term operation due to material fatigue. It is very costly to stop the turbine to replace a valve.

Since the 1960's, more and more valve failure incidents were reported due to increasing turbine size and upstream steam pressure. Because of the complicated nature of the flow through a valve, until the early 70's, there was still no big progress in this research area. There were several papers investigating the valve noise and failure problems. First, increasing the rigidity of the structure was proved insufficient. Then the

self-excited v

years of exper

vibration was

does not do ar

reason for valv

A recent valv

steam turbine i

developed in th

fully open and

seat into the stea

shown in Fig. 1.

which means tha

1.3 Objective a

As multiple-v

way, the study c

is to clarify the f

can cause valve

work has been a

1. Theory an

2. Literature

3. Numerical

4. Experimen

self-excited vibration was denied as the reason, according to Araki's research and 10 years of experience of a plant in the former Soviet Union. This means that the valve plug vibration was not a result of feedback from the flow vibration, and so adding damping does not do any good. Finally, the flow-induced vibration was believed to be the main reason for valve failure.

A recent valve failure was reported in 1998. The valve started operation in a multistage steam turbine in 1998. After 3 months of running, the No. 2 valve failed after the crack developed in the location shown in Fig. 1.3. It happened as the No.1 valve was almost fully open and No. 2 valve was at an opening of 0.147(h/D). The falling plug drove the seat into the steam chest wall approximately 0.7in. The failed valve stem surface is shown in Fig. 1.3. Before the failure, there was higher noise coming out of the machine, which means that chattering may have existed.

1.3 Objective and Structure of The Present Study

As multiple-valves are essentially several single venturi valves mounted in a parallel way, the study concentrates on the single venturi valve. The objective of the present study is to clarify the fluid and failure mechanism of venturi valves to obtain regions, which can cause valve failure and to design new valves to improve their reliability. The research work has been accomplished systematically to achieve the goals with following steps:

1. Theory analysis of fluid valve interaction and valve vibration
2. Literature review of former research
3. Numerical simulations for current valves and improved valve designs
4. Experimental investigation of current venturi valves

The cross sc

between plug

seat facing the

lifted to contro

push all the wa

lift position. M

a position after

fully open posit

reaches maximu

There were a

the result of flo

other. So it is n

clarify the intera

2.1 Flow Therm

The flow in v

unsteady. But in

and one-dimens

CHAPTER 2

FUNDAMENTALS AND THEORY ANALYSIS

The cross section of a valve passage is shown in Fig. 2.1. Flow passes the space between plug and seat. The plug is normally made as semi-sphere shape. The upper side seat facing the plug is arc shape. In response of feedback signals of turbine output, plug is lifted to control the inlet flow rate. Fully closed position was defined as when the plug is push all the way on the seat and no flow can pass by the valve, which is also called zero lift position. Mass flow rate will increase as the plug is lifted from fully closed position to a position after which the mass flow rate remains constant. This position is defined as fully open position. After fully open position, the valve plug can still be lifted until reaches maximum lift position.

There were a lot of reports on valve plug vibration and break, which were believed as the result of flow-structure interaction. It is still unclear that how they interact with each other. So it is necessary to have a study on both the fluid side and valve plug side to clarify the interaction mechanism between them.

2.1 Flow Thermodynamics

The flow in valve is highly complex, three-dimensional, turbulent, viscous, and unsteady. But important information can be obtained by the basic governing equations and one-dimensional analysis.

2.1.1 Basic g

Continuity

In most cas

in changing pl

accumulation i

continuity equa

Energy balance

The valve is

be treated as adi

thus reduces to

In the absence

the stagnation en

steady state proc

Equation of state

As the steam

as ideal gas. Wi

the gas satisfies

2.1.1 Basic governing equations

Continuity

In most cases, turbine operates with constant output, which means flow is steady. Even in changing plug lift process, as the valve is little compare with big mass flow rate, mass accumulation in valve can also be ignored. Define valve inlet as 1 and exit as 2, the continuity equation becomes

$$\dot{m}_1 = \rho_1 V_1 A_1 = \dot{m}_2 = \rho_2 V_2 A_2 \tag{2.1}$$

Energy balance

The valve is little, so fluid potential energy changing is ignored and also the valve can be treated as adiabatic wall. The energy balance relation for flow passing through a valve thus reduces to

$$h_{01} = h_{02} = h_1 + \frac{V_1^2}{2} = h_2 + \frac{V_2^2}{2} \tag{2.2}$$

In the absence of any heat and work interactions and any changes in potential energy, the stagnation enthalpy of a fluid remains constant when passing through a valve during steady state process.

Equation of state

As the steam temperature is very high when passing through the valve, it can be treated as ideal gas. With constant gas constant, R, specific heats, C_v and C_p, and their ratio, k, the gas satisfies following state equation:

$$P = \rho RT \tag{2.3}$$

Newton secon

Motion equ

Momentum

Second law of

Thermodyna

reversible comp

2.1.2 Ideal pro

As shown in

dimensional co

Newton second law

Motion equations are used to deduce vibration-governing equations

$$\sum \vec{F} = m\vec{a} \tag{2.4}$$

$$\sum \vec{F}\vec{R} = J\ddot{\vec{\theta}} \tag{2.5}$$

Momentum equation is used to analysis hydraulic forces acting on valve plug

$$\sum \vec{F} = \frac{\partial}{\partial t}\int_{c.v.} \rho \vec{V} dv + \int_{c.s.} \rho \vec{V}\vec{V} \bullet d\vec{A} \tag{2.6}$$

Second law of thermodynamics

Thermodynamics second law is used to deduce the basic thermodynamic relations for reversible compressible flow process and to define valve efficiency.

2.1.2 Ideal process for 1-D fluid passing the valve

As shown in Fig. 2.1, flow passing through a venturi valve can be idealized as one-dimensional compressible ideal gas passing through a converging-diverging

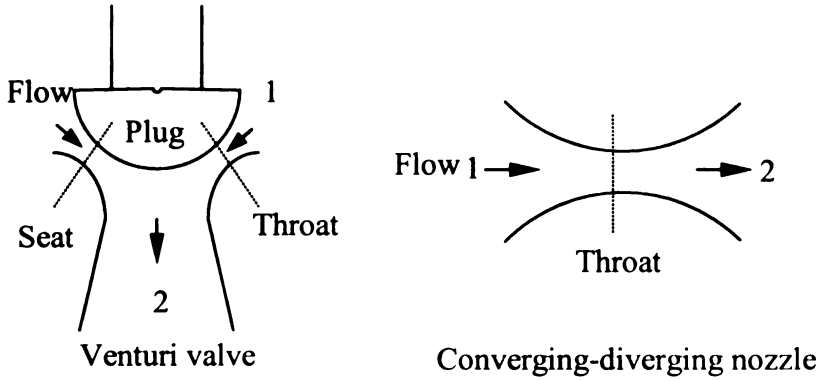

Fig. 2.1 Idealization of valve

Driven by t

valve with a l

boiler supplie

position to full

converging-di

different valve

Fig

At wide-open

accelerated befo

velocity and low

diffuser section o

throat and flow is

As the plug tra

(curve B), the thr

Driven by the pressure difference between valve inlet (1) and outlet (2), flow enters the valve with a low velocity at stagnation pressure P_{01}, which can be treated as constant as boiler supplies constant pressure steam to turbine. As plug traveling from wide-open position to fully closed position, valve exit pressure P_2 falls down. According to converging-diverging nozzle theory, the flow will experience different process with different valve lift, as shown in Fig. 2.2.

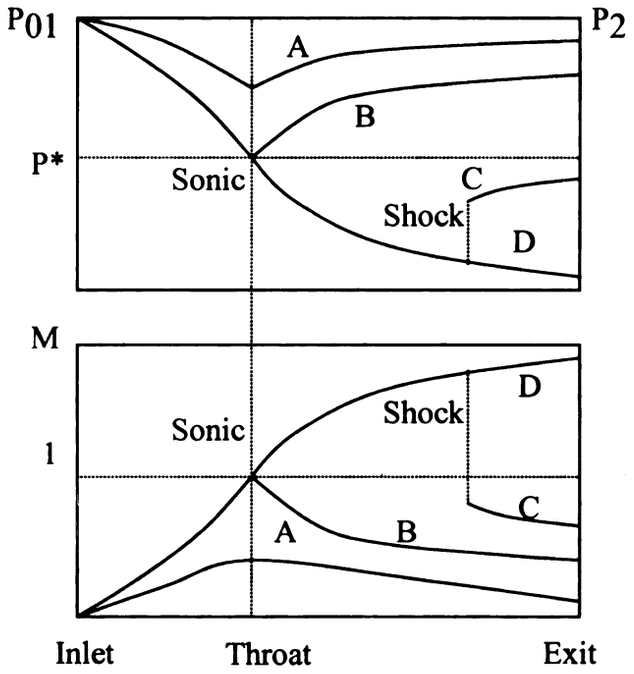

Fig. 2.2 The effects of plug travel on the flow through a valve

At wide-open position, the flow remains subsonic throughout the valve. The fluid is accelerated before throat while pressure keeps decreasing, until reaches the highest velocity and lowest pressure at throat, then slow down with pressure increasing at the diffuser section of the valve. The maximum Mach number is less than unit at the valve throat and flow is not chocked. The valve acts as a diffuser.

As the plug travels to closed position, P_2 keeps dropping. At one critical position (curve B), the throat Mach number reaches unit. The valve still acts as a diffuser. The

velocity and p

becomes soni

between critic

closed positio

When valve

accelerating to

decreases. Thi

between throat

increase in pres

valve.

In real valves

impossible to ac

much P_2 droppe

Property Relatio

Fig. 2.3 Ideal a

velocity and pressure change as same way as large open situation except at throat flow becomes sonic. This position is called critical position. It is called almost wide open between critical position and wide-open position. Between critical position and fully closed position, it is called almost close.

When valve is almost close, as shown in curve C, the sonic fluid at throat continues accelerating to supersonic velocities in the diverging section of valve as pressure decreases. This acceleration comes to a sudden stop as a shock develops at the section between throat and exit causing a sudden drop in velocity to subsonic levels and sudden increase in pressure. Then the fluid continues to decelerate further in remaining part of valve.

In real valves, because the exit section is normally designed over diffused, it is impossible to accelerate fluid to supersonic, as shown curve D, at valve exit even how much P_2 dropped.

Property Relations for isentropic flow of ideal gas passing through a valve

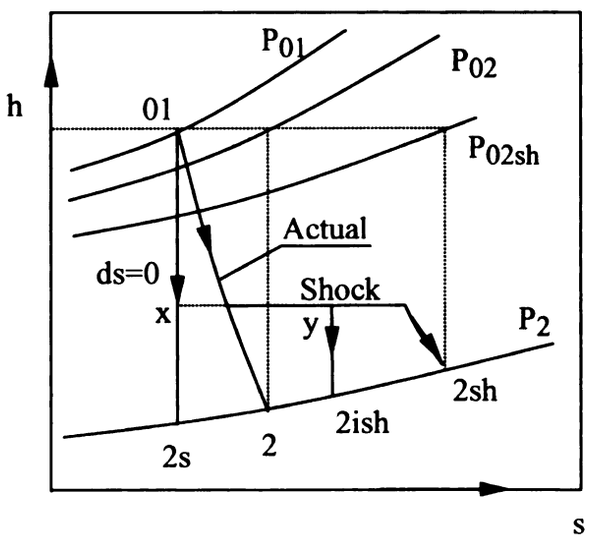

Fig. 2.3 Ideal and actual flow in a valve between same inlet state and exit pressure

Flow is ass

process, all st

relations for s

(y→2ish) shoc

$$\frac{A}{A}$$

Above equa

properties can

the function of

Mass flow rate

Under steady

number, valve

Flow is assumed isentropic except for the shock region (x→y in Fig. 2.3). As isentropic process, all stagnation properties, T_0, P_0 and ρ_0 remain constant. The basic property relations for subsonic and sonic (01→2s), and for supersonic flow before (01→x) or after (y→2ish) shock are shown as following:

$$\frac{T_0}{T} = 1 + \left(\frac{k-1}{2}\right) M^2 \tag{2.7}$$

$$\frac{P_0}{P} = \left[1 + \left(\frac{k-1}{2}\right) M^2\right]^{\frac{k}{k-1}} \tag{2.8}$$

$$\frac{\rho_0}{\rho} = \left[1 + \left(\frac{k-1}{2}\right) M^2\right]^{\frac{1}{k-1}} \tag{2.9}$$

$$\frac{A}{A^*} = \frac{1}{M}\left[\left(\frac{2}{k+1}\right)\left(1 + \left(\frac{k-1}{2}\right) M^2\right)\right]^{\frac{k+1}{2(k-1)}} \tag{2.10}$$

Above equations show that the relation between stagnation properties and static properties can be express as a function of Mach number. The Mach number is essentially the function of cross-area. In the equation, k is specific ratio and is constant for ideal gas.

Mass flow rate

Under steady flow conditions, the mass flow rate can be expressed as function of Mach number, valve throat area. R is gas constant.

$$\dot{m} = A^* M P_0 \sqrt{\frac{k}{RT_0}} \left[1 + \frac{k-1}{2} M^2\right]^{\frac{k+1}{2(1-k)}} \tag{2.11}$$

After critic

can be simpli

As both inle

proportional to

Shock Waves

Shock wave

changes in flui

occur in a very

flow process th

as being isentro

shown as follo

After critical position, flow is choked as Mach number turns to unit. Above equation can be simplified as following:

$$\dot{m} = A^* P_0 \sqrt{\frac{k}{RT_0}} \left[\frac{k+1}{2} \right]^{\frac{k+1}{2(1-k)}} \tag{2.12}$$

As both inlet conditions and specific heat ratio remain constant, the mass flow rate is proportional to throat area, which changes with plug lift.

Shock Waves

Shock wave occurs when flow in valve is supersonic, as shown in Fig. 2.2. Abrupt changes in fluid properties, such as pressure, temperature, Mach number and density, occur in a very thin section, creating a shock wave. As shown in Fig. 2.3 the curve x→y, flow process through the shock wave is highly irreversible and cannot be approximated as being isentropic. The basic property relations before (x) and after (y) shock wave are shown as following.

$$M_y = \sqrt{\frac{(k-1)M_x^2 + 2}{2kM_x^2 - (k-1)}} \tag{2.13}$$

$$\frac{T_y}{T_x} = \frac{2 + (k-1)M_x^2}{2 + (k-1)M_y^2} \tag{2.14}$$

$$\frac{P_y}{P_x} = \frac{1 + kM_x^2}{1 + kM_y^2} \tag{2.15}$$

$$\frac{P_{0y}}{P_{0x}} = \frac{M_x}{M_y}\left[\frac{2+(k-1)M_y^2}{2+(k-1)M_x^2}\right]^{\frac{k+1}{2(k-1)}} \tag{2.16}$$

$$\frac{\rho_y}{\rho_x} = \frac{P_y T_x}{P_x T_y} \tag{2.17}$$

$$\frac{P_{0y}}{P_x} = \frac{1+kM_x^2}{1+kM_y^2}\left[1+\frac{k-1}{2}M_y^2\right]^{\frac{k}{k-1}} \tag{2.18}$$

According to above equations, after shock, the stagnation pressure and velocity decrease while the static pressure, temperature, density, and entropy increase.

2.1.3 Flow through actual valves and valve performance

Actual flow process is not ideal as above discussion. Besides shock, two major factors, friction and flow separation also cause irreversibility, making the real process looks like 01→2 without shock or 01→2sh with shock instead of 01→2s and 01→2ish respectively in Fig. 2.3. The friction effects are mostly confined to the boundary layer, while separation occurs when flow area increases faster than fluid expansion, or simply, over diffusion.

Valve efficiency

To evaluate a valve, the valve efficiency can be defined by comparing actual kinetic energy at valve exit to kinetic energy at valve exit for isentropic flow from the same inlet state to the same exit pressure as shown in equation (2.19a). It can also be defined in terms of total pressure loss or total pressure ratio as shown in equation (2.19b).

For subsoni

Fig. 2.4a sho

subsonic situati

waves can prod

parameter, total

ratio portion du

predicted by equ

result from equa

Specification 50

$$\eta_v = \frac{h_{01} - h_{2\ or2sh}}{h_{01} - h_{2s}} \tag{2.19a}$$

$$\pi_0 = 1 - \frac{\Delta P_0}{P_{01}} = \frac{P_{02}}{P_{01}} \tag{2.19b}$$

For subsonic flow, they can be related as

$$\eta_v = \frac{\tau_0 \pi_0^{\frac{k-1}{k}} - 1}{\tau_0 - 1} \tag{2.20a}$$

$$\eta_r = \frac{\pi_0}{\pi_{0f}} \tag{2.20b}$$

Fig. 2.4a shows the typical relation variation of efficiency and pressure ratio for subsonic situation. The total pressure loss is due to friction. In supersonic flow, shock waves can produce much greater total pressure loss as shown in Fig. 2.13. Thus another parameter, total pressure recovery η_r, is defined as total pressure ratio over total pressure ratio portion due to friction. In theory the total pressure loss due to shock waves can be predicted by equation 2.16. In real situation, at high Mach number (bigger than 1.5), the result from equation 2.16 is higher than experiment data. Thus an equation from Military Specification 5008B can be used here as

$$\eta_r = 1 \qquad \text{M}\leq 1 \tag{2.20c1}$$

$$\eta_r = 1 - 0.075(M-1)^{1.35} \qquad 1<\text{M}<5 \tag{2.20c2}$$

$$\eta_r = \frac{800}{M^4 + 935} \qquad 5<\text{M} \tag{2.20c3}$$

The recov

Different v

efficiency un

valve has hig

smaller fracti

decreases as p

region increas

pressure loss.

Mass flow rat

The inlet co

the output of t

way that the m

In practice, the

characteristic.

valves is show

equations.

In the steep

governed by eq

linear relation

affect the mass

increasing, the

like a steep-flat

The recovery variation with Mach number based above equation is plotted in Fig. 2.4c.

Different valves have different performance. Even the same valve has different efficiency under different lift level shown as solid line in Fig. 2.4. At wide-open position, valve has higher efficiency ranges from 90-99% because the boundary layer occupies a smaller fraction of total flow volume and separation region is less. The efficiency decreases as plug moves toward seat since both boundary layer fraction and separation region increase. After the critical position, shock waves become the main cause of total pressure loss. The efficiency drops quickly.

Mass flow rate

The inlet control valve is to serve for controlling the mass flow rate to turbine. Because the output of turbine is proportional to flow rate, so it is desirable to design the valve in a way that the mass flow rate is proportional to plug lift shown as dash dot line in Fig. 2.4. In practice, the flow-lift characteristic of valve does not act like the ideal proportion characteristic. For example, a typical flow-lift characteristic line for a valve in multiple valves is shown as doted line, which can be explained, based on ideal mass flow rate equations.

In the steep linear part of the curve between critical position and fully closed position, governed by equation (2.12), the mass flow rate is proportional to throat area, which has linear relation with plug lift. After the critical position, both throat area and Mach number affect the mass flow rate, according to equation (2.11). As valve throat area continues increasing, the Mach number starts to drop. This combination makes the rest of the curve like a steep-flat shape.

a. Variation o

The goverr

parts, steep pa

the mass flow

about 10% ma

pressure ratio

decreases. For

position, while

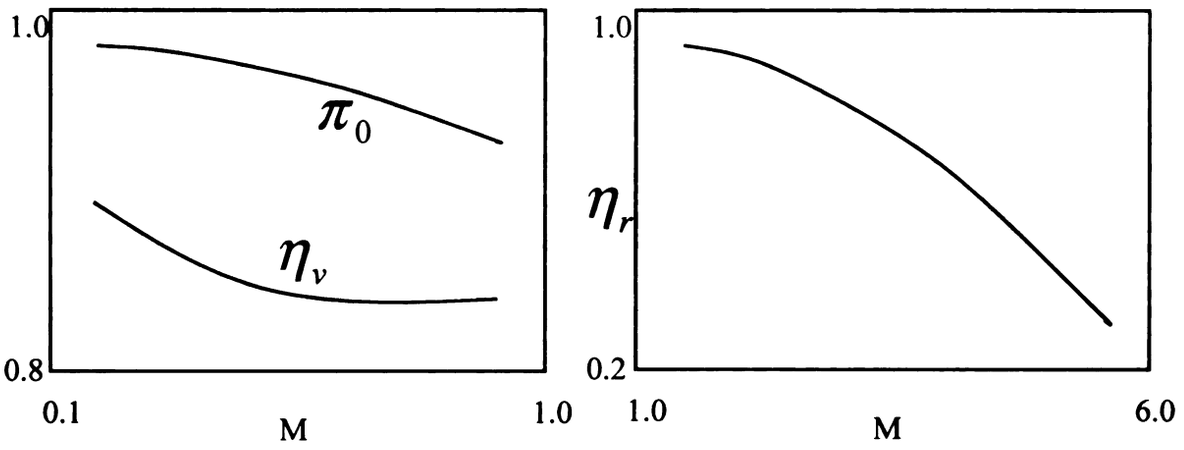

a. Variation of efficiency of subsubsonic flow b. Variation of recovery of supersonic flow

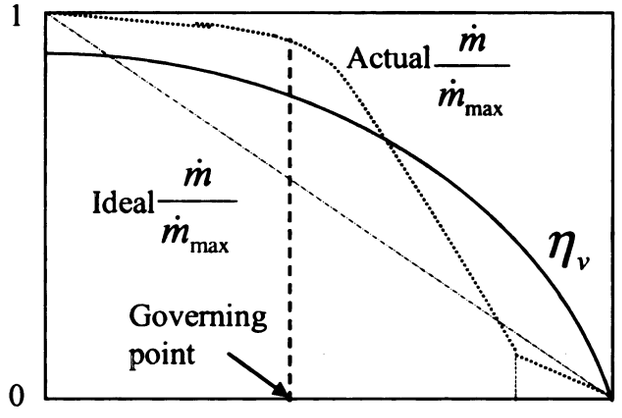

c. Efficiency and mass flow changing due to open process

Fig. 2.4 Valve efficiency and mass flow rate

The governing point is defined as shown in Fig. 2.4, which divides the curve into two parts, steep part and flat part. In the steep part, including choked or unchoked situations, the mass flow rate changes from 0 to about 90%, while the flat part only accounts for about 10% mass flow increase. The governing point moves to wide open position as the pressure ratio of downstream (turbine first stage) and upstream (steam feeding chest) decreases. For example, if the pressure ratio is 0.9, the governing point is at half open position, while if the pressure ratio is 0.5, it reaches 80% open position. This is the reason

why the flow

valves. In m

has more infl

flow-lift char

2.2 Hydrauli

2.2.1 Drag and

Passing throu

jets, vortex, and

and lift, are exte

Drag

The total drag

drag.

why the flow-lift characteristic of single valve is different with one valve of multiple-valves. In multiple valves, the pressure ratio is approximately constant, while single valve has more influence on pressure ratio when changing lift. There is still no big different for flow-lift characteristic. The curve is also steep-flat shape for single valve.

2.2 Hydraulic Forces

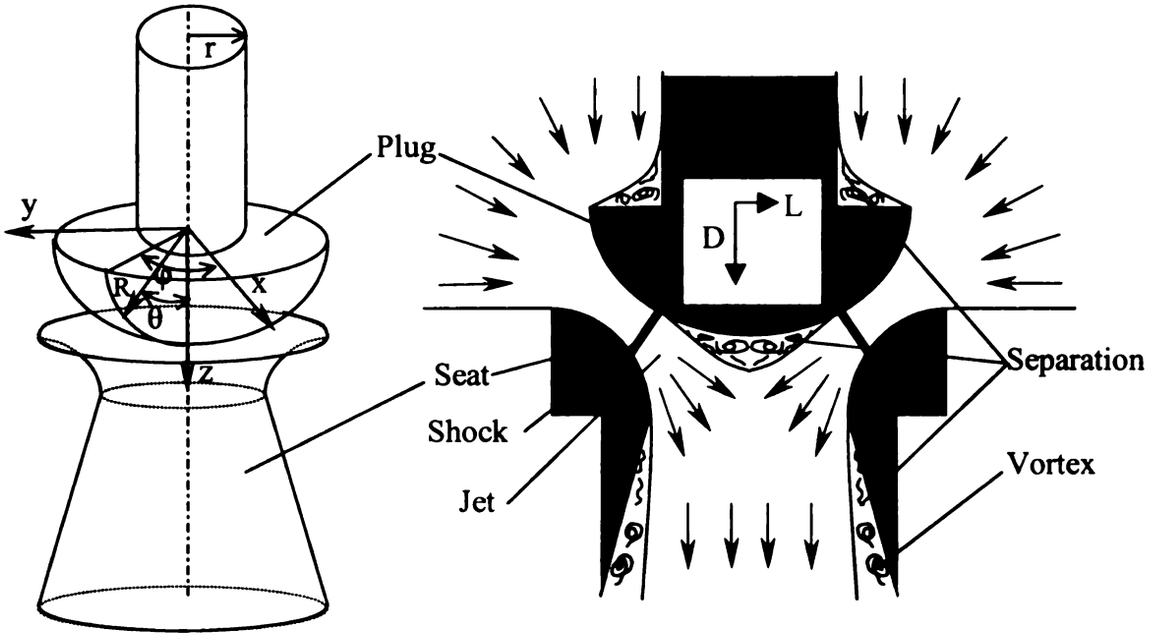

Fig. 2.5 Valve and flow pattern

2.2.1 Drag and lift extended by fluid

Passing through a valve, the flow is highly complex with friction, separation, unsteady jets, vortex, and possible shock waves as shown in Fig. 2.5. Two hydraulic forces, drag and lift, are extended on plug, which can be treated as an immersed body.

Drag

The total drag acted by fluid is composed of two parts, pressure drag and skin friction drag.

The pressu

between plug

force acted by

If the plug i

$$D_p =$$

D_{pup} is drag

component of

When viscou

be calculated b

According to b

friction drag ca

Where bas m

The fluid is tr

$$D_f$$

$$D = D_p + D_f \tag{2.21}$$

The pressure drag is net normal stress in z-direction. It is caused by pressure difference between plug upside and semi-sphere side. It can be obtained by integrating the normal force acted by pressure along the out face of plug in z direction.

$$D_p = -\oiint_s P\hat{z} \bullet d\vec{A} \tag{2.22}$$

If the plug is a semi-sphere, the equation can be specified as:

$$D_p = D_{pup} - D_{psp} = P_{01}\pi(R^2 - r^2) - R^2 \int_0^{\frac{\pi}{2}} \int_0^{2\pi} P\cos\theta d\varphi d\theta \tag{2.23}$$

D_{pup} is drag force extended by pressure on up surface, which is a ring; D_{psp} z-direction component of the normal stress of semi-sphere surface.

When viscous fluid passing through the valve, it extends skin friction drag, which can be calculated by integrating the shear stress along the semi-sphere surface in z-direction. According to boundary theory, the skin friction mainly occurs in boundary layer. So the friction drag can be expressed as:

$$D_f = \iint_{bas} \sin(\hat{R} \wedge \hat{z})\tau d\vec{A} \tag{2.24}$$

Where bas means boundary layer attached area.

The fluid is treated as Newtonian fluids. The equitation can be expressed as:

$$D_f = R^2 \int_0^{2\pi} \int_0^{\alpha_c} \left(\mu \frac{\partial V}{\partial n}\Big|_R \right) \sin\theta d\theta d\varphi \tag{2.25}$$

Where α_c i

separation. It

Lift

Lift also ca

total lift has t

The pressur

pressure differ

integrating the

The angle be

Where L_{px} an

$$L_{px} = R$$

$$L_{py} =$$

Where α_c is critical angle, which means the angle that boundary layer started separation. It can be function of φ when separation is asymmetric.

Lift

Lift also called lateral foce is defined as forces perpendicular to drag. Similar to drag, total lift has two components, pressure lift and friction lift.

$$\vec{L} = \vec{L}_p + \vec{L}_f \tag{2.26}$$

The pressure lift is net normal stress perpendicular to z-direction. It is caused by pressure difference in directions perpendicular to z-axis. It can also be obtained by integrating the normal stress as following equations.

$$L_p = \sqrt{L_{px}^2 + L_{py}^2} \tag{2.27}$$

The angle between pressure lift direction and x-direction is

$$\phi = \tan^{-1}\left(\frac{L_{py}}{L_{px}}\right) \tag{2.28}$$

Where L_{px} and L_{py} are x and y-direction components of pressure lift respectively.

$$L_{px} = R^2\left(\int_0^{\frac{\pi}{2}}\left(\int_{\frac{\pi}{2}}^{\frac{3\pi}{2}} P\cos\varphi d\varphi - \int_{-\frac{\pi}{2}}^{\frac{\pi}{2}} P\cos\varphi d\varphi\right)\sin\theta d\theta\right) \tag{2.29}$$

$$L_{py} = R^2\left(\int_0^{\frac{\pi}{2}}\left(\int_{\pi}^{2\pi} P\sin\varphi d\varphi - \int_0^{\pi} P\sin\varphi d\varphi\right)\sin\theta d\theta\right) \tag{2.30}$$

Skin fricti

stress along t

also mainly c

The angle

Where L_{px} a

$$L_{fx} =$$

$$L_{fy} =$$

Where, if tr

Analysis on li

Balanced va

seat. If the flo

such situation,

Skin friction also cause lift drag, which can be calculated by integrating the shear stress along the semi-sphere surface in perpendicular direction to z-axis. Skin friction lift also mainly occurs in boundary layer attached area and can be expressed as:

$$L_f = \sqrt{L_{fx}^2 + L_{fy}^2} \tag{2.31}$$

The angle between pressure lift direction and x-direction is

$$\gamma = \tan^{-1}\left(\frac{L_{fy}}{L_{fx}}\right) \tag{2.32}$$

Where L_{px} and L_{py} are x and y-direction components of pressure lift respectively.

$$L_{fx} = R^2\left(\int_{\frac{\pi}{2}}^{\frac{3\pi}{2}}\int_0^{\alpha_c}\tau\cos\varphi\cos\theta d\theta d\varphi - \int_{-\frac{\pi}{2}}^{\frac{\pi}{2}}\int_0^{\alpha_c}\tau\cos\varphi\cos\theta d\theta d\varphi\right) \tag{2.33}$$

$$L_{fy} = R^2\left(\int_{\pi}^{2\pi}\int_0^{\alpha_c}\tau\sin\varphi\cos\theta d\theta d\varphi - \int_0^{\pi}\int_0^{\alpha_c}\tau\sin\varphi\cos\theta d\theta d\varphi\right) \tag{2.34}$$

Where, if treat the flow as Newtonian fluid

$$\tau = \mu\frac{\partial V}{\partial n}\Big|_R \tag{2.35}$$

Analysis on lift and drag estimation for balanced valve

Balanced valve means plug is stationary without vibration and is concentric with the seat. If the flow is symmetric around z-axis, according to lift equations, lift is zero under such situation. To get the drag by theory, the shear force should be simplified as:

$$\tau = \mu\frac{2V}{d} \tag{2.36}$$

Where V

be expressed

one-dimensi

get accurate

unpredictable

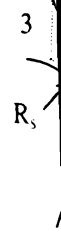

a. C
alm

A simple w

control volume

a. Flow ent

b. Ignore bo

c. The regio

no fluid f

d. Static pre

e. Flow velo

Where V is main stream velocity and d is distance shown in Fig. 2.6. Both of them can be expressed as function of passing area, or sphere profiles of seat and plug, according to one-dimensional analysis. The pressure is also a function of sphere profiles. Thus we can get accurate drag by above equations. But due to the complex geometry of valve and the unpredictable separation, drag is too complicated to be obtained by this way.

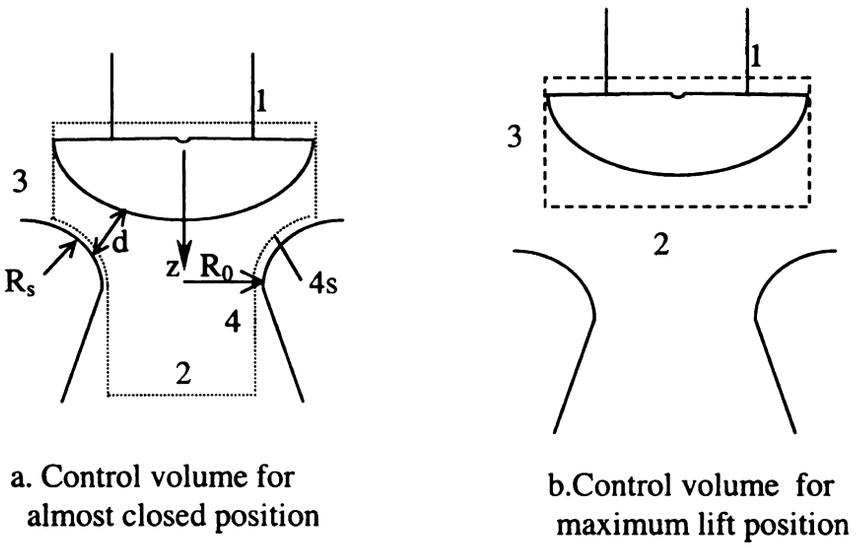

a. Control volume for almost closed position

b.Control volume for maximum lift position

Fig. 2.6 Drag estimation

A simple way is to estimate the drag by simplifying momentum equation to the control volume shown in Fig. 2.6 with following assumptions:

a. Flow enter the control surface 3 with average z-direction velocity component V_{3z}

b. Ignore body force and friction between fluid and seat

c. The region between control surface 4 and seat after seat throat is separation region, no fluid flowing out of surface 4

d. Static pressure at control surface 1 equals flow inlet stagnation pressure

e. Flow velocity at surface 2 is uniform with z-direction

f. Steady

So the mo

The second

also very diffi

along valve as

terms, inlet, o

direction char

in this term, s

The third p

set to turbine

The fifth te

difficult to si

both mass flo

ignored.

Thus the

D

For exam

in, is operat

f. Steady state, no friction between fluid and seat, ignore body force

So the momentum equation reduces to

$$D = P_{01}A_1 - \int_{c.s.4s} P\hat{z} \bullet d\vec{A}_{4s} - \dot{m}V_2 - P_2A_2 + \dot{m}V_{3z} \tag{2.37}$$

The second part in right side of equation is the support force extended by seat, which is also very difficult to determine. By considering the one-dimensional pressure analysis along valve as shown in Fig. 2.2, the pressure can be substitute by average value of three terms, inlet, outlet stagnation pressures and throat static pressure. Since the stress direction changes along the surface, while only the z-direction component can be counted in this term, so the area is approximated as half time projection area of A_{4s} on x-y plane.

The third part can be set as zero and to compensate this simplification, the last term is set to turbine first stage stagnation pressure.

The fifth term is from flow momentum when entering the control volume. It is very difficult to simplify it. Here we do force analysis on valve small open situation, so that both mass flow rate and z-direction velocity component are very small and it can be ignored.

Thus the momentum equation can be further simplified as:

$$D = P_{01}\pi\left(R^2 - r^2\right) - \frac{\pi}{6}\left(P_{01} + P_{th} + P_{02}\right)\left(R^2 - R_0^2\right) - P_{02}\pi R_0^2 \tag{2.38}$$

For example, a valve with geometry parameters, R=2 in, R_0=1.5 in, r=1 in, and R_s=0.9 in, is operated at almost closed position. The flow is choked. The inlet total pressure is

4,000 psi an

equation, the

Drag charac

Valve des

mass flow rat

lift the plug, v

controlled. Al

vibrations wil

designing the

Rearranging

dimensionless

$$D$$

Where

$$D_h = \frac{D}{\pi P_{01} R}$$

$\pi_0 = \frac{P_{02}}{P_{01}}$, To

$\pi^* = \frac{P_{th}}{P_{01}}$, Pre

4,000 psi and the pressure drop as 200 psi as we mentioned in Chapter 1. By using above equation, the drag acted on vale plug is about 1600 lb.

Drag characteristic curves at almost closed situation

Valve design need consider a lot of issues such as, turbine type, space for installing, mass flow rate, material properties, and so on. As we talked in Chapter 1, the less force to lift the plug, which equals the drag fluid acting on plug, the better the valve can be controlled. Also we will discuss later, the more drag on plug, the more possible severe vibrations will occur. So it is very important to obtain drag force characteristic when designing the turbine valves.

Rearranging the equation (2.38), we can get a functional relation between several dimensionless groups

$$D_h = \left[(1-\lambda) - \frac{1}{6}(1+\pi^* + \pi_0)(1-\varepsilon) - \pi_0 \varepsilon \right] \tag{2.39}$$

Where

$D_h = \dfrac{D}{\pi P_{01} R^2}$, is called hydraulic drag number

$\pi_0 = \dfrac{P_{02}}{P_{01}}$, Total pressure ratio

$\pi^* = \dfrac{P_{th}}{P_{01}}$, Pressure ratio between valve throat static pressure and total inlet pressure

$$\lambda = \left(\frac{r}{R}\right)$$

$$\varepsilon = \left(\frac{R_0}{R}\right)$$

Differenti

For this fun

very difficult

$\frac{\partial \pi^*}{\partial \pi_0} = 0$. TH

This term is

This term is

$\frac{\partial D_h}{\partial \lambda}$ is alwa

than D_h-π_0 line

$\lambda = \left(\frac{r}{R}\right)^2$, Plug stem and plug area ratio

$\varepsilon = \left(\frac{R_0}{R}\right)^2$, Seat throat and plug area ratio

Differentiating drag number with total pressure ratio, we can get

$$\frac{\partial D_h}{\partial \pi_0} = -\left(\frac{1}{6}\left(1+\frac{\partial \pi^*}{\partial \pi_0}\right)(1-\varepsilon)+\varepsilon\right) \tag{2.40}$$

For this function, before fluid is choked, $\frac{\partial \pi^*}{\partial \pi_0}$ is a function of Mach number, which is very difficult to get. When the flow is choked, π^* becomes constant, which means $\frac{\partial \pi^*}{\partial \pi_0} = 0$. The equation can be reduced to

$$\frac{\partial D_h}{\partial \pi_0} = -\frac{1}{6}(1+5\varepsilon) \tag{2.41}$$

This term is always negative and is a function of seat throat-plug area ratio.

$$\frac{\partial D_h}{\partial \lambda} = -1 \tag{2.42}$$

This term is also always negative constant. As ε is always less than one, which means $\frac{\partial D_h}{\partial \lambda}$ is always less than $\frac{\partial D_h}{\partial \pi_0}$. As shown in Fig. 2.7, the slope of D_h-λ line is steeper than D_h-π_0 line.

This term

pressure rati

becomes con

This is true f

pressure drop

Based on a

variables is sh

the drag alway

can be negativ

the flow sucks

values, π_0^*, λ^*

easy to be ope

design a valve

specified.

There are n

Moussa gave s

running Davis

is to use comp

explain the dat

between drag n

ratio are linearl

$$\frac{\partial D_h}{\partial \varepsilon} = \frac{1}{6}\left(1 + \pi^* - 5\pi_0\right) \tag{2.43}$$

This term is a function of throat static-inlet total pressure ratio and exit-inlet total pressure ratio. As we know π^* increases as π_0 decreases until the flow is choked. Then it becomes constant, for ideal gas, 0.528. That means if π_0>0.31, this term will be negative. This is true for most case, as we do not want fluid passing the valve with such a big pressure drop.

Based on above analysis, the drag number changing with above three dimensionless variables is shown in Fig. 2.7. When uniform flow passing through a semi-sphere body, the drag always has same direction as flow. But to valve, it is not true. The drag number can be negative, which means the flow pushes the plug outside, or positive, which mans the flow sucks the plug to seat. The drag number is zero when any of these specific values, π_0^*, λ^* and ε^*, is satisfied. This is the most favorite operating situation for valve, easy to be operated and vibration being great reduced. These should be considered when design a valve. For continence, the drag is assumed as positive in this thesis, except when specified.

There are no experiment data to show the accuracy of our model. In 1976, Zaher M. Moussa gave some data about the relation between the drag number and pressure ratio by running Davis' computer program as shown in Fig. 2.7b. The basic idea of the program is to use computer solve the equation (2.22) to obtain pressure drag. Moussa did not explain the data. Compared the 10% and 20% lift lines with our theoretical relation between drag number and pressure ratio, they match very well. The drag and pressure ratio are linearly related when flow is choked (pressure ratio less then the dotted line).

b. Relati

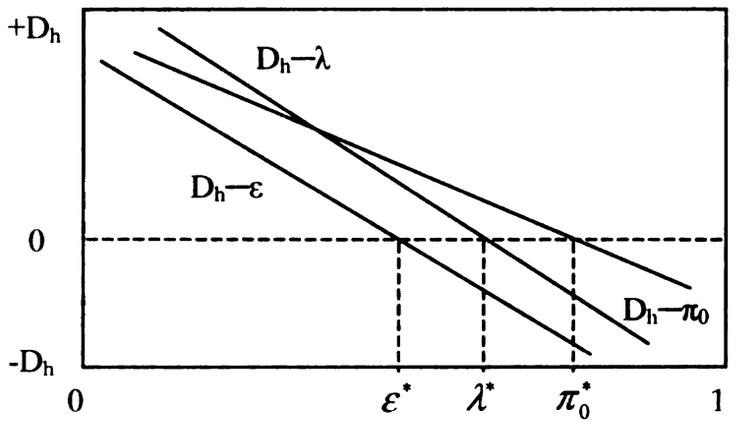

a. Relation between dimensionless groups

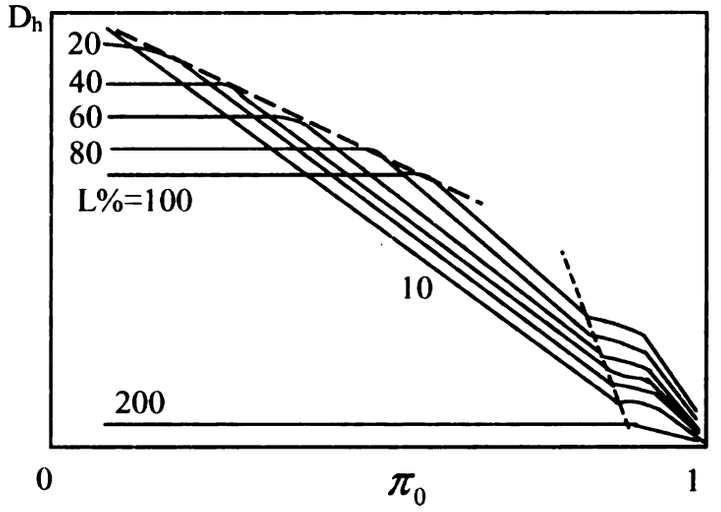

b. Relation between drag number and pressure ratio from computation result

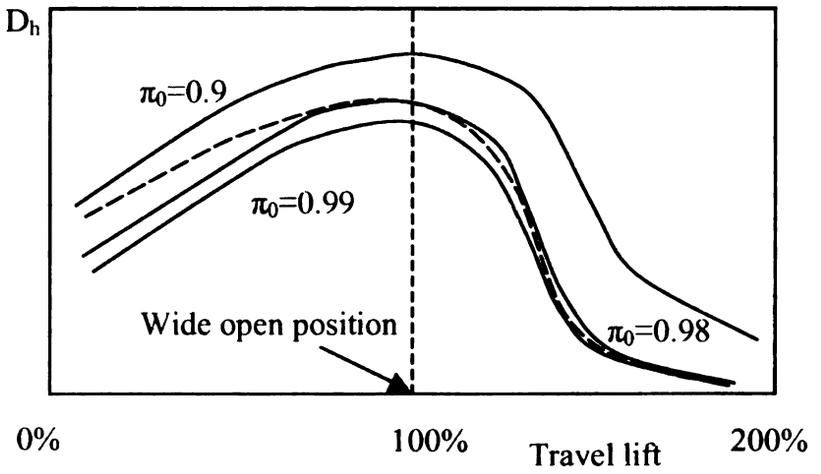

c. Plug drag-travel characteristic

Fig. 2.7 Hydraulic drag number

As plug t

independent

think the rea

thus the dow

force remain

higher the pr

outside of the

ratio between

same. This pr

ratio scale dur

maximum lift

Drag-plug trav

Not only wi

lift as shown i

Normally lift p

valves. If the v

position, the d

According t

second and fif

dimensional a

term. When th

component inc

As plug travels to fully open position, at the low pressure-ratio, the drag becomes independent on pressure ratio, as the horizontal lines on the left side of dashed line. We think the reason is that the shock waves happen outside the valve or the control volume, thus the downstream pressure has no influence on the fluid inside the valve, so that the force remain constant. This is not a big concern, because the bigger the plug lift is, the higher the pressure ratio. In real turbine, it is unlikely that the shock waves happen outside of the valve. At higher plug lift, the drag still has linear relation with the pressure ratio between the dashed and dotted lines. The slopes at different plug lift are almost same. This proved our equation (2.41). One thing needs to be mentioned that the pressure ratio scale during which curve show linearity is decreasing as the plug travels to its maximum lift position. At two times of wide-open lift, there is no such relation anymore.

Drag-plug travel characteristic

Not only with pressure ratio and geometry difference, the drag changes also with plug lift as shown in Fig. 2.7c. The solid lines are characteristic cures with fixed pressure ratio. Normally lift position changing affects the total pressure ratio, even it is one out of eight valves. If the valve affects pressure ratio from 0.9 (closed position) to maximum lift position, the drag-plug travel characteristic will look like the dashed line.

According to equation (2.37), if valve inlet and outlet total pressures are fixed, only second and fifth terms determine the drag. In valve opening process, we know from one-dimensional analysis the average pressure increases, so does the absolute value of second term. When the valve starts open, the mass flow rate and average z-direction velocity component increase quickly, then the mass flow rate slows down when plug lift reaches

the governi

So the fifth

its flat incre

each other, s

Fig. 2.7c, th

To unders

maximum lif

fifth term in e

position, the

is 45° with z-

$$D_{max} = P_{01}$$

Where $\dot{m}_{}$

equation (2.1

For maxim

becomes a sta

and drag numb

the governing point as shown in Fig. 2.4 and becomes constant after wide-open position. So the fifth term starts as a sharp increasing, then after about wide-open position, enters its flat increasing region. Because the force caused by the two terms are opposite with each other, so the combination effect results in the drag-travel characteristic as shown in Fig. 2.7c, the drag increase before the wide-open position then drops quickly.

To understand the characteristic, drags at wide-open position (maximum drag) and at maximum lift position (minimum drag) should be obtained. To get maximum drag, the fifth term in equation (2.38) can be simplified by using flow properties at throat. At that position, the valve throat area equals the seat throat area. Also we assume the jet direction is 45° with z-direction. Therefore, the equation (2.38) and (2.39) can be changed to

$$D_{\max} = P_{01}\pi\left(R^2 - r^2\right) - \frac{\pi}{6}\left(P_{01} + P_{th} + P_{02}\right)\left(R^2 - R_0^2\right) - P_{02}\pi R_0^2 + \frac{\sqrt{2}\dot{m}_{\max}^2}{2\pi\rho_{th}R_0^2} \quad (2.38a)$$

$$D_{h\max} = \frac{D_{\max}}{\pi R^2 P_{01}} \quad (2.39a)$$

Where $\dot{m}_{\max}$ is maximum mass flow rate at wide-open position, can be obtained by equation (2.11) for subsonic or (2.12) for supersonic.

For maximum lift position, we assume the plug is too far away from seat, so this becomes a static fluid problem. Define a control volume as shown in Fig. 2.6b. The drag and drag number are simply

$$D_{\min} = -P_{01}\pi r^2 \quad (2.38c)$$

$$D_{h\min} = -\lambda \quad (2.39c)$$

We do n

showing th

open positi

Where Li

almost close

open position

From wide

between them

D_{hmin} to get t

2.2.2 One-di

As discuss

are symmetri

dimensions.

2.8. lift oscil

Some reports

value of lift c

severe vibrat

mechanisms

Instability of

We do not have enough data to develop an empirical equation, but there are some data showing there is approximately linear relation between drag and plug lift, so before wide open position, the relation can be expressed as

$$D_h = D_{alc} + \frac{Li - Li_{alc}}{1 - Li_{alc}}\left(D_{h\max} - D_{halc}\right) \tag{2.40}$$

Where Li is the ratio of plug lift with wide-open position lift. The subscript, alc, means almost closed position. The equation can be only used from fully closed position to wide-open position.

From wide-open position to maximum lift position drag, there seems no good linearity between them. For guessing, we still can use the linear interpolation between D_{hmax} and D_{hmin} to get the drag.

2.2.2 One-dimensional analysis on unsteady hydraulic forces acting on plug

As discussed before, the lift acting on plug is zero if the geometry and flow patterns are symmetric. The drag is a function of pressure ratio, plug lift and geometry dimensions. In real cases, both drag and lift are also functions of time as shown in Fig. 2.8, lift oscillates around 0 while drag around a number we can get by analysis of 2.2.1. Some reports show that the peak-to-peak value of drag can reaches to 1,000 lbs, while the value of lift can reaches to 3,200 lbs. This oscillation is very dangerous, it can results in severe vibration of plug and potential failure of valve. Here we will discuss the major mechanisms that cause oscillation of hydraulic forces

Instability of highly turbulence flow

Accordin

as pressure

to time and

Where, $\overline{P}$

The pressur

as shown in Fi

drag and lift m

Fig. 2.9b and

which inverse

Influence of S

Separation

when flow is s

shown. They a

According to fluid turbulence theory, all the instantaneous continuum properties, such as pressure and velocity, fluctuate rapidly and randomly about a mean value with respect to time and spatial direction. Thus the pressure can be express as

$$P(x,t) = \overline{P}(x) + P(x,t)' \tag{2.45}$$

Where, $\overline{P}(x) = \frac{1}{\Delta t}\int_{t_0}^{t_0+\Delta t} P(x,t)dt$, is time average pressure at a fixed point x.

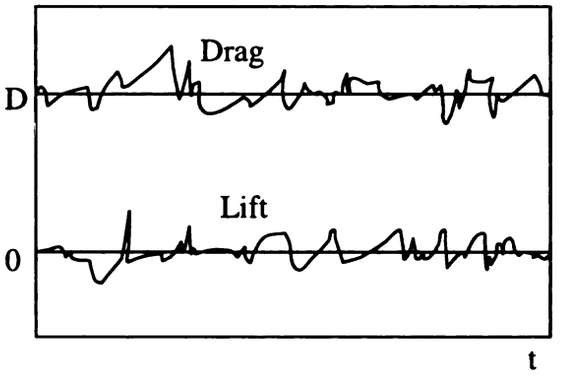

Fig. 2.8 Unsteady hydraulic forces

The pressure along upstream, downstream, and valve surface at one instant fluctuates as shown in Fig. 2.9a. If integrating the pressure on both left and right sides, the pressure drag and lift may become asymmetric in both magnitude and acting points as shown in Fig. 2.9b and moment can be generated at this instant. This will start the plug vibration, which inverse makes more pressure fluctuations.

Influence of Separation and shock instability on drag and lift

Separation occurs when flow met an adverse pressure gradient, while shock occurs when flow is supersonic and the back pressure is different with some special value, P^{**} as shown. They are different fluid phenomena's. But for this case, two characteristics are in

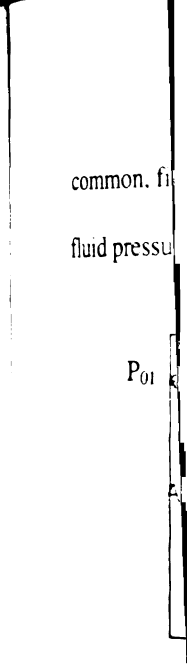

Ideally, th
central line o
vibration, the
earlier in righ
remain almos
the average p
left side is le
side is higher
Of course, in
right side, or
separation ha
annular direc
of shock or s
or with a freq

common, first they both occur in valve diffusion region or after valve throat; second, fluid pressure jump suddenly after shock or separation points as shown in Fig. 2.10a.

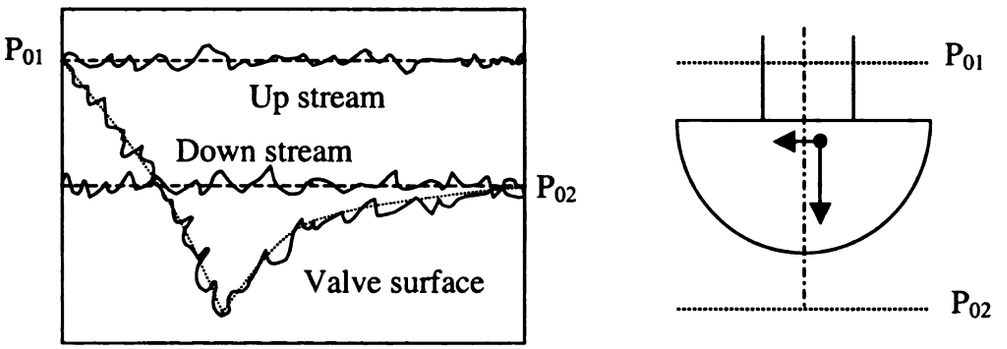

a. Pressure distribution b. Forces

Fig. 2.9 Pressure distribution and resulting forces at one instant

Ideally, the separation point and shock wave point should be symmetric with the central line of valve. Due to instability of high velocity compressible flow or structure vibration, the points become asymmetric, let's say, both separation and shock happen earlier in right side than in left side. If we assume that the pressure after separation remain almost constant, we can get same conclusion both for shock and separation that the average pressure on left side is less than right side. That means the pressure drag on left side is less and the pressure lift is more than right side. The force acting point on left side is higher and further from central line than right side. These also cause momentum. Of course, in next instant, the shock and separation may happen earlier in left side than right side, or separation earlier in one side while shock later, or in subsonic flow only separation happens. To actual three-dimensional flow, the changing also occurs in annular direction. The pressure force magnitude and acting position changes in response of shock or separation instability. The hydraulic forces can repeat the changing randomly or with a frequency depend on flow conditions. The plug will be harmonically excited, if

this frequen

valve. This

P_{01}

P*

F

D/L

0

a

Fig. 2.

Separatio

We discusse

drag/lift. Th

area ratio as

increases as

this frequency is close to plug natural frequency. Severe vibration will be experienced by valve. This situation should be avoid.

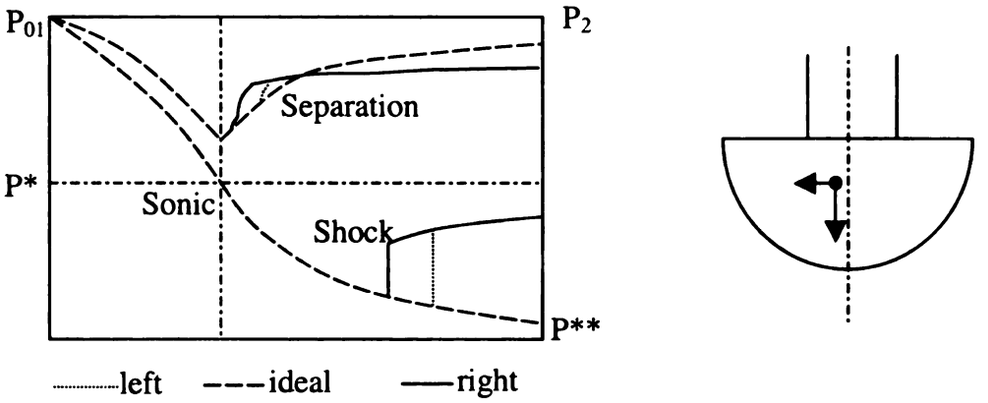

a. Pressure distribution b. Pressure Forces

Fig. 2.10 Pressure and forces at one instant with shock or separation

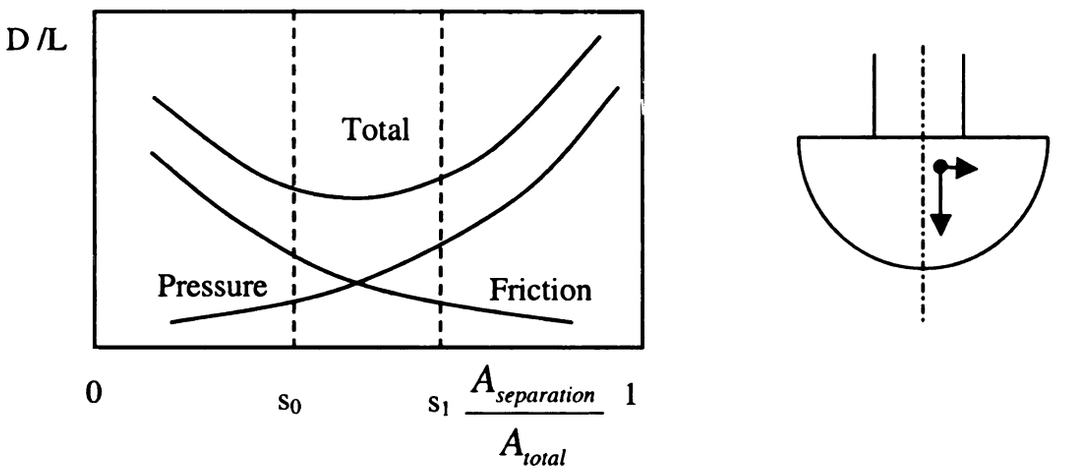

a. Drag/lift changing with area ratio b. Friction forces

Fig. 2.11 Pressure-friction drag/lift relation and friction forces due to separation

Separation has influence not only on pressure drag/lift, but also on friction drag/lift. We discussed that total drag/lift is summation of pressure drag/lift and skin friction drag/lift. The drag/lift can be expressed as function of separation area to total semi-sphere area ratio as shown in Fig. 2.11a. The pressure drag/lift decreases while friction drag/lift increases as the area ratio increases. This is because the friction mainly occurs in

boundary l

pressure dr

To discu

happens ear

drag/lift will

friction drag

According

ratio less tha

has same tren

more than s_1

The region be

drag/lift rema

results in the u

will results in

separation has

Unsteady jets a

After separa

subsonic or sup

most cases nor

becomes stable

succession of o

together results

also causes pres

boundary layer attached area, the more area in separation, the less friction. While for pressure drag, the more separation, the more the drag is.

To discuss the separation influence on friction drag, we also assume that separation happens earlier in right side than in left side. Due to the reverse trend, the friction drag/lift will have exactly opposite way with the pressure drag/lift. The forces due to friction drag/lift difference will have opposite trend as shown in Fig. 2.11 b.

According to total D/L curve, three domains can be defined. The domain with area ratio less than s_0 is called friction dominant region, in which the total drag/lift changing has same trend with friction drag/lift changing with area ratio. The domain with area ratio more than s_1 is called pressure dominant region, in which pressure drag/lift dominates. The region between dashed lines is called separation insensitive region, in which total drag/lift remains almost constant. So in pressure dominant region, separation instability results in the unbalanced force pattern like Fig. 2.10b, and in friction dominant domain, it will results in the force pattern like Fig. 2.11b. In separation insensitive region, the separation has no effect on valve.

Unsteady jets and vortex

After separating from both seat and plug, the flow can be idealized as free jet, either subsonic or supersonic. The shock we discuss before is normal shock wave. We think in most cases normal shock waves happen if the flow is supersonic and after that flow becomes stable free subsonic jet. There is still possibility that the jet is supersonic with a succession of oblique expansions and shocks or possible conical waves, which combined together results in the basic characteristic of supersonic jet, instability. The instability also causes pressure fluctuation resulting in unbalanced forces as shown in Fig. 2.8b.

Actual fl

shown in F

asymmetri

generated d

side to side

the plug nat

Expansi

We belie

side and sea

separation.

and mass fl

plug is later

shown in F

causes lift.

Vortex c

big velocit

Actual flow is constrained by seat wall and encountering with the jet from other side as shown in Fig. 2.12. Also it is three –dimensional. The annular jet flow may become asymmetric, thus the flow leave valve with x and y-direction velocity component. Lift is generated during this process. This asymmetry can change in annular way or simply from side to side and can be random or with a frequency. If the frequency equals or is close to the plug natural frequency, resonance will happen, great vibration altitude will occur.

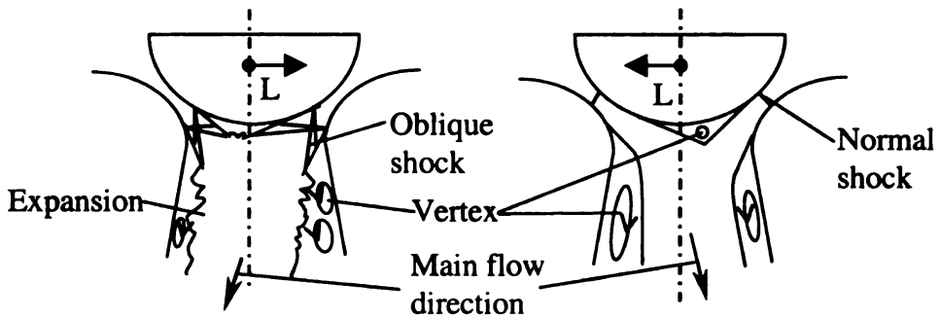

a. Supersonic jet b. Subsonic jet

Fig. 2.12 Asymmetric jet flow after valve throat

We believe that the jet instability is the result of instability of separations on both plug side and seat side. The separation we discussed before just focus on the plug side separation. We assume the valve geometry is symmetric, so does velocity distribution, and mass flow rate is same. According to continuity, if the flow separation on left side of plug is later than right side, the flow separation on the left side of seat will be earlier. As shown in Fig. 2.10b, the main flow velocity has momentum normal to z-direction which causes lift.

Vortex occurs in the separation region as shown in Fig. 2.12, because jet flow causes big velocity gradient. The 3-D flow is too complex to have regular vortex arrangement

like vorte

structure.

Other mech

There are

such as ups

secondary f

these have

act as key r

2.3 Analys

Normall

or simply f

induced vi

structure a

internal flo

flow patte

structure v

of flow-in

induced vi

strengther

due to the

about self

like vortex wake. The irregular arrangement of vortex still has random impulses on structure.

Other mechanisms

There are also other possible flow mechanisms counting for the unbalanced forces, such as upstream flow instability, upstream vortex direct impingement on plug, and secondary flow in jet region. We believe that compared with above three mechanisms, these have much less influence on plug. They may behave like vibration trigger, but not act as key roles to maintain or strengthen the plug vibration.

2.3 Analysis on Fluid Structure Interaction

Normally, fluid structure interaction means flow instability caused structure vibration, or simply flow-induced vibration. For a pure flow-induced problem, like the wind-induced vibration of bridges, the interaction is one way, from flow to structure while the structure almost has no influence on flow. For this valve problem, because it is an internal flow passing an immersed body, the structure vibration has strong influence on flow pattern and instability. The structure vibration caused by flow instability due to structure vibration is called self-excited vibration. So the plug vibration is a combination of flow-induced vibration and self-induced vibration. We think in this problem, flow-induced vibration plays major role, while self-induced vibration is auxiliary to either strengthen or weaken the vibration. In this part, we will analysis how the plug vibrates due to the flow instability mechanisms discussed in 2.2, meanwhile, do some analysis about self-induced excitations.

2.3.1 Flow

Flow-in

induced vi

We dis

result in h

the valve p

and down

associated

resonance

For loca

forces cau

interactio

induced v

on the flo

research v

more gen

Based o

moment a

directions

system, z_1

two coord

plug leng

2.3.1 Flow-induced vibration

Flow-induced vibration can generally be divided into two categories: local flow induced vibration and piping system-induced vibration.

We discussed the mechanisms that cause unsteady hydraulic forces on plug and finally result in hydraulic induced vibrations. All these forces are extended by the flow around the valve plug. This kind of vibration is called local flow induced vibration. The valve and down stream pipe form a piping system. The vibration in response of mechanism associated with the system is called system-induced vibration. Most known is acoustic resonance in valve piping system.

For local flow induced vibration, the mechanism is like direct feedback. The unsteady forces cause plug vibration and vice verse. The research focuses on valve and local flow interaction. The vibration is normally random. While mechanism of acoustic resonance induced vibration is like a feedback loop as shown in Fig. 2.11. The research is focused on the flow valve piping system. The plug will vibrate with one dominant frequency. Our research will focus on local flow induced vibration, because we think this mechanism is more general and basic.

Based on one dimensional hydraulic force analysis, three dimensional forces and moment acting on plug at t instant are shown in Fig. 2.13. Thus vibrations in three directions, axial, lateral and spinning, are generated. For convenience, another coordinate system, z_l-α-β, is defined from the plug stem beginning position. The relation between two coordinates at t instant is: $\vec{z}_l = \vec{z} + \vec{l}(t)$, where l(t) is the stem length at t instant, the plug length without stress is l_0.


L(t)

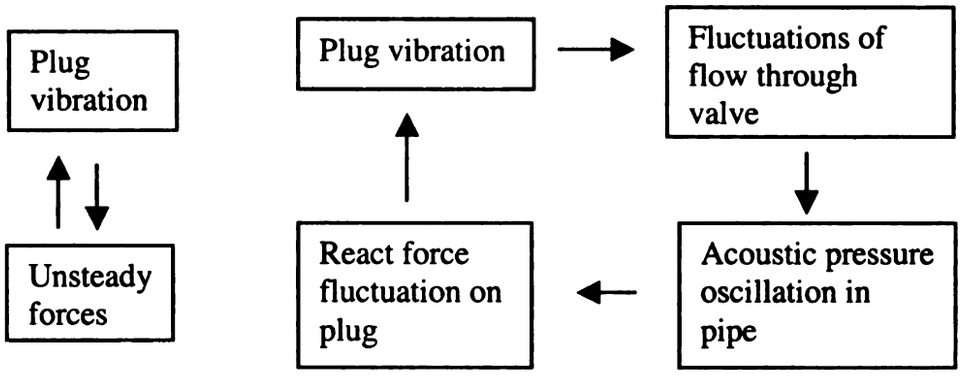

a. Local flow induced vibration

b. Acoustic resonance

Fig. 2.13 Flow induced vibration mechanism

Assumptions

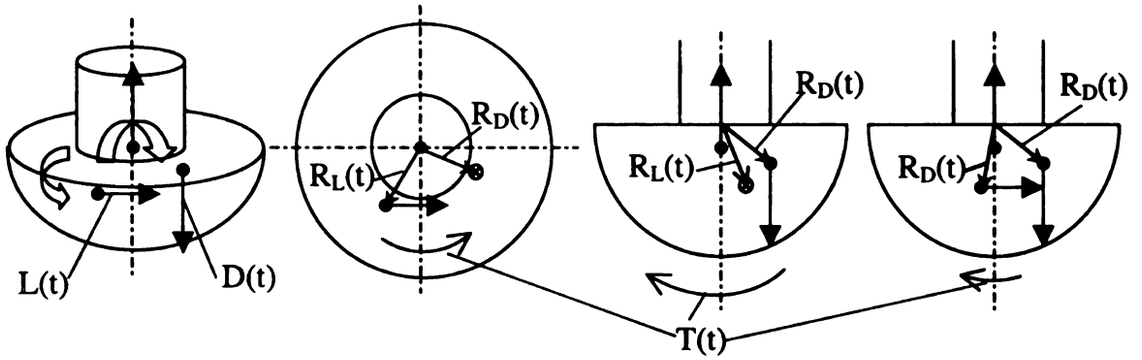

a. 3-D view b. Up view c. Side view c. Front view

Fig. 2.14 3-D view of unbalanced forces

Flow induced vibration can be modeled as a second-order mass-spring-damping system in response to hydraulic force excitation as shown in Fig. 2.14. We do not deal with the vibration due to lift changing or control induced vibration. From Fig. 1.2, the valve plug is mounted on a beam to be operated. The whole multiple-valve vibrates as a whole structure. The beam vibrates due to vibration from all the valves and pressure oscillation around it as a continuous system serving as a base excitement for single valve. Because the beam is much stronger than plug stem, from practice, in most cases, the

beam expe

remains st

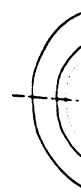

a. A

In reality,

vibration go

the vibration

know in real

the "severe"

um. That me

hydraulic for

Axial vibrati

beam experiences much less vibrations. Due to above reasons, we assume that the beam remains stationary, which means z_l-α-β coordinate remains stationary.

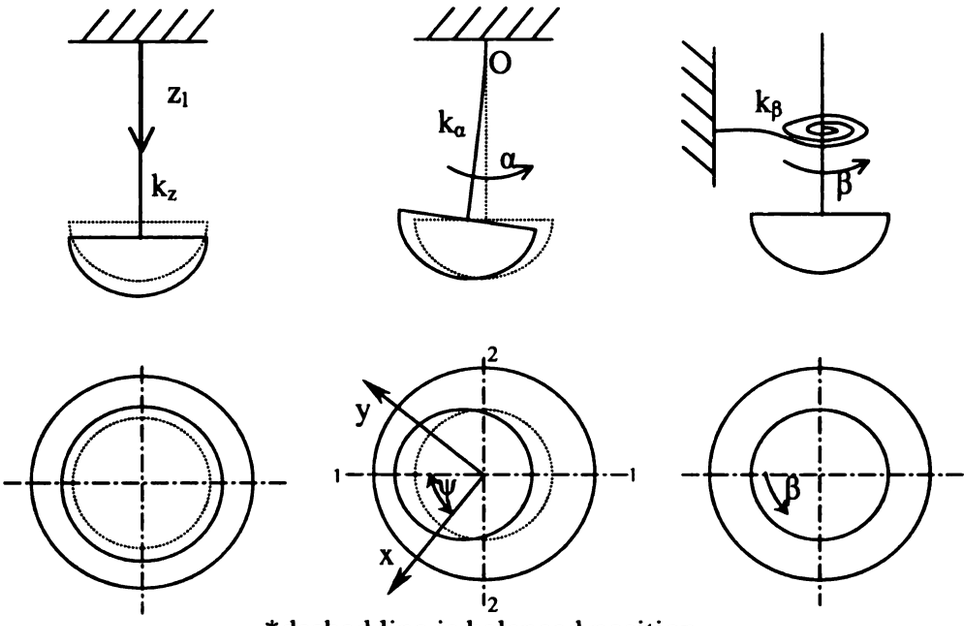

*dashed line is balanced position

a. Axial vibration b. Lateral vibration c. Spinning vibration

Fig. 2.15 Plug vibrations due to unbalanced forces

In reality, the three direction vibrations occur simultaneously. This make the three vibration governing equations coupled by nonlinear terms. So another assumption is that the vibrations are not influenced with each other, they can be treated separately. We know in real situation, the vibrations in three directions are not very big. In some report, the "severe" vibration, which causes valve failure, can only reach amplitude of 100-400 μm. That means we can get a decent result with such an assumption. Compared with the hydraulic forces, body force is too small. Thus plug and stem body force is ignored.

Axial vibration

The plug

vibration i

in z-directi

The firs

the mass o

The sec

structural

Damping

damping f

energy los

which car

vibration,

viscous da

to be the r

The thir

for stem. T

in stem stre

The plug can be treated as a point mass attached at the end of mass less shaft. The axial vibration is due to the unsteady drag. By using Newton second law, the motion equation in z-direction is derived as:

$$m_{eq}\frac{d^2l(t)}{dt^2}+c\frac{dl(t)}{dt}+k_z\left(l(t)-l_0\right)-D(t)=0 \tag{2.45}$$

The first term is inertia force. The plug equivalent mass can be obtained by integrating the mass of plug and stem.

The second term is damping force mainly from stem internal friction, which is called structural damping, and friction from fluid, which can be treated as viscous damping. Damping factor c thus is summation of structural damping factor, cs, and viscous damping factor, c_v. For harmonic vibration, $c_s=\frac{\Delta E_{cyc}}{X^2\pi\omega_s}$. $\frac{\Delta E_{cyc}}{X^2}$ is the ratio of energy loss per cycle to the square of displacement amplitude. It is a property of material, which can be obtained from experiment. ω_s is plug vibration frequency; For random vibration, it is very difficult to get exact value of structural damping factor. In this case, viscous damping is also impossible to get from theory. The structure damping is believed to be the major damping in this case.

The third term is spring force. $k_z=\frac{Em_s}{\rho l(t)^2}$ is equivalent spring constant or stiffness for stem. The stem density ρ is treated as constant. E is Young's modulus. The stiffness in stem stretching process is less than in depressing process. This term is nonlinear.

D(t) is t

plug vibra

position to

which mea

drag increa

excitation t

weaken the

$$\omega_{\pi} = \sqrt{}$$

Lateral vi

In later

point mas

position,

amplitude

to elimina

equation c

First ter

from mainl

term comes

D(t) is the drag on plug at t instant. Drag is unpredictable due to flow instability. The plug vibration also has influence on drag. When the plug is stretched from the balanced position to positive deviation as shown in Fig. 2.15a, the valve throat area decreases, which means pressure loss increases and downstream total pressure decreases. Thus the drag increases during this process. Combined with decreasing of stiffness, this self-excitation tends to strengthen the axial vibration when plug has positive deviation and weaken the axial vibration when the plug deviation is negative. The natural frequency is

$$\omega_{zn} = \sqrt{\frac{k_z}{m_{eq}}}$$

Lateral vibration

In lateral direction, the vibration can be idealized as a mass less cantilever with end point mass. The vibration is due to the moment of forces around the fixed stem holding position, O. When we analysis moment, the geometry of plug is considered. For small amplitude oscillation, which is true in practice, we approximate sinα by α, and cosα by 1 to eliminate nonlinear terms. By using equation (1.2) in vibration direction, the motion equation can be

$$m_{\alpha eq} l^2 \frac{d^2\alpha}{dt^2} + c_\alpha l \frac{d\alpha}{dt} + k_\alpha \alpha d^2 = M(t) \qquad (2.46)$$

First term is inertia moment of plug with equivalent mass; Second term is the moment from mainly structural internal and flow friction damping with damping factor, c_α. Third term comes from spring force of stem. Spring stiffness, $k_\alpha = \frac{3EI_s}{l^3}$, can be treated as

constant, $\bar{v}$

The natura

$\bar{M}(t)$ i

defines the

important

unstable. S

model.

The thro

2.16a, whe

left throat

Different f

based on o

constant, while I_s is the polar moment of inertial of the cross-sectional area of the shaft.

The natural frequency is $\omega_{on} = \sqrt{\frac{k_\alpha}{M_{eq}}}$.

$$\vec{M}(t) = \vec{D}(t) \times \left(\vec{R}_D(t)\right) + \vec{L}(t) \times \left((\vec{l} + \vec{R}_L(t)) \bullet \vec{z}\right)\vec{z} \qquad (2.47)$$

$\vec{M}(t)$ is the momentum due to hydraulic drag and lift. Its direction, ψ with x-axis, defines the vibration direction and its amplitude, M(t), affects the vibration. So it is very important to determine this term. It is very difficult because all the terms in equation are unstable. Some qualitatively analysis must to be done to simplify the lateral vibration model.

The throat area of valve shown in Fig 2.15b becomes asymmetric as shown in Fig. 2.16a, when plug starts vibration. For example, at t moment, it is moving to left side, the left throat area is less than right side. Thus the pressure distribution becomes asymmetric Different flow situation causes different pressure distribution along the valve surface, based on one-dimensional analysis.

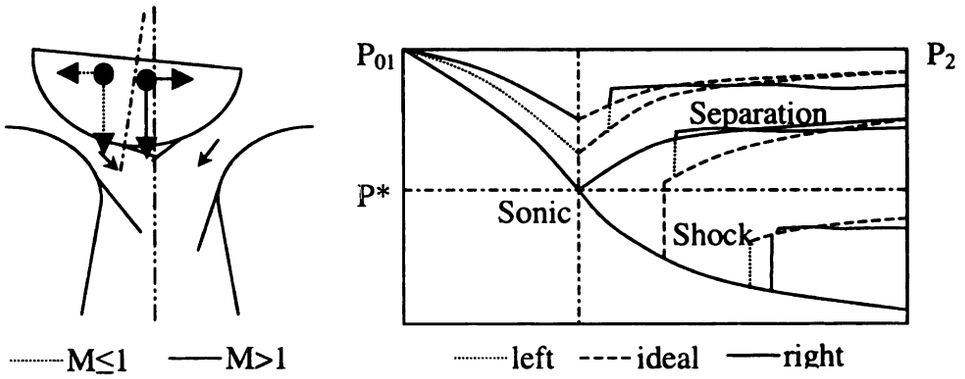

a. Vibration and forces b. Asymmetric pressure distribution

Fig. 2.16 Pressure distribution and forced in response of vibration

For son

of valve is

possibility

big pressu

left side is

acting pos

moving to

moment

moment

Normally

less than

before, th

moment

In case

more dif

total drag

solid arro

each othe

moment

will expe

Of cour

like turbul

as above d

For sonic or subsonic flow, the integration of fluid pressure (doted line) along left side of valve is less than right side (solid line) when flow is subsonic. There is also another possibility that left side is supersonic while left side is sonic or subsonic, which causes big pressure difference as shown in Fig. 2.16b. Under both situations, the lift and drag in left side is less than right side. Thus the overall lift points to left and the overall drag acting position moving to left shown in dotted arrow in Fig. 2.16a. As plug continues moving to left, both lift and drag acting point deviation becomes bigger. Thus the moment of lift pushes the plug further left side to strengthen the vibration while the moment of hydraulic force pushes the plug to its balanced position to stabilize the plug. Normally, the drag is much bigger than lift. So even its acting distance around O is much less than lift, we still think it can play a big role in valve stability. As we discussed before, the drag goes down to zero or a value not strong enough to overcome the lift moment at some open position. The plug will experience severe vibration.

In case of supersonic flow, shock waves in right side occur earlier than left side due to more diffusion in left side. Thus left side average pressure is higher than right side. The total drag and lift will behave in opposite way to subsonic flow situation as shown in solid arrows in Fig. 2.16a. The moment of drag is minimized as two trend encounter with each other, the plug move to left while the drag acting point moving to right. This is lift moment dominant region. As the lift moment tries to stabilize the plug, we think the plug will experience a high frequency low amplitude vibration compared with sonic flow.

Of course, the plug vibration also has strong influence on other instability mechanism, like turbulence, separation, and jets. But the way is quite unpredictable or not as regular as above discussion. For turbulence, this is always a random excitement mechanism to

plug vibra

boundary

gradient a

separates a

side the flo

flow has m

Based o

situation.

to drag an

For sup

Spinning

In β di

mass less

Fig. 2.15

The firs

around th

and skin f

plug vibration. For separation, adverse pressure gradient and flow kinetic energy in boundary layer determine the separation area. In diverging region, both the pressure gradient and kinetic energy of flow are larger than right side. So we just assume the flow separates at almost same place in both sides with oscillation. For jets, because even in left side the flow velocity is bigger and the mass flow rate is less. Thus we assume that the flow has moment oscillating around a same value in both sides.

Based on above analysis, the moment term can be simplified according to flow situation. For sonic flow, the moment direction is combination direction of moment due to drag and lift, the amplitude is:

$$M(t) = \left(\alpha D(t) + L(t)\right)l \tag{2.49}$$

For supersonic flow, the lift defined the vibration direction, the moment of lift is:

$$M(t) = L(t)l \tag{2.50}$$

Spinning vibration

In β direction, the valve also experiences vibration, like a disk attached at the end of a mass less shaft, as shown in Fig. 2.13c, in response of torque caused by lift as shown in Fig. 2.15c. The motion equation can be derived as

$$J_{eq}\frac{d^2\beta}{dt^2} + c_\beta \frac{d\alpha}{dt} + k_\beta \beta = T_L(t) \tag{2.51}$$

The first term is inertia term. J_{eq} is equivalent moment of inertia of the stem and plug around the center point of semi-sphere. Second term is damping moment due to internal and skin friction. c_β is equivalent damping factor. The third term is moment of spring

force. k_j

term is to

$\omega_{\beta n} =$

The spin

less due to

axial vibrat

plane as sh

with same

direction. S

direction is

angle ψ to

a. Rot
vib

Relation bet

force. $k_\beta = \frac{GI_s}{l}$ is equivalent torsion stiffness, while G is the shear modulus. The last term is torque of lift, $T_L(t) = L(t)(\vec{R}_L(t) \times \vec{z})$. The natural frequency is

$$\omega_{\beta n} = \sqrt{\frac{k_\beta}{J_{eq}}}.$$

The spinning vibration is believed as the weakest vibration because the torque is much less due to little acting distance of lift. But it is still believed to be more dangerous than axial vibration, because it cause the lateral vibration keeping changing directions in x-y plane as shown in Fig. 2.17a. Assume, at t instant, the lift acts on plug as dashed arrow with same direction as +x. If drag moment is ignored, the plug lateral vibration is in x-direction. Some moment later, due to the spinning vibration in β direction, the lift force direction is rotated ψ anti-clock wise. Thus the lateral vibration changes direction with an angle ψ to x-axis. Also, the rotation can cause rotation of asymmetric jet.

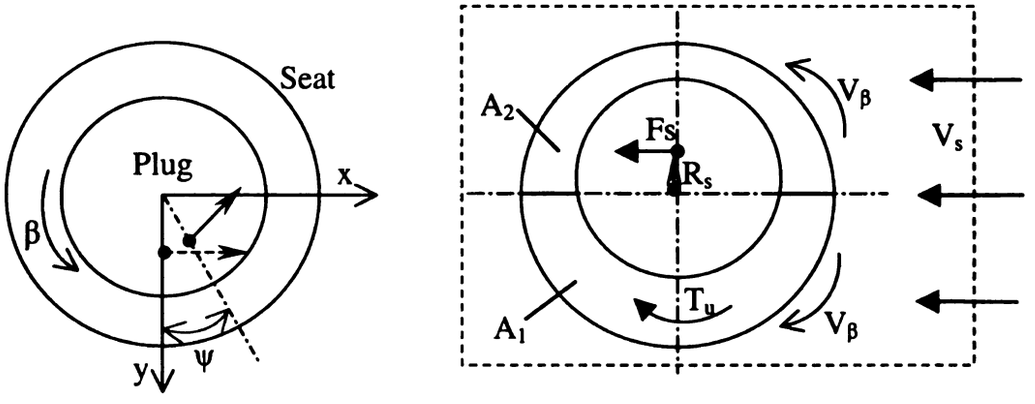

a. Rotation changes lateral vibration direction

b. Lateral vibration influence on spinning vibration

Fig. 2.17 Interaction of lateral and spinning flow

Relation between flow-induced excitation and self-excitation

As sho

direction

causes tan

applying

By assu

into the va

by using r

Now if

flow insta

finally ca

instability

mechanis

If we a

with time

section. A

(2.52a) ca

As shown in Fig. 1.2, the steam flow normally enter the chest mounted valves with the direction normal to valve plug. Assume the velocity, V_s as shown in Fig. 2.5b. Thus causes tangential velocity, V_β. Flow enters the valve with z-direction velocity, V. By applying Momentum equation in β-direction, we can get torque acting on plug

$$T_u = \rho\left[\int_{A_1} VV_\beta dA - \int_{A_2} VV_\beta dA\right] \tag{2.52a}$$

By assuming all the flow enter the control volume (dashed rectangle) at right side goes into the valve and no flow exit and enter at left side, we can get the force acting on plug by using momentum equation in x-direction

$$F_s = \dot{m}V_s \tag{2.53a}$$

Now if we assume, the plug is at this balanced position, eccentric with seat. Due to flow instability, the velocity in three directions and oscillating mass flow rate, which finally cause unbalanced force and torque. This mechanism is called upstream flow instability. It is a kind of flow-induced excitation, but as we mentioned in 2.2, this mechanism is not a key role in flow-induced vibration.

If we assume the plug is vibrating, and the velocity of three directions are constant with time changing; V_β is symmetrically distributed; The V is uniform in this cross section. At t moment when the plug moves to –y-direction with angle α, the equation (2.52a) can be reduced to

$$T_u = \rho VV_\beta\left(A_1 - A_2\right) \tag{2.52b}$$

Also d

effect on

This is

have effec

mechanism

Valve opti

Based o

strong vib

of drag ac

optimizin

frequentl

lateral an

asymmetr

the valve

We are

on vibrati

and struct

2.3.2 Ran

The equ

equations

can be obta

Also due to eccentric, the force in equation (2.53a) excites a moment, which can have effect on spinning vibration and direction changing of lateral vibration.

$$M_s = F_s R_s = \dot{m} V_s l \tag{2.53b}$$

This is a typical self-excitation mechanism. The actual situation is both mechanisms have effect on plug vibration. The above example is just to show how these two mechanisms interact with each other and contribute to plug vibration.

Valve optimum design

Based on above analysis, the valve should be designed following some rules to avoid strong vibration. We believe that the severe axial vibration occurs when large amplitude of drag acts on valve. When designing a valve, it is recommended to use equation (2.40) optimizing valve geometry to minimize the drag at that point to about zero at the valve frequently opening postion. This can great reduces the axial vibration amplitude. For lateral and spinning vibration, the basic rule is to reduce the flow instability or asymmetry, which is defined by the plug and seat shapes. So it is important to optimize the valve shape to guide the flow in a symmetric way.

We are not concentrate on material properties of plug. But according to above analysis on vibrations of three directions, materials with higher shear modulus, Young's modulus, and structural internal friction are preferred when design a valve plug.

2.3.2 Random model for random vibration

The equations of motion in three directions are obtained. So if the right side terms of equations or excitation terms, D(t), M(t), and $T_L(t)$ can be determined, the valve motions can be obtained. As we discussed before, because so many factors, like instability of

turbulenc

be predict

This kind

excitation

By using

Because th

can be l for

input term,

Where m_i c

damping rat

Thus we c

turbulence, separation or shock waves, affect the lift and drag, the excitation terms cannot be predicted or cannot be expressed as explicit time description as shown if Fig. 2.18. This kind of excitation is called random excitation. The response of a system to random excitation is called random vibration.

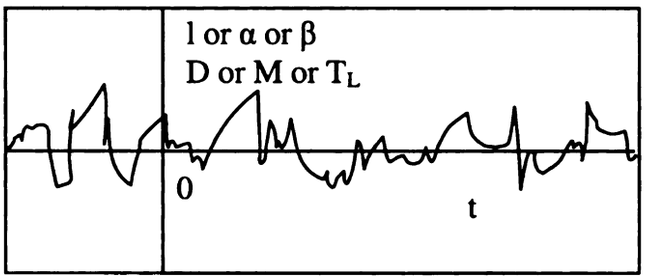

Fig. 2.18 Random phenomena

By using Fourier transform, the three motion equations can be transformed to

$$\hat{O}(\omega) = \hat{H}(\omega)\hat{I}(\omega) \tag{2.54}$$

Because they have similar form, so we write three equations as one. $\hat{O}(\omega)$ is output term, can be l for axial vibration, α for lateral vibration and β for spinning vibration; $\hat{I}(\omega)$ is input term, can be any of the three excitation, D, M and T_L.

$$\hat{H}(\omega) = \frac{1}{m_i\left(\omega_n^2 - \omega^2 + i2\zeta\omega\omega_n\right)} \tag{2.55}$$

Where m_i can be m_{eq}, $m_{eq}l^2$, or J_{eq}, depending on direction of vibration. $\zeta = \frac{c_i}{2\sqrt{k_i m_i}}$ is damping ratio.

Thus we can get the relation between input and output as

$$O(t) = \int_{-\infty}^{+\infty} I(t-\varpi)h(\varpi)d\varpi \tag{2.56}$$

Where

Relation

First, w

The me

Autoco

f, at two t

The me

associate

Power

time dom

If we k

Two im

Where $h(\varpi)$ is system response to a unit impulse.

Relation of mean value of input and response

First, we need introduce some basic conceptions in random vibration theory.

The mean value means time average value. For function f, the mean value is

$$\bar{f} = E(f) = \lim_{t\to\infty}\frac{1}{t}\int_0^t f(t)dt \tag{2.57}$$

Autocorrelation is the mean value of products of the instantaneous values of function, f, at two times t=t and t=t+τ.

$$R_f(\tau) = E[f(t)f(t+\tau)] \tag{2.58}$$

The mean squared value is a random variable provides a measure of the energy associated with the function.

$$\bar{f}^2 = E[f^2] = R_f(0) = \lim_{t\to\infty}\frac{1}{t}\int_0^t f^2(t)dt \tag{2.59}$$

Power spectral density (PSD) is variable concerning properties of a random variable in time domain. It shows the spectral distribution of average energy.

$$S_f(\omega) = \int_{-\infty}^{+\infty} R_f(\tau)e^{-i\omega\tau}d\tau \tag{2.60}$$

If we know the PSD, the autocorrelation can be obtained as

$$R_f(\tau) = \int_{-\infty}^{+\infty} S_f(\omega)e^{i\omega\tau}d\omega \tag{2.61}$$

Two important relations between excitation and response variable are

From b

value for

direction

PSD r

signal. A

unknow

excitati

the exp

Simplif

We

effect c

equatic

At d

$$\overline{O} = E\big(O(t)\big) = \hat{H}(0)E\big(I(t)\big) = \frac{\bar{I}}{k_i} \tag{2.62}$$

$$S_O(\omega) = S_I(\omega)\left|\hat{H}(\omega)\right|^2 \tag{2.63}$$

From basic physical knowledge about the valve vibration we can get that the mean value for Drag is D, while both moment and torque are zero. Thus the mean value in axial direction vibration is $\frac{D}{k_z}$ and is zero in both α and β direction vibrations.

PSD relation is still unknown because we do not know either the excitation or response signal. Also the value of $\left|\hat{H}(\omega)\right|^2$ cannot be obtained by theory, as damping factor is unknown. So experiment data is needed. As it is difficult to measure all information of excitation and response of three directions, a more simplified model is needed to direct the experiment.

Simplify excitation as dynamic pressure oscillation

We know the basic excitation is drag and lift for plug vibration. Ignoring the viscous effect on valve, we assume the total drag and lift equal pressure drag and lift. Discretizing equation with equal area in semi-sphere, we can get

$$D = P_{01}\hat{z} \bullet \vec{A}_{up} - \sum_{k=1}^{N} P_k \hat{z} \bullet \Delta\vec{A} \tag{2.64}$$

At direction $\vec{n}$, the lift is

$$L = \sum_{k=1}^{N} P_k \vec{n} \bullet \Delta\vec{A} \sin\theta_k \tag{2.65}$$

The pres

considered

random vi

and torqu

shown in

In abov

reflect up

instabilit

seat side.

points to

this mod

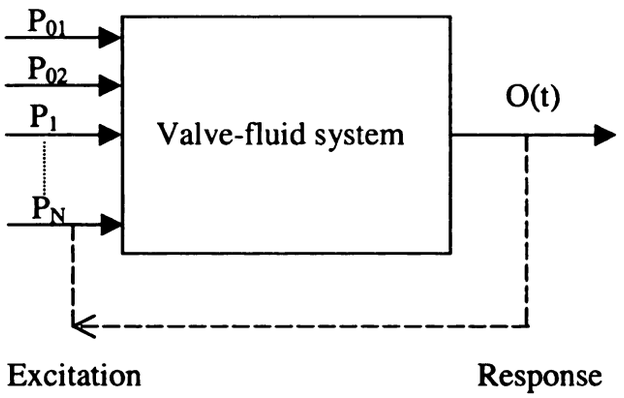

Fig. 2.19 Simplified excitation-response model for plug vibrations

The pressure is not been considered as a function of space domain. They were considered as N independent variables that influence the drag and lift resulting in plug random vibration. Thus we can get a simple model. Rather than consider force, moment and torque as input, we consider the pressure oscillation as plug system excitation, as shown in Fig. 2.16.

In above model, we consider pressure as basic excitation for the system. P_{01} and P_{02} reflect up and down stream turbulence instability, P_1 to P_N represent the turbulence instability of flow when passing through a valve. Some pressure points also are taken in seat side, we can get information of jet and vortex instability. Thus we use finite pressure points to represent integration of pressure along plug surface. This is the basic purpose of this model and basic theory of experiment.

3.1 Flow

Stall in diff

For diffu
separates fr
which is ca
boundary l
dimension
patterns w
L/W=5, w
range of l
develope
When di
jet flow
flow is
stall hap
pressur
valve a

All
proble
theory
is easi

CHAPTER 3

LITERATURE REVIEW

3.1 Flow Asymmetry and Instability

Stall in diffusion process

For diffusing flow in a divergent passage, stall or backflow happens as boundary layer separates from the wall. The boundary layer separation is due to the adverse pressure gradient, which is caused by pressure rise due to diffusion. Kline et al reviewed the topic of stall and boundary layer theory in 1956. In their study on diffusion process in straight-walled two-dimensional diffusers for incompressible flow, stall regimes were identified. Four typical flow patterns were found as shown in Fig. 3.1. For a fixed diffuser length and inlet width ratio, L/W=5, when flow is low turbulence, at small diffuser angle, no stall happens (Pattern a); In the range of larger angles, from 16° to 20°, large transitory stall zone was found (Pattern b); Fully developed steady stall (Pattern c) occurs in the range of 20° to 80°. This pattern is nearly steady; When diffuser angle is wider than 80°, flow separates from both sides and become nearly steady jet flow (Pattern d). The inlet flow condition has some effect on the flow patterns. But before the flow is choked in the inlet, the stall happens in a similar way. It was also pointed out that stall happens in a position where the wall curvature changes sharply or under a high adverse pressure gradient due to shock wave. This can be used to explain flow phenomena in venturi valve and to improve valve design.

All above analysis is about symmetric straight 2-D diffuser. Kline et al did not discuss the stall problem in a general asymmetric curved wall diffusion passage. Referring to boundary layer theory, we make an assumption here that the flow behaves like in a symmetric diffuser, but stall is easier to occur in the sharper curvature side due to larger adverse pressure gradient.

The val

analysis, th

valve. Thu

other with

nozzles.

a. F
wit

Based o

D. Zhang

developed

The valve can be treated as an annular of 3-D converging diverging nozzles. To simplify analysis, the valve is further idealized as 2-D infinite wall with same cross-section area as real valve. Thus the valve becomes a combination of two converging diverging nozzles facing each other with an angle. Here the major concern goes to the interaction of two converging diverging nozzles.

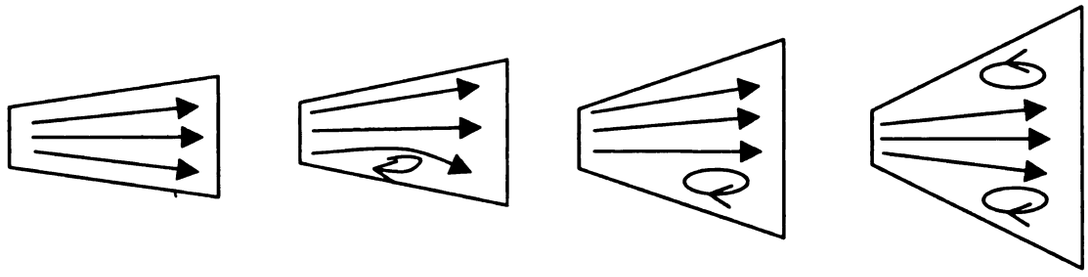

a. Flow without stall | b. Large Transitory stall | c.Fully developed steady stall | d. Jet flow

Fig. 3.1 Stall in diffuser

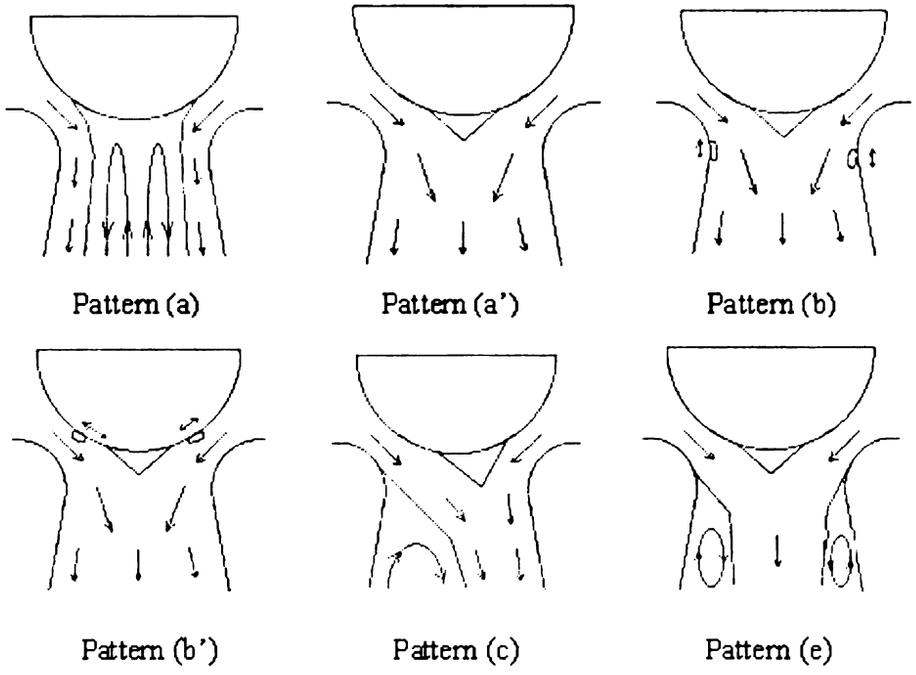

Fig. 3.2 Possible flow patterns due to stall in valve

Based on 1-D stall analysis, 6 basic flow patterns may possibly occur according to the paper of D. Zhang and A. Engeda. Pattern (a') occurs when there is no stall in both sides. When fully developed steady stall happens in plug side, pattern (a) occurs. When stall happens in plug side at

right and

unsteady.

in one side

also possib

High veloc

The ver

formed by

symmetri

the conve

and decre

flow is di

flow. flow

happen fo

(convergi

transonic

A. Sha

consideri

a region

velocity i

pressure

backside

shock wa

right and seat side at left, pattern (c) happens. Due to transitory stall, pattern (b) and (b') are unsteady, which may be symmetric or asymmetric (not shown in Fig. 3) with one stall near plug in one side and another stall near seat in the other side. Pattern (e) is caused by jet flow. There are also possible intermediate flow patterns not shown here either.

High velocity compressible flow theory

The venturi valve can be considered as an annular of converging diverging nozzles formed by plug surface and seat surface. In Chapter 2, one-dimensional theory for symmetric nozzle is summarized. The compressible flow is considered as isentropic. In the converging part of valve, the flow will be accelerated with increasing Mach number and decreasing static pressure. In diverging part, for subsonic flow, after valve throat, flow is diffused with decreasing velocity and increasing static pressure. For supersonic flow, flow will be continuing accelerated with decreasing static pressure. Shock may happen for supersonic flow. The transition flow changing from pure subsonic (converging and diverging) to pure subsonic-supersonic (converging-diverging) is called transonic flow. In one-dimensional theory, the transition is a process with continuities.

A. Shapiro explained the study done by Emmons about the transition process while considering two-dimensional effects. For pure subsonic flow, as the back pressure drops, a region of supersonic flow develops near the throat wall as shown in Fig. 3.3a. The flow velocity is sonic at the boundary of this region and main flow is subsonic. As the back pressure is reduced further, the supersonic region grows with shock wave happening at backside region as shown in Fig. 3.3b. Then two growing regions join together with shock waves happening in the plane of after the throat as shown in Fig. 3.3c. The

supersonic

and finally

Fig

supersonic region keep growing with the shock plane moving toward the exit of nozzle, and finally becomes pure subsonic-supersonic flow inside the nozzle.

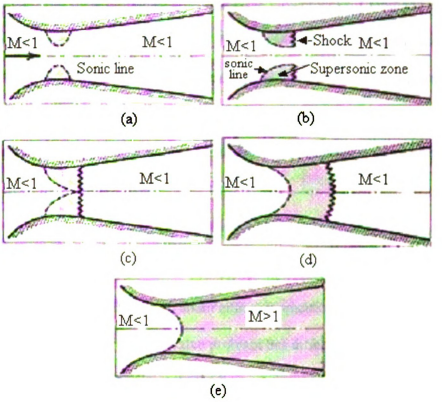

Fig. 3.3 2-D flow changing from subsonic to supersonic (after A. Shapiro)

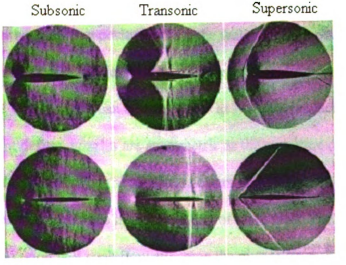

Fig. 3.4 Visualized transonic flow for airfoil (after Becker)

Becker

supersoni

flow is un

the interac

boundary

pulses in t

like airfoil

unstable fl

Fighting T

All abov

valve, whi

uniform ex

papers of

geometry

pressure g

separation

under a hi

cross sect

an angle.

sharper th

that press

seat side

two nozz

Becker visualized the flow patterns for airfoil as shown in Fig. 3.4. The subsonic and supersonic flow is stable. The boundary layer is thin and wake is small. But transonic flow is unstable with thick boundary layer and large violent wake. Liepmann et al studied the interaction between boundary layer and shock wave and pointed out the way boundary layer affect flow stability. Kuo investigated the flow instability due to pressure pulses in transonic flows. For the valve, the plug can be considered as immersed body like airfoil in wind tunnel. In our point of view, the transonic flow is one cause of unstable flow in the venturi valves.

Fighting Theory

All above theory can be very useful to understand the flow phenomena in a venturi valve, which is similar. But they were about either symmetric nozzle internal flow or uniform external flow of airfoil. The valve problem has different focus with them. In the papers of D. Zhang and A. Engeda, a theory is generalized by considering the valve geometry and basic fluid theories. According to boundary layer theory, the adverse pressure gradient in diffusion process can cause boundary layer separation. The separation normally happens in a position where the wall curvature changes sharply or under a high adverse pressure gradient due to shock waves. As mentioned before, the cross section of the venturi valve can be considered as two nozzles facing each other with an angle. For current design, nozzles are asymmetric as the curvature of seat side is sharper than that of plug side. Thus separation is easier to happen in seat side. We know that pressure in separation region is higher than that of main flow. The high pressure in seat side separation region will push flow attaching the plug surface. Because flows in two nozzles mirror each other, they will fight for the attachment of plug. As the result,

either flo

sides keep

the plug a

3.2 Fluid

It is nec

from them

when desi

actuator tr

Fig. 3.5

balanced p

compressi

direction b

drag decre

becoming

value. The

with our th

Chapter 2.

Fig. 3.5

shows stro

from 0 to

vibration c

plug will e

either flow in one side retreat to form a stable asymmetric flow pattern or flow on both sides keep fighting to form unstable flow patterns. In a real valve, the interaction between the plug and flow makes the flow more unstable.

3.2 Fluid Forces

It is necessary to understand fluid forces to minimize control valve problems arising from them. Drag is mostly concerned because it is very important factor to be considered when designing control valves. Thus how drag, or vertical force, changes with plug or actuator travel becomes a major topic in this field.

Fig. 3.5, given by Schuder, shows a typical plug force-travel characteristic curve for balanced plug travel process. The tension is essentially defined as positive drag. The compression force is defined as negative drag. At almost closed position, the drag is –z-direction by using same coordinate system as Chapter 2. Then as valve starts opening, the drag decreases almost linearly with the plug lift. At about 0.55in lift, it changes direction becoming positive drag. At about 0.7 inches lift, it reaches its maximum positive drag value. Then it changes its direction again and increases with the plug travel. It agrees with our theory analysis and force-travel characteristic by Moussa's computation data in Chapter 2.

Fig. 3.5a shows only steady state component of the drag. The actual experiment data shows strong oscillation in Fig. 3.5b. The time-varying drag has a fairly flat spectrum from 0 to 100 Hz. The peak-to-peak values exceed 1000 lbs. This can cause strong vibration of valve plug. If the plug axial direction natural frequency is at this range, the plug will experiences large amplitude vibration. This is quite possible, because normally

the plug s

is little re

It is no

drag osc

plug. sh

conclus

design a

linearly

the plug stiffness in any direction is large, while the plug equivalent mass or polar inertia is little resulting in small value of natural frequency.

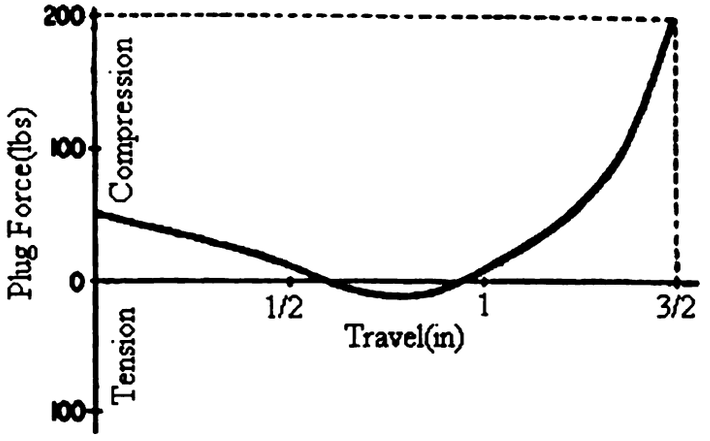

a. Steady state drag

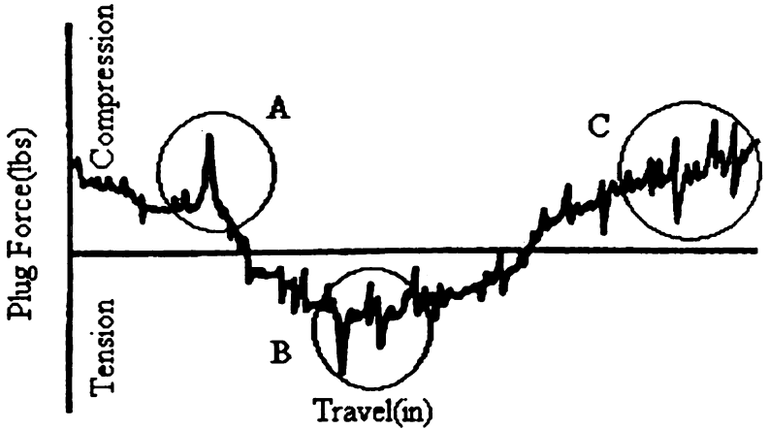

b. Drag oscillation

Fig. 3.5 Drag-plug travel characteristic (after Schuder)

It is not generalized by Schuder, but in our view by studying the Fig 3.5b, the large drag oscillation probably occurs at the places where there are large drag acting on the plug, shown as A, B, C at Fig. 3.5b. We do not have enough data to prove our conclusion. But at least, for this case, it is true. This is the one reason that it is better to design a valve with minimizing drag on it in Chapter 2. We know that the drag increases linearly with the pressure ratio decreasing. This point can also be proved by one

conclusi

across th

3.3 Flow

There

velocity

velocity.

3.3.1 Low

Excitation due to	
Excitation function of	
Cylindrical Structure	
Conduit Gate	

conclusion of Schuder, "buffeting forces are proportional to ΔP". ΔP is the pressure drop across the valve.

3.3 Flow-Induced Vibration

There are a lot of papers on flow-induced vibrations. Most of them are about low velocity incompressible flow. For turbine inlet valve, the flow is compressible with high velocity. But still some mechanisms are in common for them.

3.3.1 Low velocity incompressible flow-induced vibration

	EXTRON-EOUSLY INDUCED EXCITATION (EIE)	INSTABILITY INDUCED EXCITATION (IIE)			MOVEMENT INDUCED EXCITAT-ION (MIE)
		Excitation unaffected by oscillators Fluid-Dynamics	Excitation unaffected by fluid oscillators Fluid-Resonance	Excitation unaffected by body oscillators Body-Resonance	
Excitation due to	Flow pulsations not intrinsic to system	Flow instability	Flow instability controlled by		Self-excited movement of structure
			Fluid resonator	Body resonator	
Excitation function of	Flow conditions alone (not affected by structure dynamics)		Flow conditions + dynamics of		Fluid conditions +structure dynamics
			Fluid oscillator	Body oscillator	
Cylindrical Structure			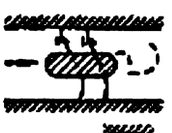	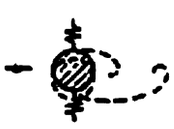	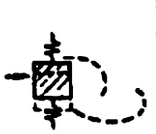
Conduit Gate	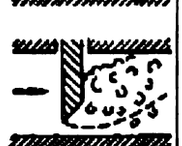		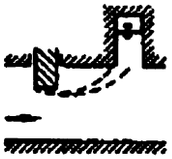		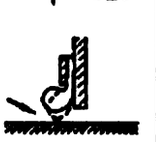

Fig. 3.6 Fluid excitation mechanisms (after Naudascher)

In 198

categorie

movemer

flow insta

structure.

Fig. 3.6.

Weaver

the flow-i

methods o

vibrations

also prove

induced vi

high energ

damping b

vibrations

effective v

possible s

3.3.2 Flo

In 198

vibration

study rev

instabilit

effective

In 1980, Naudascher classified the basic flow-induced excitation into three main categories, extraneously induced excitation (EIE), instability induced excitation (IIE), and movement induced excitation (MIE). EIE is caused by the flow pulsation; IIE is due to flow instability when passing a structure; MIE arises from movement of vibrating structure, or can be called self-excitation. Each category can be subdivided as shown in Fig. 3.6.

Weaver generalized jet flow-inertia mechanism, turbulence and acoustic resonance as the flow-induced excitation mechanisms for valves operated at small openings. Some methods of alleviation are given. The basic method to reduce jet flow-inertia type vibrations is to design valve in a way avoiding large closing force at small openings (this also proved our point that large drag can cause severe axial vibration); For turbulence induced vibrations, which caused by broad band random pressure or impingement with high energy levels in the lower frequency range, increasing the plug stiffness and damping becomes very important to reduce the vibrations, of course, this is true for vibrations due to any excitation. For Acoustic resonance induced vibration, the most effective way to reduce vibration is to design the valve-piping system with the widest possible separation between the valve natural frequency and acoustic frequencies of pipe.

3.3.2 Flow induced vibration for steam turbine inlet control valve

In 1980, Araki et al investigated the plug vibrations phenomena. A mathematic vibration model was built and a 1/3-scaled valve and an improved valve were tested. The study revealed that it was the random pressure fluctuation on valve surface due to flow instability that causes the plug vibration. Changing the valve geometry can be an effective method to reduce the vibration due to pressure oscillation.

Plug vibr

The pl

The vibr

600 to 3.

the high f

frequency

freedom v

By assu

Plug vibration models

The plug vibration at different opening is different due to the pressure drop difference. The vibration frequency of small valve opening (almost closed position) is in the range 600 to 3,500 Hz, while at wider opening is about from 100 to 300 Hz. It is believed that the high frequency is corresponding to the primary longitudinal (axial) vibration and low frequency is corresponding to the bending (lateral) vibration. The two degrees of freedom vibration models are shown as Fig. 3.7.

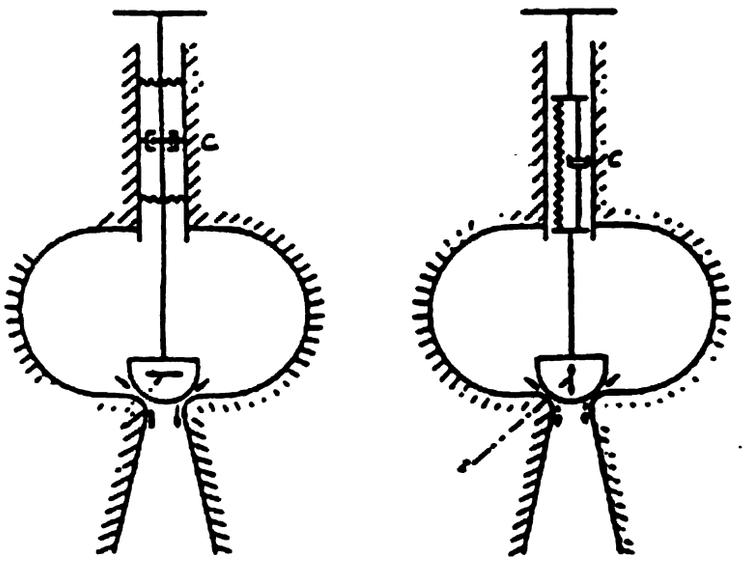

Fig. 3.7 Lateral and axial vibration models (after Araki)

By assuming the plug stem is mass less, equations of motion are derived as

$$m\frac{d^2x}{dt^2} + c_b\frac{dx}{dt} + k_b x = F_x \tag{3.1}$$

$$m\frac{d^2z}{dt^2} + c_v\frac{dz}{dt} + k_v z = F_z \tag{3.2}$$

m is th

are the la

forces in

D is th

is the den

and P_2 are

brackets i

percentage

Assume

The restor

with the hy

following

The firs

defines sys

m is the mass, c_b and c_v are the lateral and longitudinal damping coefficients. k_b and k_v are the lateral and longitudinal spring constants. F_x (Lift) and F_z (Drag) are the directional forces in the x (lateral) and z (longitudinal) directions respectively.

$$Fx, Fz = \frac{xD^2}{4}(P_1 - P_2) f\left[M, \frac{Uh\rho_2}{\mu_2}, \frac{\omega D}{U}, \frac{P_1}{P_2}, \frac{h}{D}\right] \tag{3.3}$$

D is the diameter of the plug and seat contacting place. U is the flow of the velocity. ρ is the density. M is Mach number. ω is the angular vibration frequency of the valve. P_1 and P_2 are valve inlet and exit pressure. The second dimensionless variable in the brackets is the Reynolds number, then Strouhal number, pressure ratio, and a plug lift percentage with respect to D.

Assume that the damping forces are proportional to the velocity of the plug vibration. The restoration or spring forces are proportional to valve plug displacement. Combining with the hydraulic forces, these three types of forces defined the valve vibration as following way:

$$\frac{x}{D} = f\left[\sqrt{\frac{k_b}{m}}t, \frac{c_b}{\sqrt{mk_b}}, \frac{D(P_1 - P_2)f}{k_b}\right] \tag{3.4}$$

$$\frac{z}{D} = f\left[\sqrt{\frac{k_v}{m}}t, \frac{c_v}{\sqrt{mk_v}}, \frac{D(P_1 - P_2)f}{k_v}\right] \tag{3.5}$$

The first term in the bracket is actually system natural frequency times time, which defines system property of the valve. The second term is the ratio of damping force and

spring fo

force. Th

Two-Dim

The tw

in tank (

controlle

to visual

pressure

The test

or flow pat

When va

side adhere

jet is free je

shown in Fi

called regio

spring force in respect to mass. The third term is the ratio of hydraulic forces with spring force. The value f is determined by equation (4.3).

Two-Dimensional model test and model improvement

The two-dimensional model test was constituted as shown in Fig 3.8. The air pressure in tank (1) is 30Kg/cm^2. After a control valve (2), the air pressure in the surge tank (3) is controlled to be constant. The outside of model test valve (4) is made of optical material to visualize the flow patterns. Another valve (5) is used to control the down stream pressure to change the inlet and outlet pressure ratio.

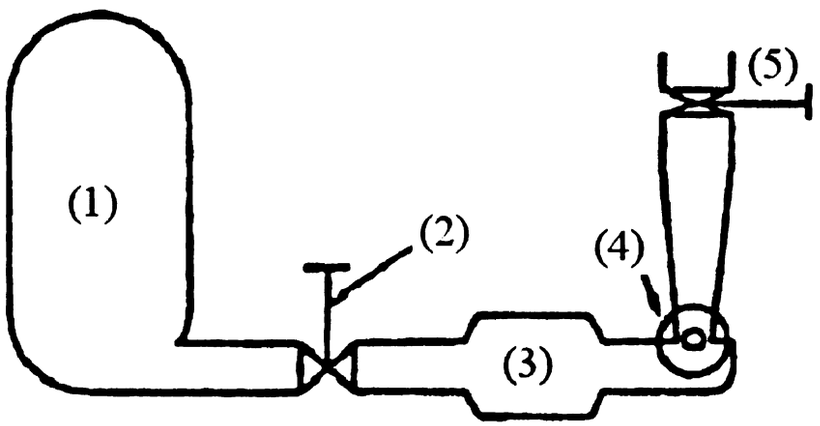

Fig. 3.8 Two-dimensional model test equipment (after Araki)

The test result shows that two jets occur at both sides of the valve. The shapes of jets or flow patterns are defined by pressure ratio and plug opening as shown in Fig. 3.9.

When valve opening is fixed, at large outlet-inlet pressure ratios, the jet flow on one side adheres to the plug up to the point near the center of the valve, while the other side jet is free jet departing from the plug and seat immediately after the valve throat, as shown in Fig. 3.10a. This flow pattern is called type B pattern. The region it occurs is called region B. When the pressure ratio is small, jets of both sides become free jets.

They are almost symmetric joining at about the center as shown in Fig. 3.10c. This flow pattern is called type C pattern. The region it occurs is called region C. When pressure ratio at a middle value, there is a transient pattern as shown in Fig. 3.10b. This flow pattern is called type D pattern. The region it occurs is called region D. In the region D, the type B pattern and type C pattern occur at irregular intervals.

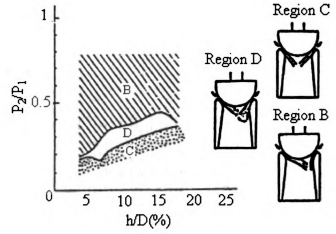

Fig. 3.9 Flow patterns with different valve opening and pressure ratio (after Araki)

a. Pattern B (P_2/P_1=0.42) b. Pattern D (P_2/P_1=0.30) c. Pattern C (P_2/P_1=0.19)
Fig. 3.10 Visualized flow pattern at a different pressure ratios (after Araki)

Jets are unstable phenomena especially when two jets meet together. The jets turning from one side to another at regular intervals is unstable. Correspondingly, the pressure at wall side or plug side turns irregularly. For example, under some small pressure ratio, the jet vibrates at 2.8 KHz. For most cases, the spectrum is randomly patterned. Not like flow

passing immersed cylinder, neither a random wake nor a turbulent flow vortex is produced.

The test result also shows that under high pressure ratio, jet pattern keep turning from one side to another. The jet adhering area also changes from one side to another, thus cause large pressure oscillation on the valve plug, which very possibly causes plug vibration. So to keep the jet adheres to the seat instead of plug becomes a possible way to reduce pressure oscillation.

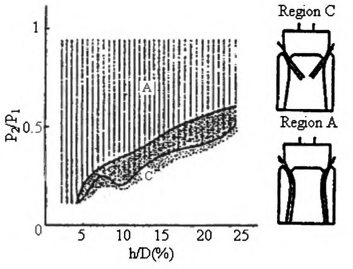

Fig. 3.11 Improved valve design and flow patterns (after Araki)

When passing through the gap between two cylinder columns with different radii, under a large pressure ratio, the flow was found to adhere to the cylinder of larger radius of curvature. As the pressure ratio decreases to some value, the flow moves away from both cylinders becoming a free jet. Based on above phenomena, an improved 2-D valve plug model is designed by making the seat radius larger than plug and cutting the nose of valve plug as shown in Fig. 3.11. The test result of this improved model shows that the magnitude of pressure variation is extremely smaller in comparison with the unimproved

one. The flow patterns are also different with the old type valve. The improved model has type A pattern instead of type B. The flow adheres to both side of seat after valve throat. In a transient pattern region, type A pattern and type B pattern turns to each other irregularly.

Three-Dimensional model test and improved valve design

As the real flow passing through a valve is three dimensional, a 1/3-scaled valve is designed as shown in Fig. 3.12.

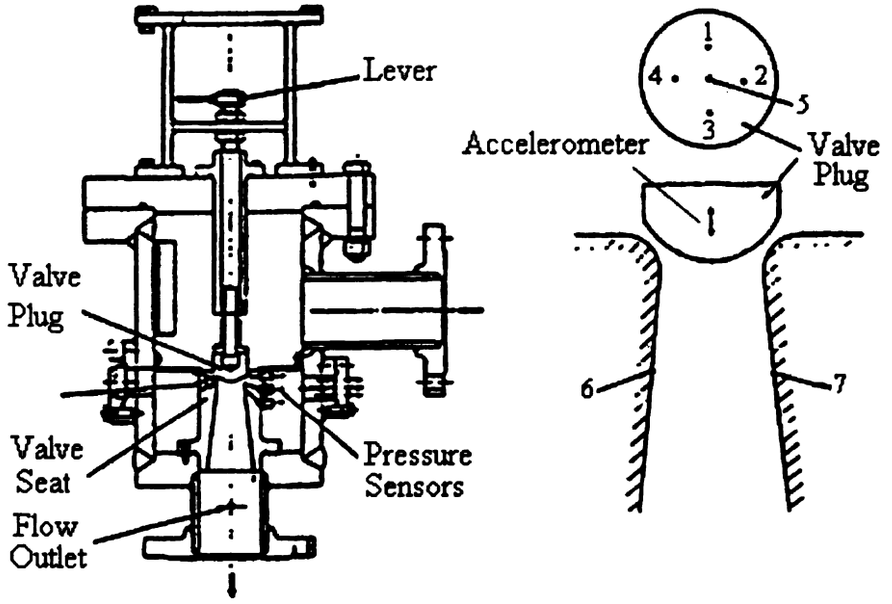

Fig. 3.12 3-D test valve and pressure sensor positions (after Araki)

The valve is also put into the same place of same test system of 2-D model. Dynamic pressure sensors for measuring pressure oscillation and accelerometers for measuring plug vibration were installed as shown in Fig. 3.12 (b).

Flow patterns

Both old and improved valves are tested, the result shows that they have difference with their 2-D models. The improved valve design has much less pressure oscillation and structure vibrations than the old valve. Fig. 3.13 shows the flow patterns for both valves. Fig. 3.14 shows the pressure oscillation and plug vibrations corresponding to different flow pattern regions for both valves.

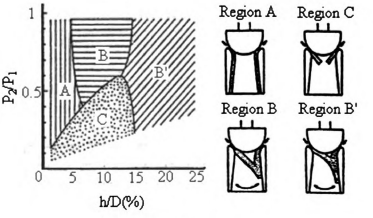

a. Old valve model

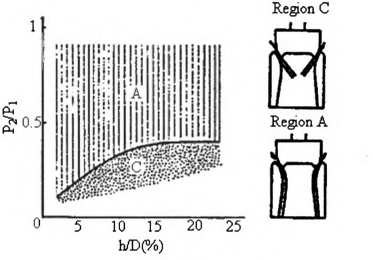

b. Improved valve model

Fig. 3.13 Flow patterns for 3-D valve test (after Araki)

For the old valve, only type C pattern is in common. For 2-D model, it is symmetric in left and right way, while for 3-D, it is axially symmetric, so does the type A pattern. In

transient regions, type D pattern turns irregularly from one side to the other, while type B or B' varies irregularly in the circumferential direction with time.

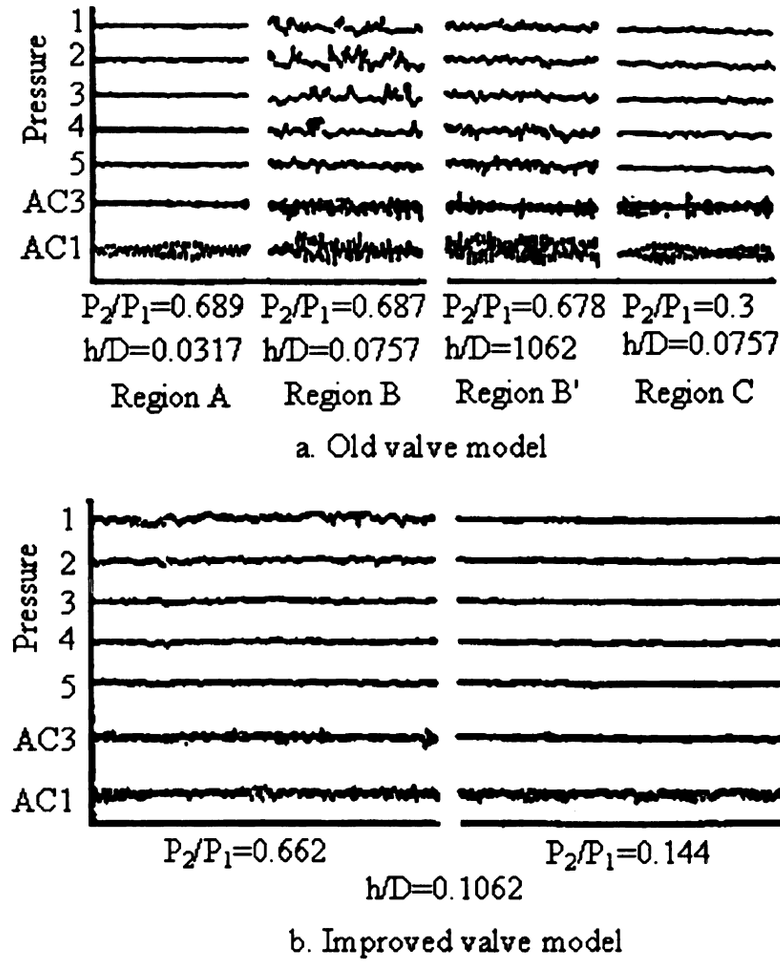

Fig. 3.14 Pressure oscillation and plug acceleration at different patterns (after Araki)

For improved design, the 3-D model does not have transient region. The pattern boundary pressure is lower than 2-D valve at same opening. For 3-D models, the improved valve has much less pressure oscillation and plug vibration amplitude than the old one. For the old valve, the most unstable regions are region B and B'. Strong pressure oscillation and structure vibration occur due to the flow pattern instability.

Pressure oscillation

Fig. 3.15 shows the maximum amplitude of the pressure oscillation using the pressure ratio and the valve-opening ratio as parameters. They have something in common, when the valve opening is large, the pressure oscillation reaches a maximum value at the pressure ratio of about 0.7. When the valve opening is small, the pressure oscillation maximum value occurs at the pressure ratio about 0.25.

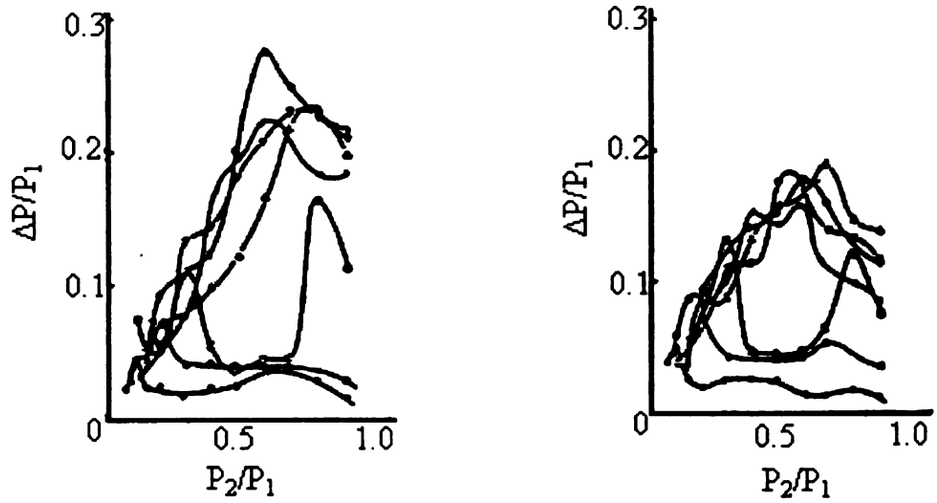

a. Pressure at valve throat b. Pressure at valve center

Fig. 3.15 Surface pressure oscillation of old valve model (after Araki)

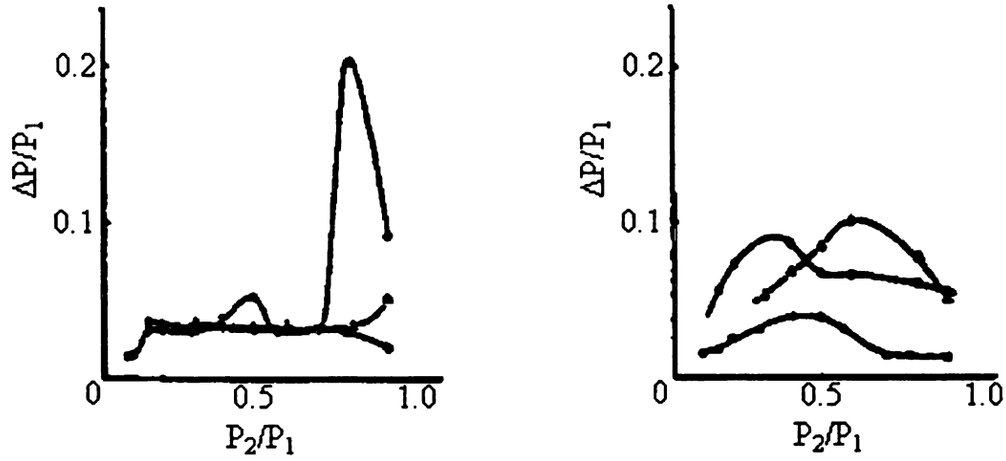

a. Pressure at valve throat b. Pressure at center

Fig. 3.16 Surface pressure oscillation of improved valve model (after Araki)

For improved design, since the flow pattern is symmetric in all the regions, no unstable flow is produced. The pressure oscillation is generally constant and smaller in comparison with the old design as shown in Fig. 3.16.

Plug acceleration

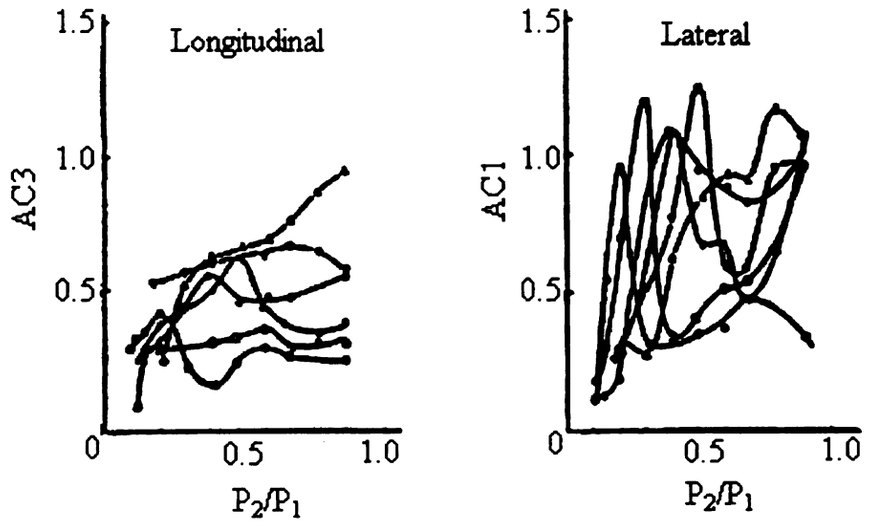

a. Old valve model

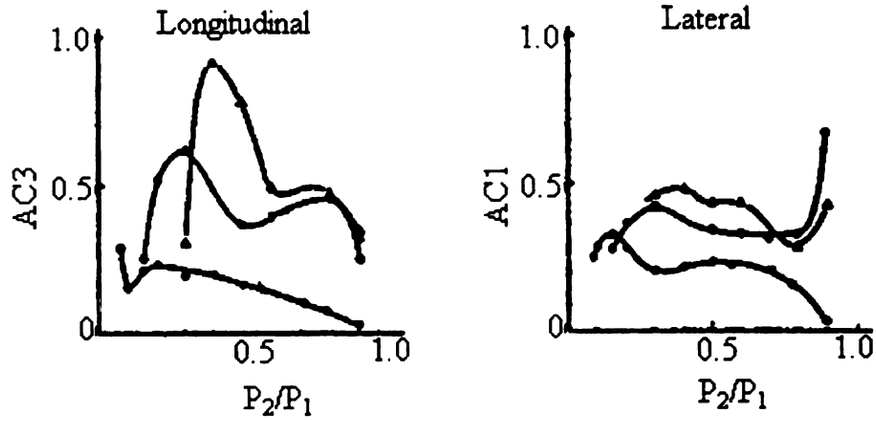

b. Improved valve model

Fig. 3.17 Plug acceleration (after Araki)

Fig. 3.17a and 3.17b show the changes by pressure ratio and the valve-opening ratio in the maximum amplitude of the valve acceleration corresponding to the pressure oscillation. For the old design, the acceleration is great in the region of large pressure

ratios when the valve opening is large and in the region of small pressure ratios when the opening is small. The same tendency is shown in both lateral and longitudinal directions. The regions with large vibration amplitude coincide with the regions with large pressure oscillation. For the improved design, the lateral acceleration is reduced to about 1/3 of the old valve and its maximum acceleration amplitude is at the opening ratio of about 0.1 or more than 0.8. The longitudinal acceleration reduced to about ½ of the old valve and reaches maximum value at 0.3 and 0.5.

Relation between pressure oscillation and plug vibration

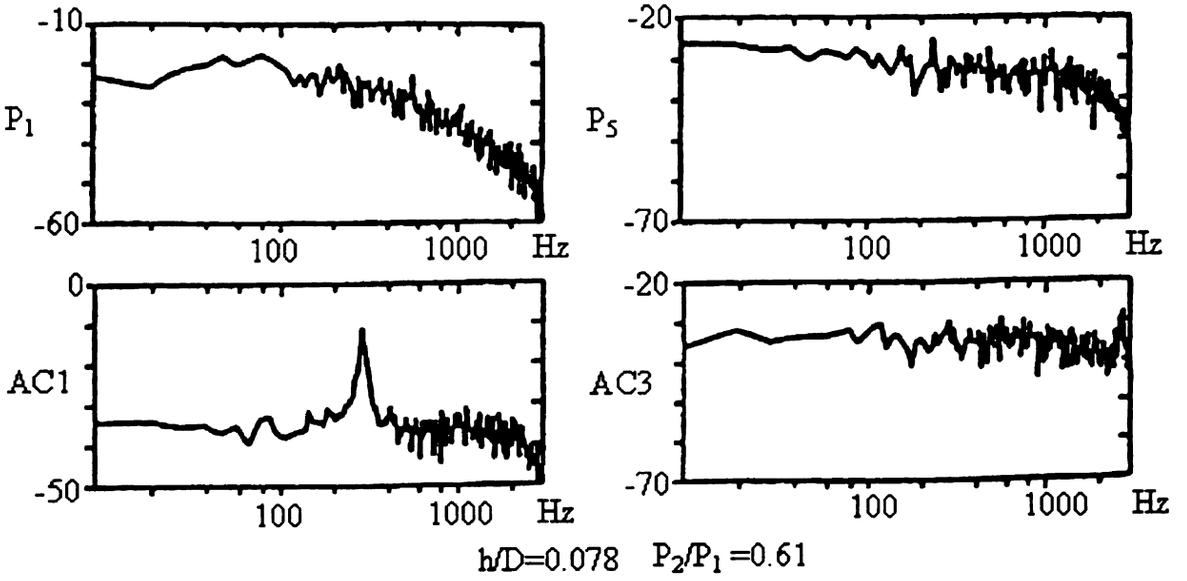

Fig. 3.18 Power spectra of surface pressure oscillation and acceleration (after Araki)

Fig. 3.18 shows the spectrum analysis result of the flow pattern B for the old valve. For pressure oscillation, the spectrum is randomly patterned without containing any outstanding component. For valve acceleration, the prominent components are shown at 300 Hz and 2,500 Hz respectively in the lateral and longitudinal directions corresponding to the plug natural frequencies. This means resonance occurs due to unstable hydraulic forces caused by pressure oscillation.

As shown in Fig. 3.19, there is an approximate linear relation between the square root of the power spectrum density (PSD) of fluid force and root mean square (RMS) valve of the vibration displacement, which can be expressed as

$$\sqrt{\overline{x^2}} = C_0 \sqrt{Wq(p)\frac{x}{4}\frac{p}{\zeta}} \tag{3.6}$$

Where $W_q(p)$ is the power spectrum density, $p = \omega_n$, is natural frequency; ζ is damping ratio; x is displacement; C_0 is constant.

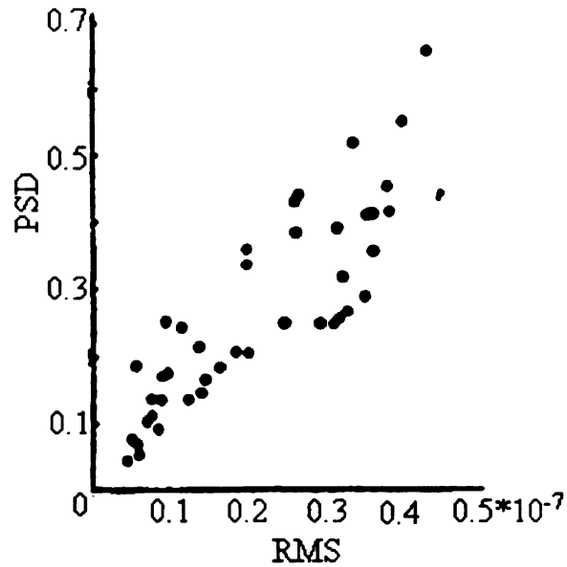

Fig. 3.19 Correlation between square root of PSD and RMS (after Araki)

Valve operation characteristics and surface pressure oscillation

In Fig. 3.20, the dashed line is a typical pressure ratio along opening curve for single valve. At fully closed position, the pressure ratio is zero. Then it increases quickly with plug lift. After some point, the increasing slows down until reaches about 1. Considering the pressure ratio and lift changing, the pressure oscillation amplitude is shown for both old and new valves.

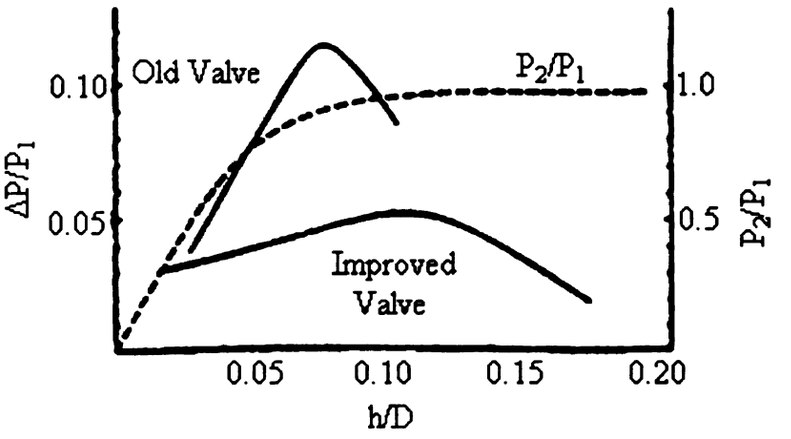

Fig. 3.20 Typical valve lift characteristic curve and pressure oscillation (after Araki)

3.3.3 Self-Excited Vibration

Self-excited vibration is still believed not as the major mechanisms to cause plug vibration for turbine valve in most cases. This is not only because the fluid-induced excitations, which also serves as negative damping, are stronger than self-excitation, but also because the self-excited vibration can be effectively restricted by increasing the system damping.

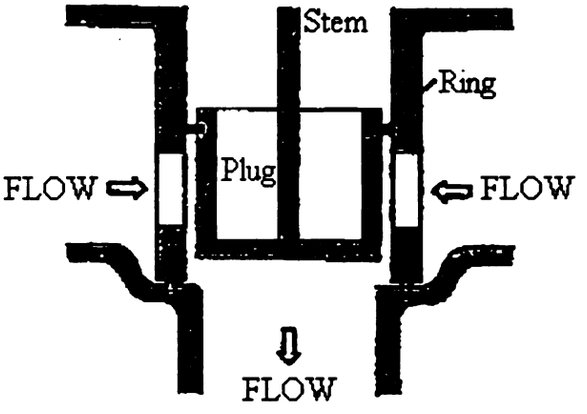

Fig. 3.21 Valve configuration (after Eguchi)

But at almost closed position, the self-excitation becomes a factor to be considered. According to the only test with an actual turbine in the former Soviet Union, it is

confirmed that self-excited longitudinal vibration occurs when the valve opening is small. Self-induced vibration is the product of aerodynamic instability.

Eguchi et al investigated the self-excited vibration of inlet control valves for large turbines. As shown in Fig 3.21, the valve studied is different with venturi valves. But the method and the mathematic models are useful for research in the self-excited vibration of the venturi type valve.

Theory analysis

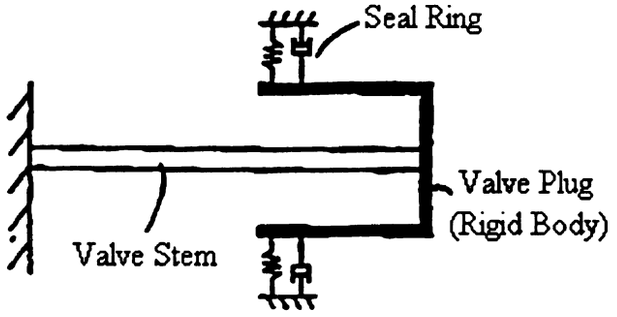

Fig. 3.22 Schematic of the system (after Eguchi)

The plug is simplified as a spring damping system with two-degree-freedom with small vibration as shown following Fig. 3.22. Knowing the fluid force is very important to understand valve vibration. To estimate the fluid forces, the relation between plug displacement and force should be identified. The basic relation between them is shown as matrix form,

$$\begin{pmatrix} K_{xx} & K_{xy} \\ K_{yx} & K_{yy} \end{pmatrix}\begin{pmatrix} x \\ y \end{pmatrix}+\begin{pmatrix} C_{xx} & C_{xy} \\ C_{yx} & C_{yy} \end{pmatrix}\begin{pmatrix} \dot{x} \\ \dot{y} \end{pmatrix}+\begin{pmatrix} M_{xx} & M_{xy} \\ M_{yx} & M_{yy} \end{pmatrix}\begin{pmatrix} \ddot{x} \\ \ddot{y} \end{pmatrix}=\begin{pmatrix} F_x \\ F_y \end{pmatrix} \qquad (3.7)$$

k_{xx}, k_{xy}, k_{yx}, k_{yy} are from the sum of flows: induced stiffness and stem stiffness; C_{xx}, C_{xy}, C_{yx}, C_{yy} are from the sum of flows: induced damping and stem damping; M_{xx}, M_{xy}, M_{yx}, M_{yy} are the sum of the added masses and valve masses; F_x, F_y are the self-induced

forces; x, y are the valve displacements in the x and y axis. Because there are too many unknowns in the equation 3.7, a practical more simple matrix form can be derived from above equation

$$\begin{pmatrix} Z_{xx} & Z_{xy} \\ Z_{yx} & Z_{yy} \end{pmatrix} \begin{pmatrix} x \\ y \end{pmatrix} = \begin{pmatrix} F_x \\ F_y \end{pmatrix} \tag{3.8}$$

$Z_{xx} = K_{xx} + i\omega C_{xx} - \omega^2 M_{xx}$; $Z_{xy} = K_{xy} + i\omega C_{xy} - \omega^2 M_{xy}$; $Z_{yx} = K_{yx} + i\omega C_{yx} - \omega^2 M_{yx}$; $Z_{yy} = K_{yy} + i\omega C_{yy} - \omega^2 M_{yy}$. Thus the number of unknowns in the equation is reduced to eight. In experiment, F_x and F_y can be calculated from the output of the pulse counter targeting for the unbalanced mass. The x and y displacements are measured by a displacement sensor. To obtain the unknown Z coefficients, two types of excitation under same condition are applied to system, a forward circular excitation and a backward circular excitation. Thus the equation is changed to

The forward circular excitation matrix form

$$\begin{pmatrix} Z_{xx} & Z_{xy} \\ Z_{yx} & Z_{yy} \end{pmatrix} \begin{pmatrix} x_F \\ y_F \end{pmatrix} = \begin{pmatrix} F_{xF} \\ F_{yF} \end{pmatrix} \tag{3.9}$$

The backward circular excitation matrix form

$$\begin{pmatrix} Z_{xx} & Z_{xy} \\ Z_{yx} & Z_{yy} \end{pmatrix} \begin{pmatrix} x_B \\ y_B \end{pmatrix} = \begin{pmatrix} F_{xB} \\ F_{yB} \end{pmatrix} \tag{3.10}$$

Combine equation (3.9) and (3.10),

$$\begin{pmatrix} Z_{xx} \\ Z_{xy} \\ Z_{yx} \\ Z_{yy} \end{pmatrix} = \begin{pmatrix} x_F & y_F & 0 & 0 \\ 0 & 0 & x_F & y_F \\ x_B & y_B & 0 & 0 \\ 0 & 0 & x_B & y_B \end{pmatrix}^{-1} \begin{pmatrix} F_{xF} \\ F_{yF} \\ F_{xB} \\ F_{yB} \end{pmatrix} \tag{3.11}$$

Experiment to determine the fluid force coefficients

The Z coefficients can be determined by experiment method. The experiment set up is shown in Fig. 3.23. The test result shows that the fluid force coefficients have relation with frequency. Fig. 3.24 shows the relation between Z_{xx} with frequency. Following the same method, other coefficients can be obtained.

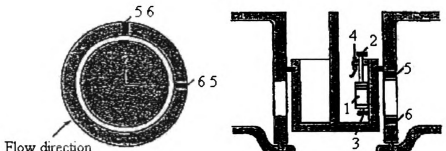

Fig. 3.23 Fluid force coefficients test model (after Eguchi)

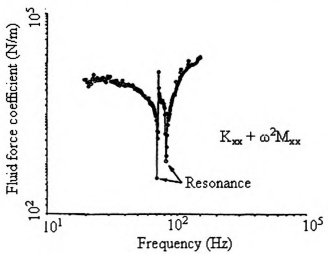

Fig. 3.24 Fluid force coefficient, Z_{xx}, determined by test result (after Eguchi)

Fluid force estimation

For same valve under same opening, the coefficients remain constant. As these coefficients are known, they will be putted into the equation (3.9) to predict the forces when knowing displacement and vice visa. So in real valves as flow passing by, the self-induced fluid force can be known if the displacement of the value plug is measured.

Stability analysis

If the vibration mode is unstable, the valve experiences severe vibration. So stability analysis is very important. Above motion of equation is derived to get the fluid force coefficients. For actual valve, the equation of motion can be

$$\begin{pmatrix} M_{st} & 0 \\ 0 & M_{st} \end{pmatrix}\begin{pmatrix} \ddot{x} \\ \ddot{y} \end{pmatrix}+\begin{pmatrix} C_{st} & 0 \\ 0 & C_{st} \end{pmatrix}\begin{pmatrix} \dot{x} \\ \dot{y} \end{pmatrix}+\begin{pmatrix} K_{st} & 0 \\ 0 & K_{st} \end{pmatrix}\begin{pmatrix} x \\ y \end{pmatrix}$$
$$=\begin{pmatrix} \overline{M}_{xx} & \overline{M}_{xy} \\ \overline{M}_{yx} & \overline{M}_{yy} \end{pmatrix}\begin{pmatrix} \ddot{x} \\ \ddot{y} \end{pmatrix}+\begin{pmatrix} \overline{C}_{xx} & \overline{C}_{xy} \\ \overline{C}_{yx} & \overline{C}_{yy} \end{pmatrix}\begin{pmatrix} \dot{x} \\ \dot{y} \end{pmatrix}+\begin{pmatrix} \overline{K}_{xx} & \overline{K}_{xy} \\ \overline{K}_{yx} & \overline{\hat{K}}_{yy} \end{pmatrix}\begin{pmatrix} x \\ y \end{pmatrix} \tag{3.12}$$

$\overline{M}_{ij}$ is the added mass; $\overline{C}_{ij}$ is the induced damping; $\overline{K}_{ij}$ is the flow-induced stiffness; M_{st} is the valve mass, C_{st} is the stem damping, and K_{st} is the stem stiffness. The eigenvalue matrix form equation of 3.12 can be reduced to

$$\left\{\lambda\begin{pmatrix} M & 0 \\ 0 & 1 \end{pmatrix}+\begin{pmatrix} C & K \\ -1 & 0 \end{pmatrix}\right\}\{X\}=0 \tag{3.13}$$

This equation is very useful to analysis the stability, while instability occurs when the real part of the complex eigenvalues become positive. The M, C, and K are essentially the sum of fluid force coefficients and structure coefficients, which depend on frequency. Then, two ways can be done to analysis the flow stability. One method is to assume the frequency first, then calculate the matrix and eigenvalue using the frequency, Fig. 3.23a shows a typical analytical result for the different modes in terms of assumed frequency

and damping ratio; The other way is to calculate the relation between assumed frequency and calculated frequency for each mode, as shown in Fig 3.25 b. The result should be same, for example, the two figures both show the first mode with frequency of 50 Hz and damping ratio of 0.12, is stability mode; while second mode with frequency 65 Hz and damping 0.04, is unstable.

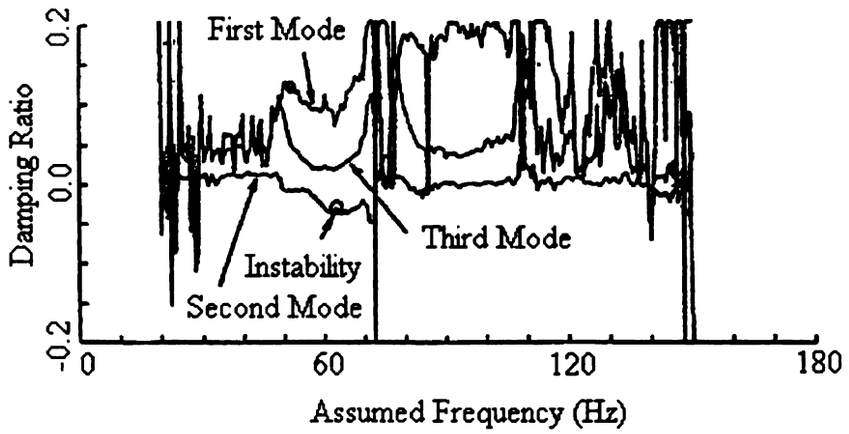

a. Relationship of damping ratio and assumed frequency

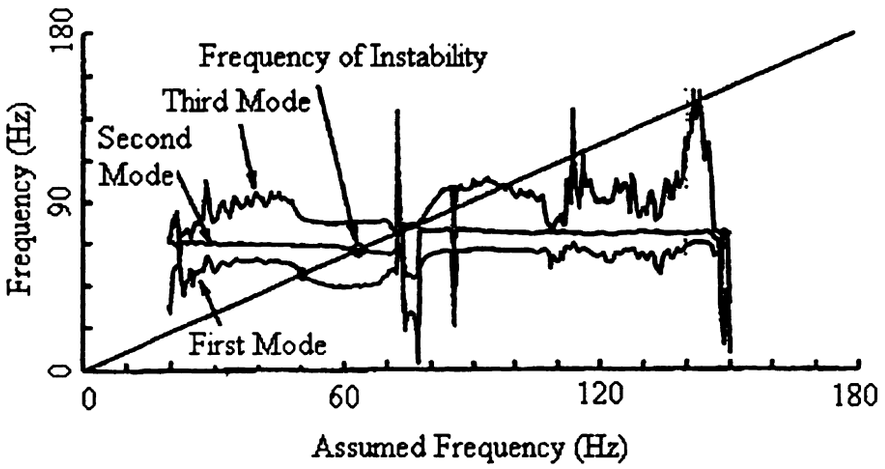

b. Relationship of calculated and assumed frequency

Fig. 3.25 Stability analysis of vibration modes (after Eguchi)

By using this method, the frequencies, vibration modes and damping values can be predicted. These results can easily be extended to obtain an estimation of the performance of an actual machine by just looking at the structural and fluid properties. Also the mode

stability can be analysis. Same process can be followed for self-excited vibration of venturi type valve.

3.3.4 Acoustic effects

Two acoustic phenomena cause problems for turbine inlet valve, noise and acoustic resonance. The noise is somehow a result of structure vibration and acoustic resonance is a cause of vibration.

Noise

Valve noise is notorious phenomena. Two main reasons are responsible for noise, first, structure vibration, second, the transmission through the structure of fluid-borne sound wave. Former is dominant reason while the downstream piping is short; later is predominant cause of noise when the downstream pipe is long.

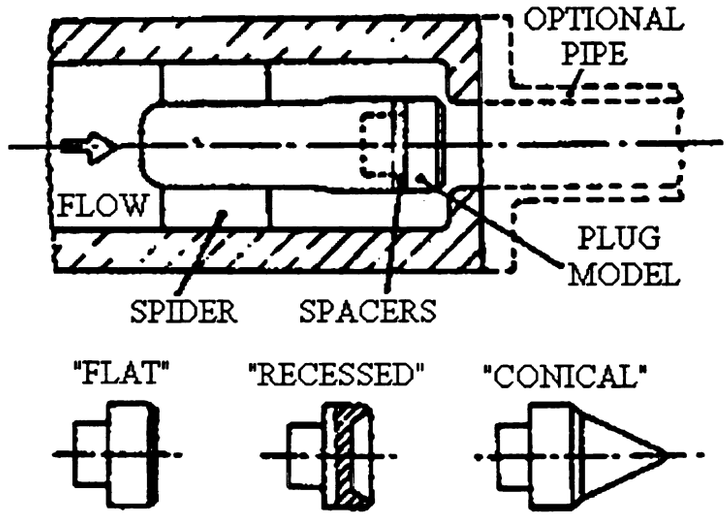

Fig. 3.26 Test valve for noise (after Heymann)

Heymann investigate the relation between noise level and Mach number for different shapes of valves at different plug lift. The basic test valve configuration is shown in Fig. 3.26, air goes through from a high pressure inlet chest to a low pressure outlet chest.

Acoustic efficiency is defined as $\eta_a = \frac{w_a}{w_f}$. w_a is sound power and $w_f = \frac{1}{2}\dot{m}V^2$. As shown in Fig. 3.27, the test result shows that the normally the acoustic efficiency increase with the increasing Mach number. It reaches maximum value at some point. Then it starts decreasing. The turning point is different due to different valve shape and lift ratio.

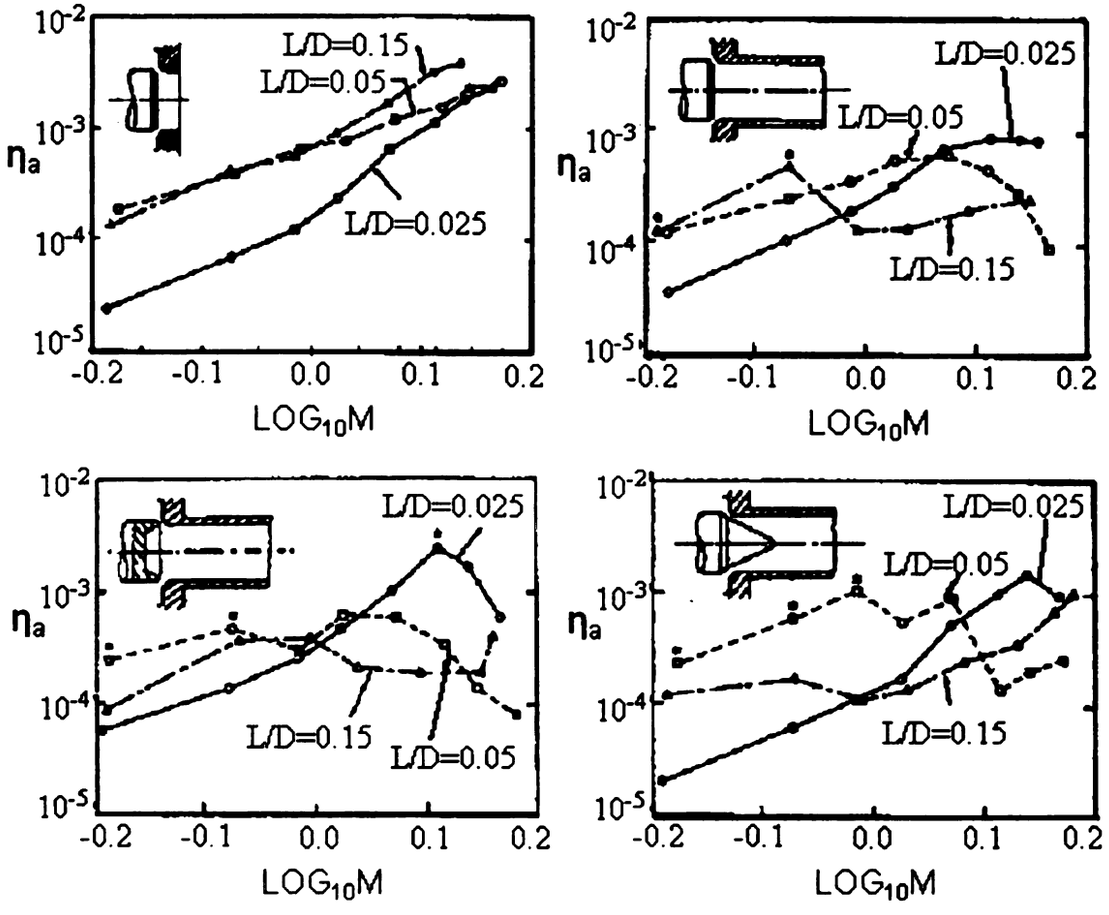

Fig. 3.27 Result of noise tests for different valve configurations (after Heymann)

We know the Mach number is a function of pressure ratio. For a valve with fixed opening, the smaller pressure ratio is, the higher the Mach number. The recessed shape valve looks like the improvement valve in the paper of Araki at el. According to our observation, the curve at the lift ratio of 0.15 for recessed shape valve in Fig. 3.27 is actually the combinations of the curves for lateral and longitudinal vibrations at lift ratio

of 0.175 in Fig. 3.17b, if we look the acceleration and acoustic efficiency as same physical meaning terms. There are two peak points in Fig. 3.27, first one is at low Mach number, which means high pressure ratio. We think this peak is due to lateral acceleration peak in Fig. 3.17b; The second peak is at high Mach number or small pressure ratio. We think this one is due to severe longitudinal vibration peak in Fig. 3.17b. Our conclusion is that even the downstream piping systems are different for two experiment, the results match in a qualitative way.

Heymann also observed the flow pattern changing phenomena as shown in Fig. 3.28. The annular flow and core flow pattern are actually called type A and type C pattern respectively in Araki's paper. The flow pattern regions also match with the Fig. 3.13a and with a little difference with Fig. 3.13b. The opposite region boundary in two figures is because here pressure drop ratio is used while in Fig. 3.13, the pressure ratio is used.

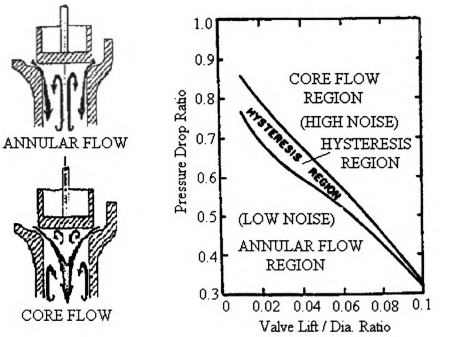

Fig. 3.28 Flow patterns and regions (after Heymann)

Acoustic resonance

As we mentioned in Chapter 2, for the acoustic resonance the research subject should be the valve piping system. Even same valve design, due to different down stream piping system, the valve may experiences different vibrations. So the research in this field is case by case.

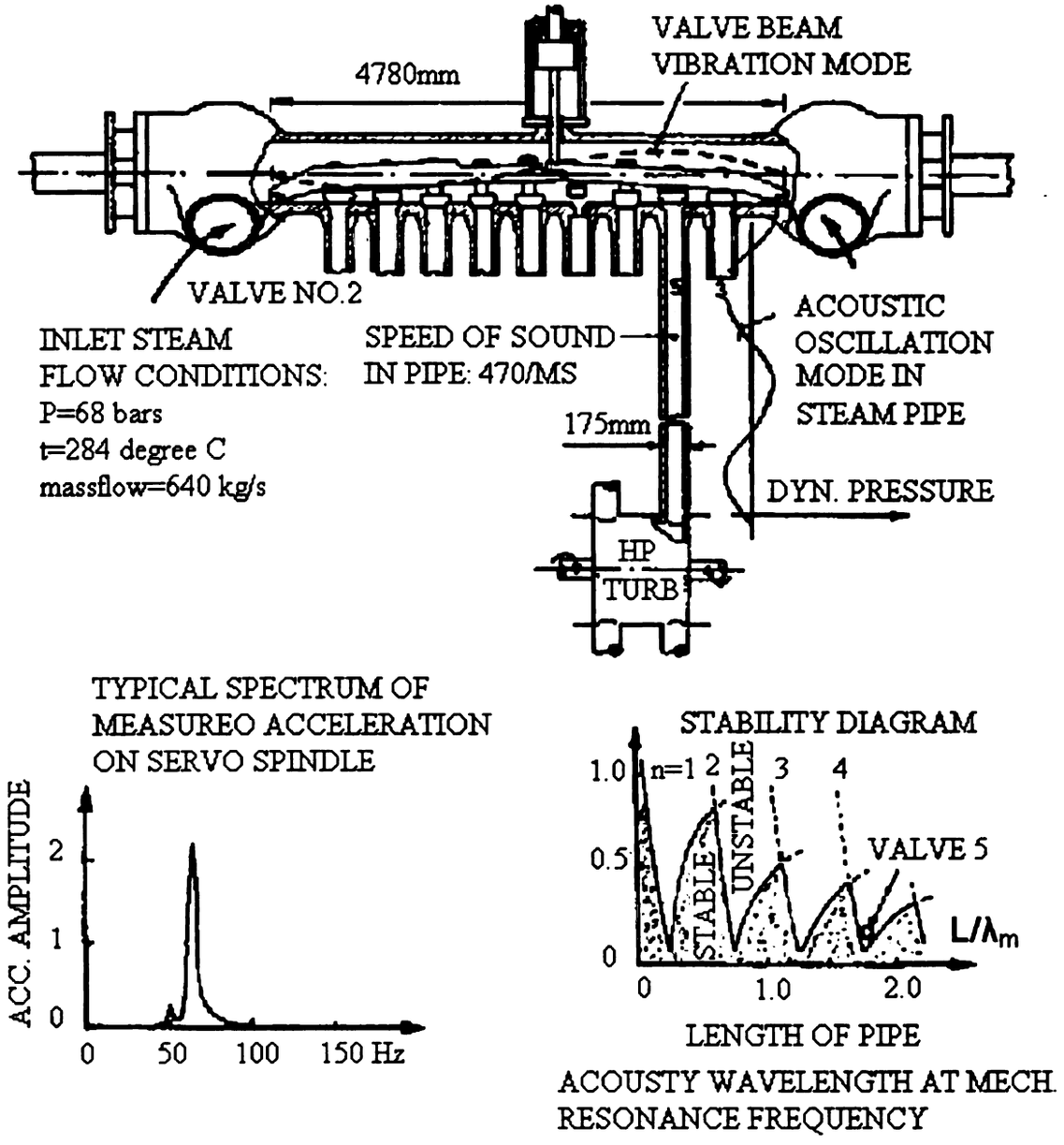

Fig. 3.29 Solving of acoustic resonance for an operating turbine valve (after Widell)

Widell studied the failures of servo spindle and couplings for an operating turbine inlet valve as shown in Fig. 3.29. The bar lift type multiple-valve is composed of 9 separated mushroom-like valves. The valves are lift one by one by two hinged beams, which is controlled by servomotor. Two inlet emergency stop valves supply steam to valve casting. After the casting, the steam is led by valve downstream pipes with different lengths to two steam chests, one on each side of the first stage of the turbine.

Severe vibration of casting and servo spindle with frequency 63 Hz and amplitude about 100-400 μm occurs in the No. 5 operating range. The power output is between 270 and 320 MW. By both using theory analysis and experiment of testing the beam vibration mode, an S-shaped mode with a frequency close to 64 Hz is confirmed. Then acoustic impedances of No. 5 downstream pipe and terminal impedance at turbine end are calculated and proved by test. From all above information, No. 5 valve is judged unstable while all others are stable. Acoustic resonance occurs between the beam and No. 5 valve-piping system.

The logical method is suggested to lengthen the downstream pipe after No. 5 valve. But considering the real situation, it is more convenient to removal the No.5 valve with less influence on turbine performance. The valve is removed, then after 7 years of operating, the vibration never happened again

3.3.5 Flow impingement

Powell (1953) recognized the impingement mechanism of shear flows as shown in Fig. 3.30. The vortex caused by velocity gradient is strengthened as traveling down stream producing regular pressure and velocity fluctuations. These fluctuations are drastically

self-enhanced at some frequencies when meet an edge. It causes severe structure vibration or noise problems.

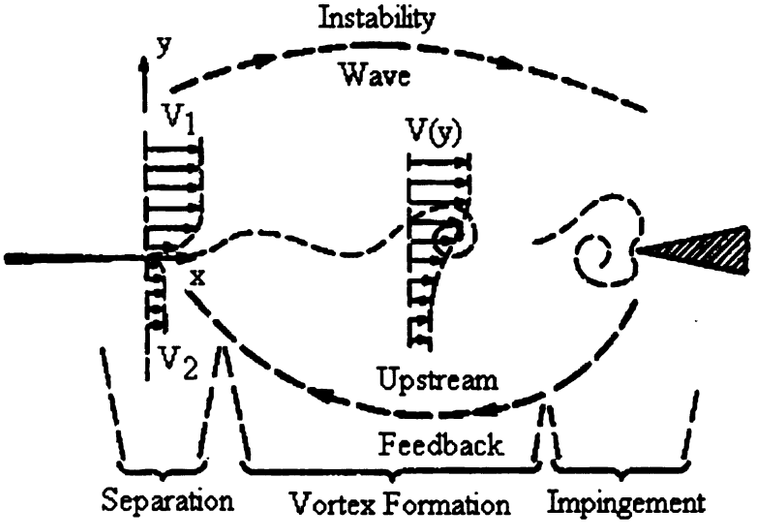

Fig. 3.30 Impingement mechanism (after Ziada)

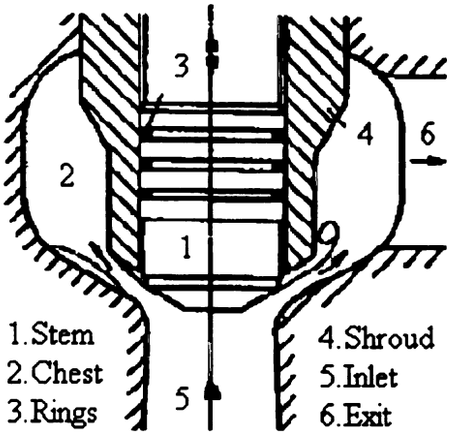

Fig. 3.31 Valve configuration for impingement analysis (after Ziada)

By using above theory, Ziada et al, studied the excitation mechanism of a kind of turbine control valve as shown in Fig. 3.31. When passing through the valve throat, flow separation occur possibly form the valve stem or seat. Then due to the flow impingement on the downstream corner of plug shroud, the flow instability is enhanced. Repeating separation and reattachment of the jet to downstream corner would generate great

pressure fluctuations. If the pressure fluctuations were coupled to the acoustic resonance of the valve chest, severe vibration and noise would occur. It was found that this kind of excitation likely occurs when high-speed jet separates after valve throat and the valve dimension is much small than the jet movement in unit time. An effective counter-measure is suggested to eliminate the impingement boundary, when impingement excitation occurs.

3.3.6 Valve improvement design

Two directions to improve valve design by either cutting the nose semi-sphere shape of venturi plug or extending it as shown in Fig. 3.32. As we mentioned before, Araki designed an improved valve by cutting the semi-sphere nose. The better performance was observed by experiments and practical operation in turbines. Zarjankin and Simonov designed a valve by extending the nose as shown in Fig. 3.33. The new valves were installed in all kinds of turbines like R-50-130, PT-80-130, K-300-240, T-100-130, and T-250-240. In more than 15 years observation in some turbines, the new design was proved to have high reliability.

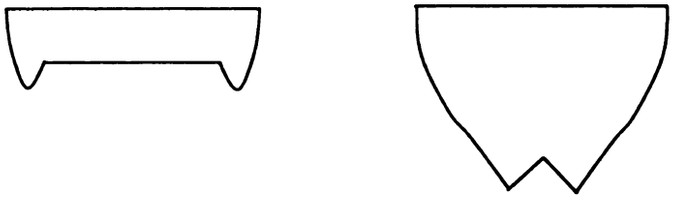

Cutting Extending

Fig. 3.32 Two directions for optimize valve plug shape

In our view, because the flow is better guided passing through a valve with extending nose, the thermal efficiency of extending nose valve is higher than the valve with cutting nose.

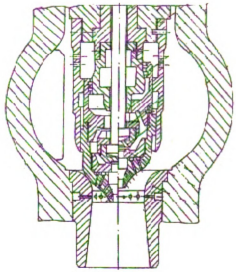

Fig. 3.33 An improved valve design (after Zarjankin and Simonov)

3.3.7 The recent research

In 2003, two papers were published about the failure cases of steam turbine venturi valves. D. Zhang and A. Engeda reviewed the literature in this field and investigated the flow phenomena by using CFD tools for the valve. Improved designs were also reported. The detail CFD results will be shown in Chapter 4. Recently, J. Hardin, F. Krushner and S. Koester published another paper describing two turbine venturi valve failures and designed a new valve that showed good flow stability.

A recent valve failure was reported in 1998 at Elliott Turbomachinery Co. The valve (shown in Fig. 1.2 and 1.3) is a real valve, which started operation in a multistage steam turbine in 1998. After 3 months of running, the No. 2 valve failed after the crack developed in the location shown in Fig. 1.3. It happened as the No.1 valve was almost fully open and No. 2 valve was at an opening of 0.147(h/D). The falling plug drove the seat into the steam chest wall approximately 0.7 in. The failed valve stem surface is

shown in Fig. 1.3. Before the failure, there was higher noise coming out of the machine, which means that chattering may have existed.

Just before the valve has the severe vibration, the frequency spectrum for the pressure port transducer at downstream of No.2 valve was tested. Fig. 3.34 shows the high amplitude, 66.6 psi, of valve vibration occurs at frequency of about 350Hz. This is due to the "organ pipe" resonance since the transducer was not flush-mounted. The long time trace period of four seconds of pressure pulsations is shown in Fig. 3.35. Zooming in the Fig. 3.35 for a quarter-second time trace of pressure pulsations, Fig. 3.36 shows clearly that the sharp drops in pressure are at an average of 35Hz. The pressure pulsation during high valve vibration is also tested as shown in Fig. 3.37. The frequency is 32 Hz. So the pressure pulsation at frequency between 30 and 40 Hz is caused by unstable flow.

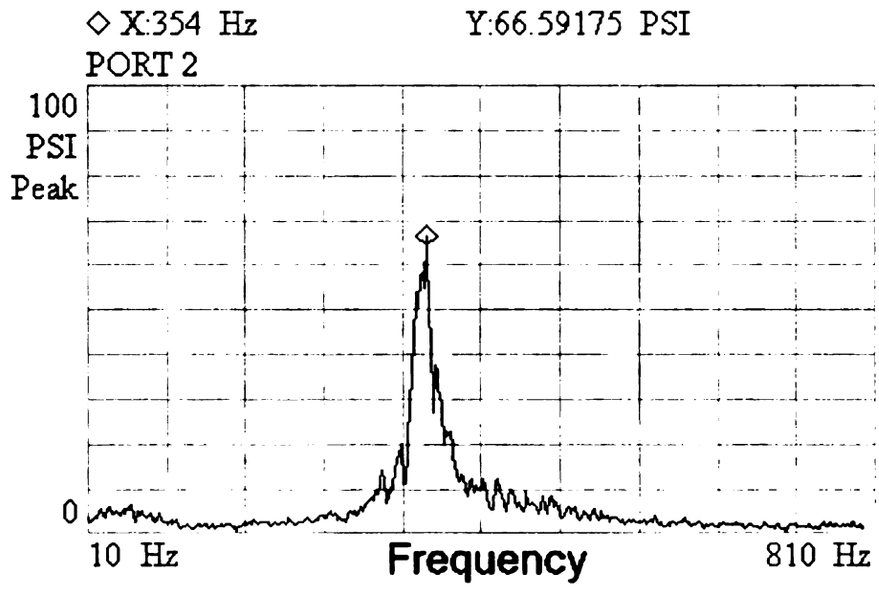

Fig. 3.34 Pressure pulsations before high vibration of No.2 valve (after J. Hardin)

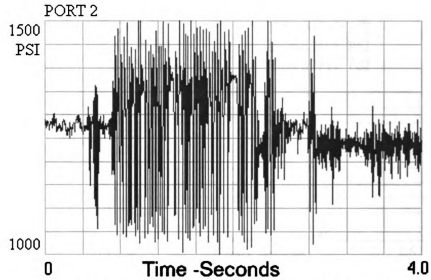

Fig. 3.35 Time trace of pressure pulsations (after J. Hardin)

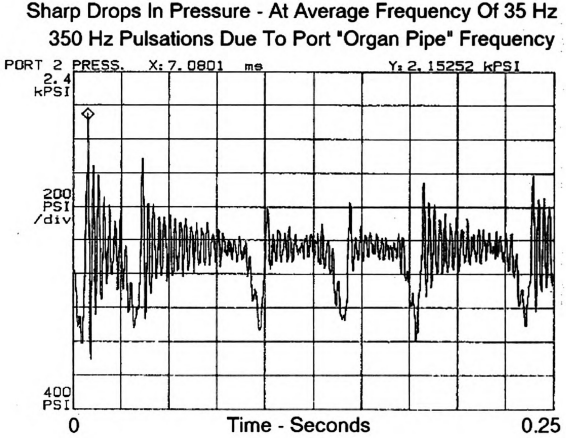

Fig. 3.36 Zooming in view of the pressure pulsations (after J. Hardin)

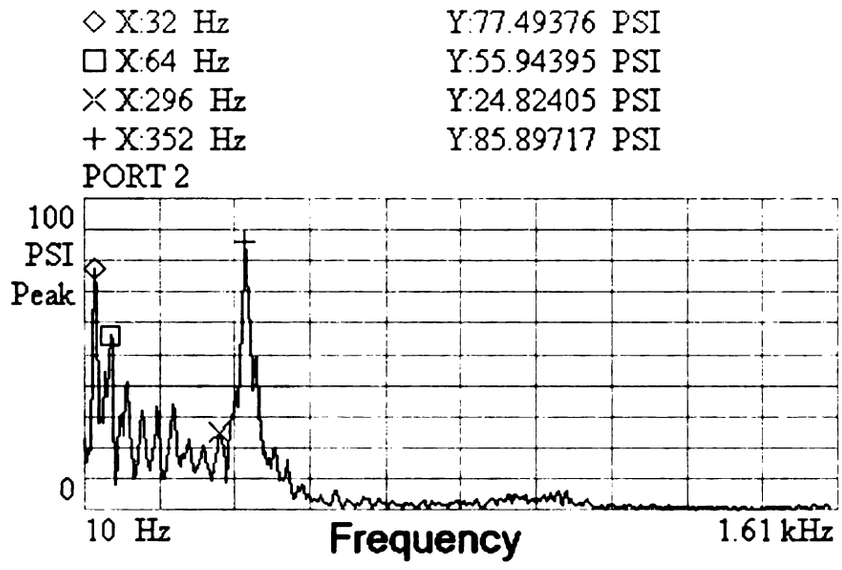

Fig. 3.37 Pressure pulsation frequency spectrum during valve vibration (after J. Hardin)

The valve natural frequency was tested as shown in table 3.1. Both bending mode frequency and torsion mode frequency decreases with decreasing pressure load of the valve. This is due to the changing of stem length and mass as the valve moves to change the pressure load.

Table 3.1 Original Valve Natural frequency (after J. Hardin)

Pressure Load (Lbs.)	Bending Mode Freq.(Hz)	Torsion Mode Freq. (Hz)
325	208/238	850/930
675	268/282	1050/1160
1325	290/310	1200/1240

The steady state CFD analysis was performed in the paper. By changing the curvature of plug, three new valves, cutoff, concave and hybrid, were designed. Three new valves at both large and small openings are simulated and the streaklines of results are shown in Fig. 3.38. The flow is annular flow for each case. The annular flow pattern is preferred and proved more stable by Araki et al. In terms of this, the new designs are better than old one. According to test data, the hybrid valve is more stable and is with less vibration.

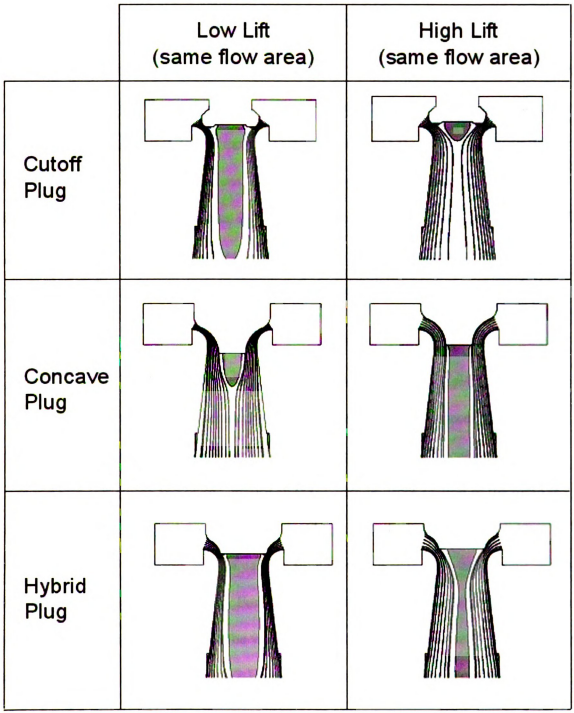

Fig. 3.38 Streaklines and reverse flow region of new valves (after J. Hardin)

CHAPTER 4

2-D NUMERICAL INVESTIGATION

Because it is very difficult to express the drag and bending moment as function of time due to complicity of flow structure interaction, it is very difficult to get analysis solution for equations in Chapter 2. Experiment is very important to help us to understand fluid nature, but due to some reality issues, we have no way to obtain a lot of detail important information from experiment alone. 2-D model was calculated by using commercial CFD package, TASCFLOW. The steady state flow field, forces and moment at plug balanced position and fluid structure interaction mechanisms by arbitrarily adding displacement on valve plug were investigated.

4.1 Numerical Modeling

TASCGRID was used to generate the grids. The whole grid composes four blocks, left and right side chest (i=50,j=30,k=4 for each), throat (i=50,j=150,k=4), and downstream seat (i=50, j=50,k=4), totally 46,000 nodes. A cross section of the mesh is shown in Fig. 4.1. The grid density around the plug (the darker area) is much greater because this is the most concerned area. The flow is treated as steady state, compressible, turbulent ideal gas with high speed. For inlet boundary condition, constant total pressure and total temperature is imposed. The wall is treated adiabatic. Constant static pressure is used at valve exit. Because this is a 2-D problem, symmetric boundary condition is used at k=1 and 4 surface. All cases were convergence to maximum residence in the order of 10^{-4}. The y+ value of the valve plug surround region is allowed to vary from 40 to 400. Except the plug geometry, same grid is used for improved valve design simulations.

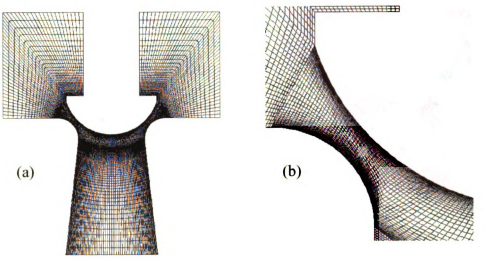

Fig. 4.1 Sample computational grid

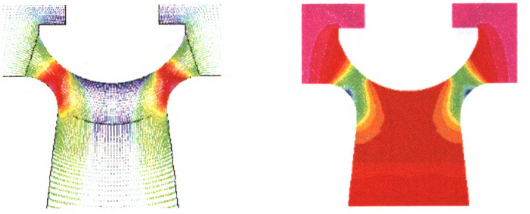

Pattern (a)

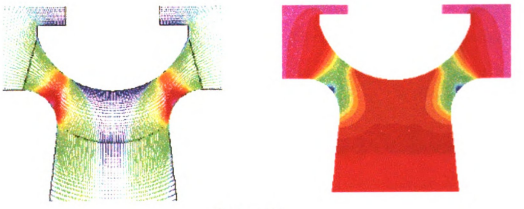

Pattern (b)

Pattern (c)

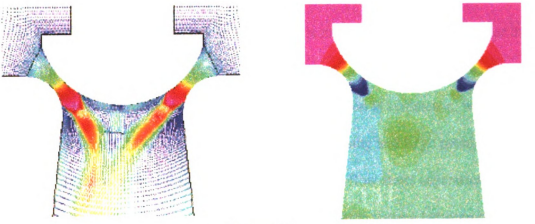

Pattern (d)

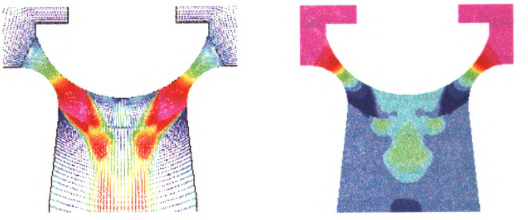

Pattern (e)

Fig. 4.2 Flow patterns and pressure field

4.2 Results and Discussion

4.2.1 Asymmetric flow pattern

Five basic flow patterns are found at different pressure ratio, defined as downstream static pressure over upstream total pressure, and valve opening ratio, defined as plug opening over plug diameter, as shown in Fig. 5.2. The plots at right show the velocity field while plots at left show the corresponding static pressure field. Even the boundary conditions and geometry are perfect symmetric, three patterns are asymmetric, especially pattern (c) showing strongly asymmetric. Pattern (a) is most wanted flow pattern for the valve. The flow accelerates before the valve throat, then slows down at valve diverging part and attached to the seat on both side. Pressure distribution is symmetric, which means less force occurs. This pattern happens in large opening and large pressure ratio situation. The difference between pattern (b) and (a) is that flow starts separation from seat in both sides. It is also relatively symmetric as a transition pattern between pattern (a) and (c). Pattern (c) is most unwanted flow pattern. Passing through valve throat, flow decelerates with one side attaching the seat and another side attaching the plug. Pressure is asymmetric essentially causing huge hydraulic forces and moment. This is dominant flow pattern as valve large (not as large as pattern (a)) opening. One thing interested is that the right side flow always attaches the plug at this pattern (In coarse grid with 1/4 density as this one, we do have some results that flow attaches left side plug. For that grid at 10.6% opening and pressure ratio 0.9, from same initial guess, one result show the flow attaching left while another attaching right looking like flip imagine. We did not try in fine grid, because converging is time consuming). Pattern (d) is transition pattern between pattern (c) and (e). At down steam of the seat, the pressure is asymmetric, while

relatively symmetric surrounding the valve. According to former visualized result done by Araki et al, this is a transient region. Pattern (d) is symmetric pattern, normally occurs in small pressure ratio situations. Above flow patterns agree well with our predicted flow patterns in Fig. 3.2.

When opening ratio is less than 20%, flow pattern changes from (c) to (d) as the pressure ratio drops from 0.98 to 0.2. No pattern (a) and (b) found. For example, when the opening ratio is 10.6%, pressure ratio between 0.98 and 0.51 is the pattern (c) region; between 0.51 and 0.28 is pattern (d) region and then becomes pattern (e) region. Similar experiment has been done by Araki et al, their visualized flow pattern shows the two critical pressure ratio are about 0.46 and 0.25 instead of our result of 0.51 and 0.28, we can say that somehow our CFD results are confirmed. The region of pattern (c) decreases as pressure opening increasing.

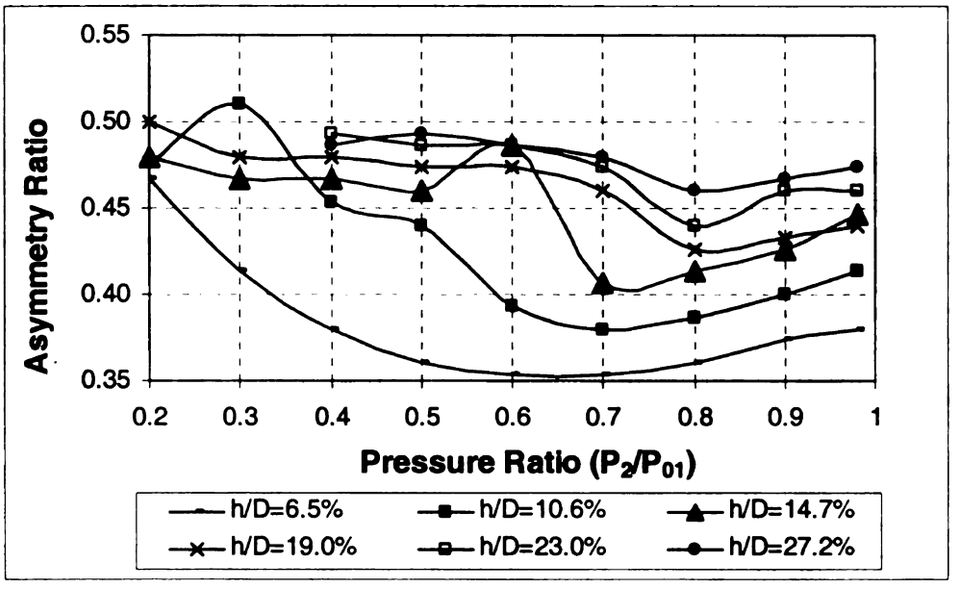

Fig. 4.3 Variation of asymmetry ratio

When opening ratio is more than 20%, which is the region not shown in the former research, the flow pattern changes in the sequence of pattern (a), (b), (c), (d) and (e). Not

as dominant as in small opening, the pattern (c) occurs at the pressure ratio of about 0.8. Before pattern (c), it is the region of Pattern (b), which is very narrow. Large pressure ratio is the region of pattern (a). Pattern (d) is dominant pattern.

It is not enough to just understand the visualized flow pattern, because even in the same pattern, the intensity is different. Thus two dimensionless parameters are defined to describe the asymmetry of flow pattern in a quantitative manner. Asymmetry ratio is defined as the arc length between center of downstream separation area and left end along the valve surface over the plug arc length. The center position is defined as the lowest average Mach number plane normal to plug surface. This means how far the attaching flow reaches. When the ratio is 0, it means the right side flow attaches all the way along plug surface while 0.5 means perfect symmetric flow pattern. As shown in Fig. 4.3, the asymmetry ratio changes with the pressure ratio in a similar manner at different valve openings. At fixed opening, as pressure ratio decreasing, the center meet point moves further and further to left until it reaches some point, then it starts to retreat and flow becomes more and more symmetric. At same pressure ratio, the flow is more symmetric at larger valve opening. The peak point occurs at higher and higher pressure ratio as valve opening larger and larger. At small opening and small pressure ratio situation, the asymmetry ratio has large oscillation. This is because at down stream there are big vortexes, which affect the accuracy of the asymmetry ratio.

To show the flow pattern in another way, the average velocity ratio between tangential component and overall velocity is defined to capture the speed angle at the center plane normal to plug surface. The more the tangential velocity ratio is, somehow means the more asymmetric the flow pattern is. It means that flow fully attaching the center point

of plug without any departure velocity component when the ratio is 1, and 0 means no attachment at the center point. The asymmetry trend in Fig. 4.4 confirms the trend in Fig 4.3.

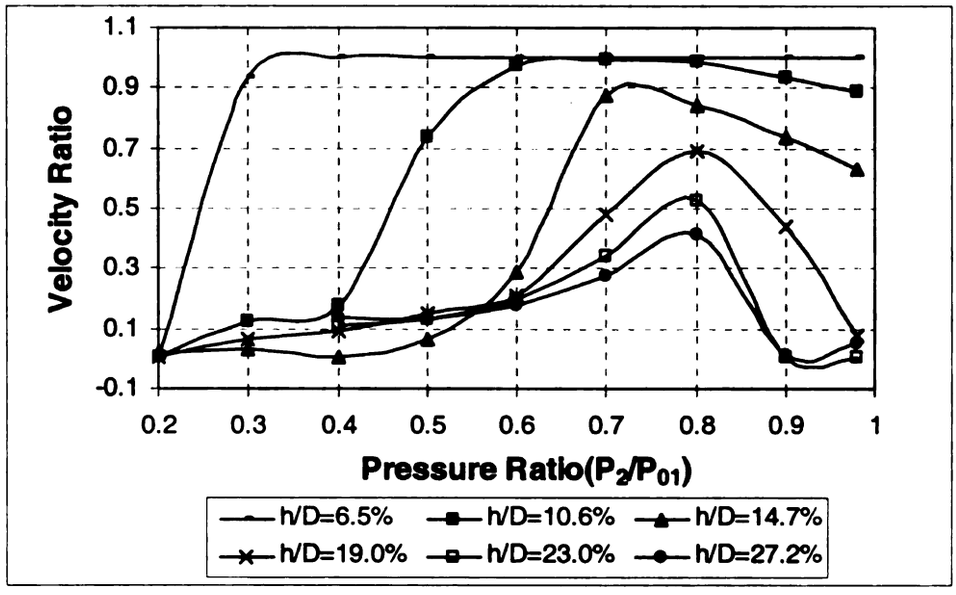

Fig. 4.4 Variation of average velocity ratio at center plane

To understand why the flow pattern phenomena happen, the passage of valve at each side is considered as a converging diverging nozzle. As the curvature of seat side is sharper and over diffuses the flow, the adverse pressure gradient is larger than plug side, which turns slowly. Thus separation is easier to happen in the seat side. At large pressure ratio, when the flow does not have enough momentum to form free jet, the separation in the seat side pushes it attaching to the plug surface. Because in the opposite side, flow has the same trend to attach to the plug, They fight each other for attaching to the plug. As the result, one side, for some reason has more momentum, pushes the other side flow attaching to the seat to reach a relative stable state. As a result, flow pattern (c) happens. At same opening, as pressure ratio keeps decreasing, both sides of flow have more momentum to become more straight instead of bending attachment, pattern (d) happens.

Finally both of them become symmetric free jets meeting at the center point, which form the pattern (e). This is how flow pattern changes at small openings. At large opening, the converging part of flow passage becomes shorter. Guided by upper side of plug surface, the flow has more vertical velocity component. The flow has more momentum to overcome the separation in seat side while the adverse pressure in plug side is larger. So flow of both sides attaches to the seat forming pattern (a). As pressure ratio decreases, flow departures from the seat side to form pattern (b). As pattern (b) developing further, two jets meet at down stream of seat. Commonly two meeting flow are not stable. Even the flow become more and more straight, they still do not have enough momentum to become free jets. So a more stable pattern (c) happens. After that, as pressure ratio decreases more, same story happens as small opening situation. The flow patterns change from (c) to (d) and (e).

4.2.2 Mass flow rate and total pressure ratio

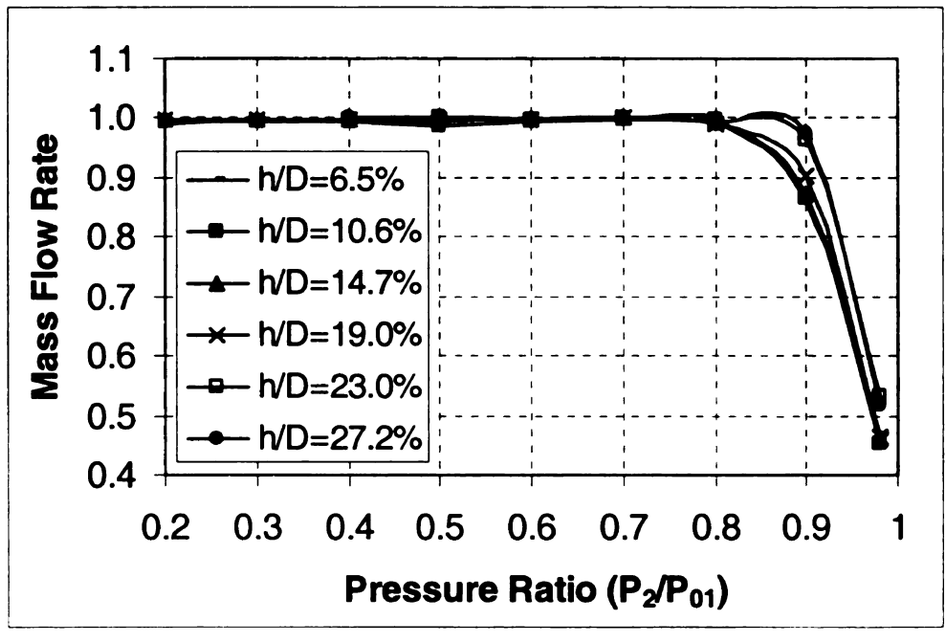

Fig. 4.5 Mass flow rate

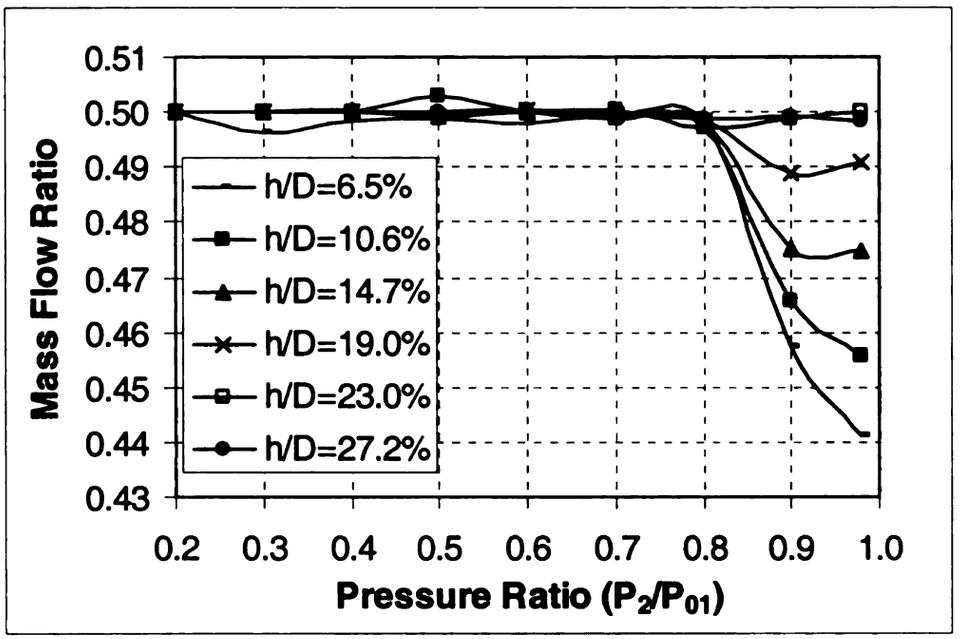

Fig. 4.6 Mass flow rate ratio between left side and overall

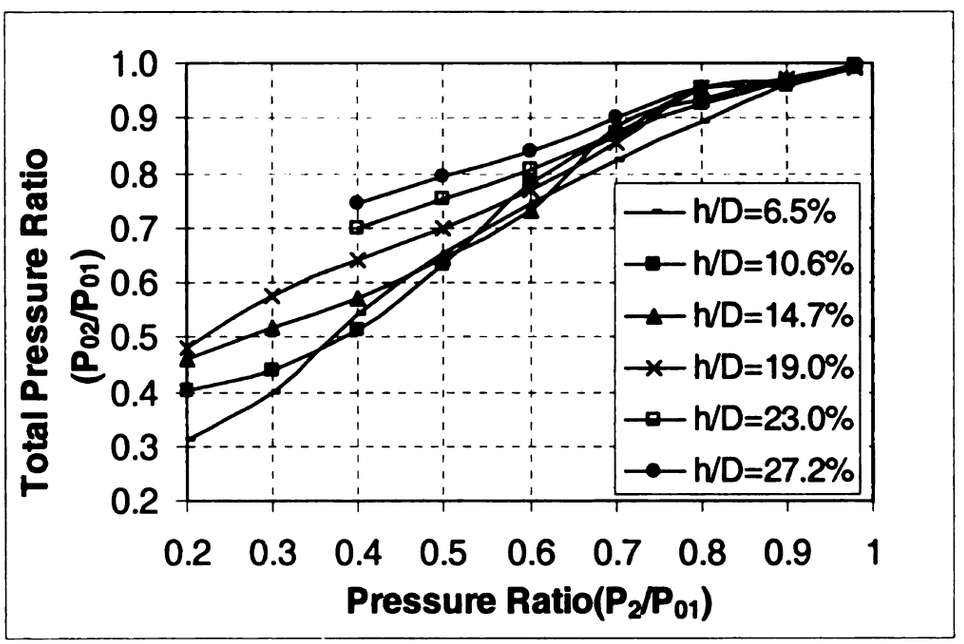

Fig. 4.7 Total pressure ratio

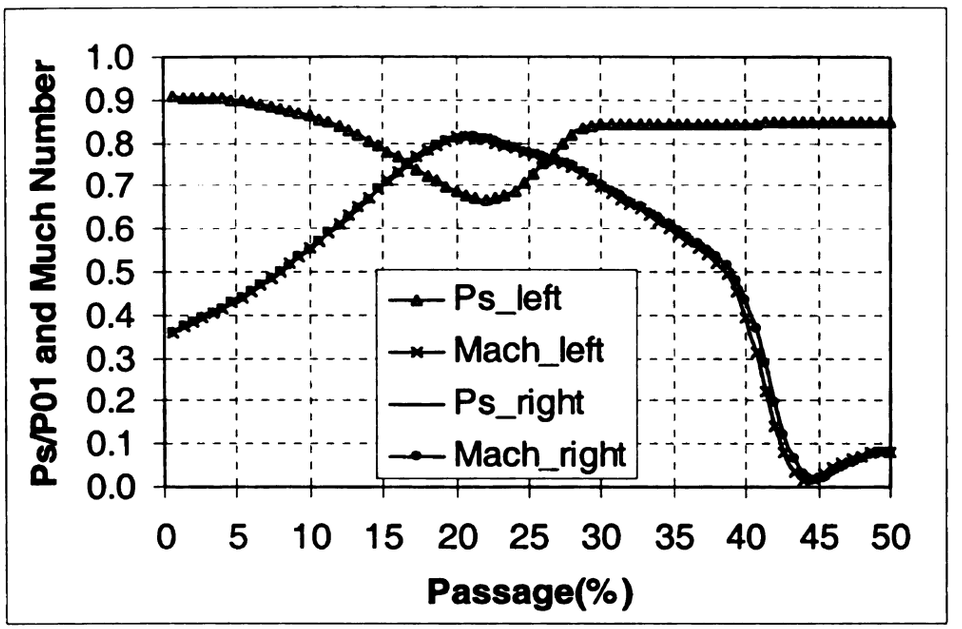

a. Pressure & Mach distribution for Pattern (a) h/D=10.6% P_2/P_{01}=0.2

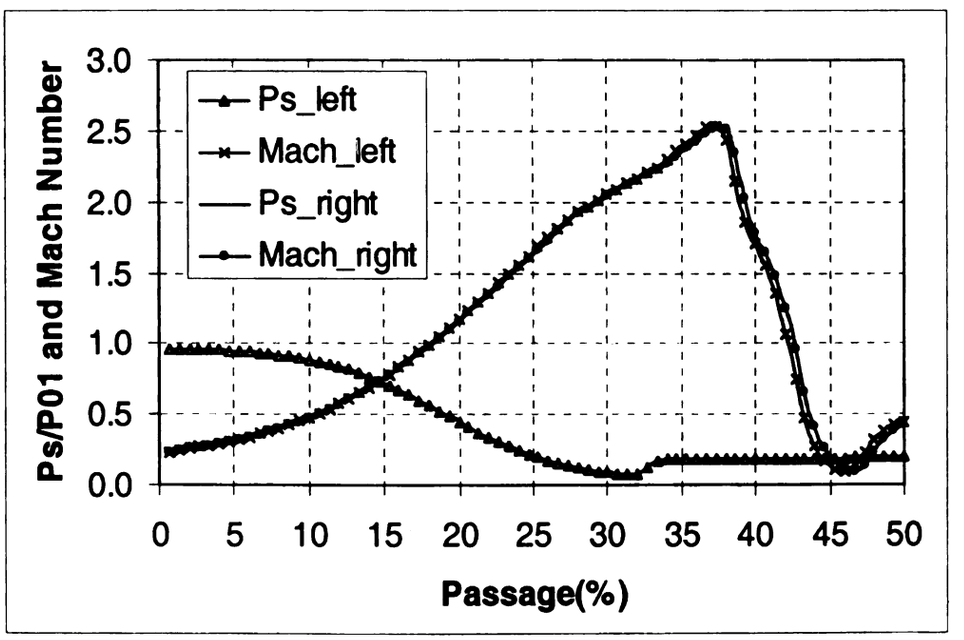

b. Pressure & Mach distribution for Pattern (e) h/D=23.0% P_2/P_{01}=0.9

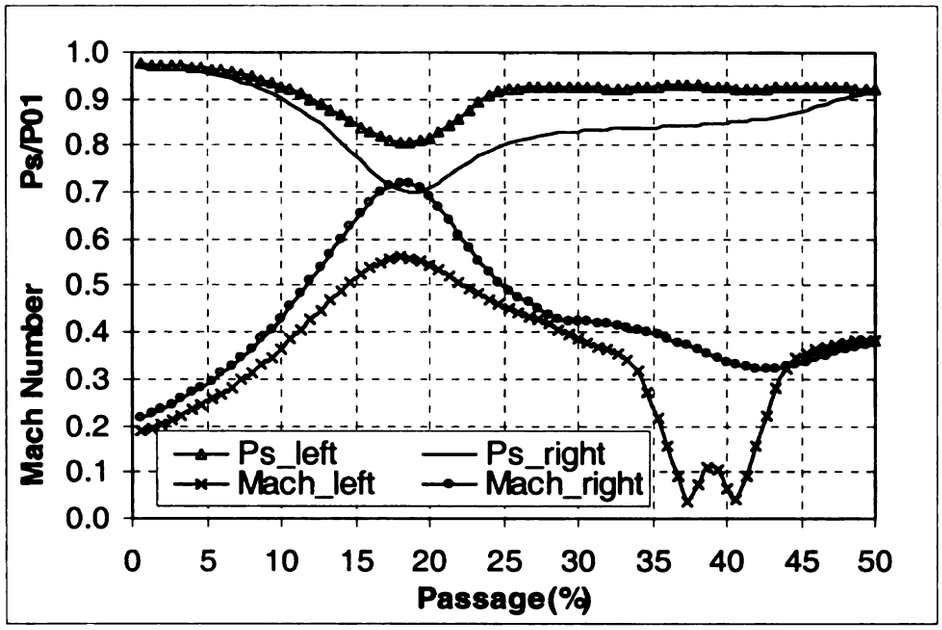

c. Pressure & Mach distribution for Pattern (b) Subsonic h/D=10.6%, P_2/P_{01}=0.9

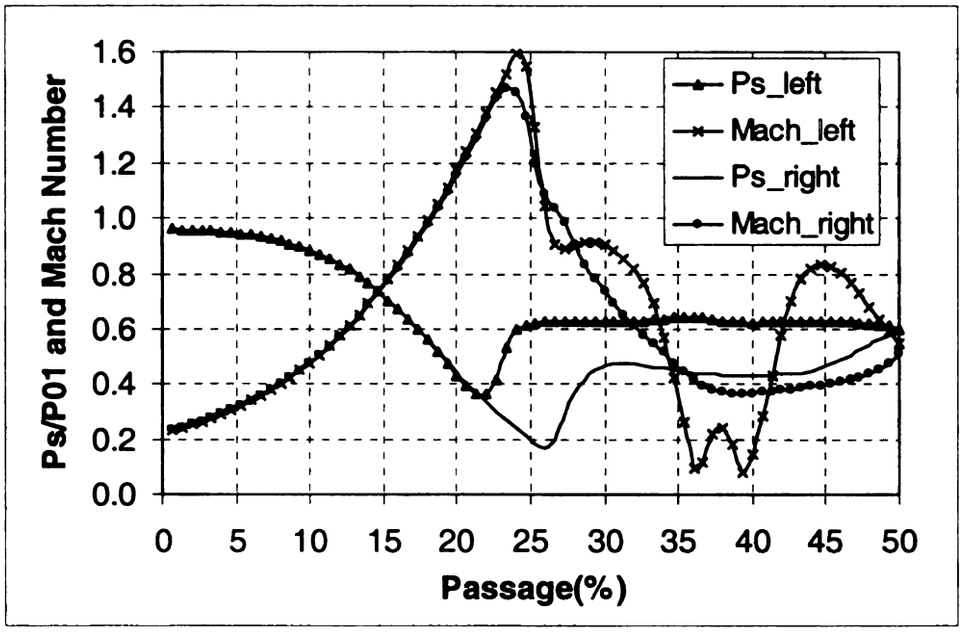

d. Pressure & Mach distribution for Pattern (c) Supersonic h/D=10.6%, P_2/P_{01}=0.6

Fig. 4.8 Pressure and Mach number distribution

Fig. 4.5 shows how mass flow rate changes with the pressure ratio at different valve opening. Because the valve exit area is much larger than valve throat area, the flow can

be choked at large pressure ratio. Mass flow rate passing the left side valve passage over overall mass flow rate is defined as mass flow ratio. As shown in Fig. 4.6, at large opening, they are symmetric. While at less opening and large pressure ratio, the mass flow rate at right side, which flow attaches to the plug, is more than the side, which flow attaches to the seat. This is either the reason or the result of asymmetric flow pattern. Less mass means less momentum in this side. So the flow retreats to attach to the seat in the battling with the other side, which attaches to the plug. This also can explain why the flow at large valve opening is choked at larger pressure ratio than small openings in Fig. 4.5, because for symmetric inlet mass flow rate, two passages choke at same time, while for asymmetric situation, one chokes after another.

Total pressure ratio changing with the pressure ratio and opening is shown in Fig. 4.7. It drops as pressure ratio decreasing. Normally, at same pressure, at larger opening, total pressure ratio is larger, which means total pressure loss is less. There is no big difference at large pressure ratio.

4.2.3 Pressure along the valve surface

Corresponding to flow pattern, there are symmetric or asymmetric pressure patterns as shown in Fig. 4.2. The pressure ratio and Mach number along the plug surface are shown in Fig. 4.8 for pattern (a), (c) and (d). 1 of x-axis means value in left or right end (i=1), while, 50 means data gotten from the center of plug (i=75). The Mach number is obtained at j=25 (j=1 is plug surface, j=50 is seat curve and interface between center block and seat block) to capture the main flow situation. Except d. in Fig. 10, which shows the Pattern b in supersonic flow situation, all other plots are identical cases with corresponding plots in Fig. 4.2.

For symmetric pattern (a) and (e), the pressure and Mach number distribution are symmetric also as shown in a. and b. in Fig. 4.8. Pressure drops and Mach number increases. The sudden flat pressure line in converging part is due to separation. For Mach number, because it is not following the flow direction after throat, it does not capture the shock wave accurately in supersonic flow situation. But it captures the vortex phenomena. The minimum Mach number captures the center of vortexes in both sides.

The pressure and Mach number is asymmetric when flow pattern is asymmetric. For pattern (c) at large pressure ratio, flow is subsonic. As the mass flow rate of flow attaching side is larger than the other side, the Mach number is larger and pressure is less. Because the separation happens much earlier in left side and no separation happens in attaching side, there is a pressure jump in left side. For supersonic flow, before throat, every thing is symmetric. After throat, pressure is recovering in both sides. Because separation happens earlier, the pressure jumps earlier in left side.

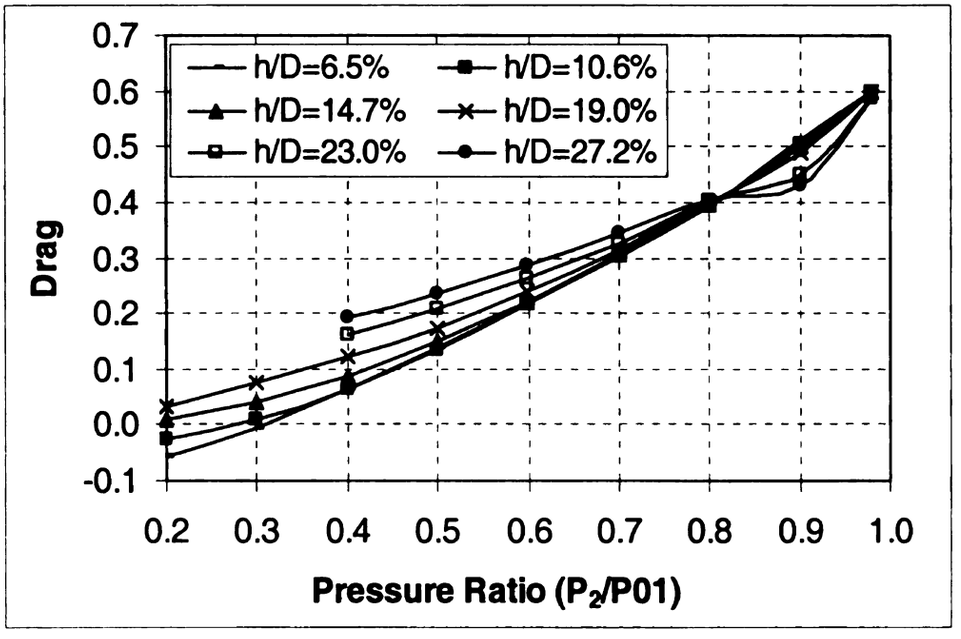

Fig. 4.9 Vertical force on plug

4.2.4 Forces and moment caused by fluid

In highly turbulence flow, there are many mechanisms that can cause unsteady forces and moment, such as pressure oscillation and instability of separation or even plug asymmetry with seat by manufacturing error. All of these make it almost impossible to predict forces acting on valve. But it is very important to understand the steady forces and moment acting on plug, which can help to understand fluid structure interaction mechanism.

The dimensionless drag is shown in Fig. 4.9. Drag increases as pressure ratio increases. The curves are almost linear at small valve opening or after choke at large valve opening. This trend agrees with the theory analysis in Chapter 2. At different opening under same pressure ratio, the drag is less at large opening after flow is choked. The equation cannot predict this changing, but according to some data from industry, this is true.

Dimensionless lateral force and moment caused by drag are shown in Fig. 4.10 and Fig. 4.11 respectively. They are defined as same way as dimensionless vertical force, for lift, substituting drag with lift and for moment, with moment over plug radius in numerator. Essentially, they are caused by the asymmetric pressure distribution along plug surface. They have same trend and almost similar amplitude, which can be proved analytically by integrating along the plug surface. The positive value means that for moment the direction is clockwise, while the lateral force points to right. At fixed valve opening, as pressure decreasing, the lift and force increases until reaching a peak value then decreases. At same pressure ratio, as valve moving toward the seat from wide opening, the moment and force increases until reaching peach point at about 11% of

opening ratio, then started decreasing. Even they are not simulated, for maximum opening and fully closed situation, this becomes fluid static problem, both moment and force become 0.

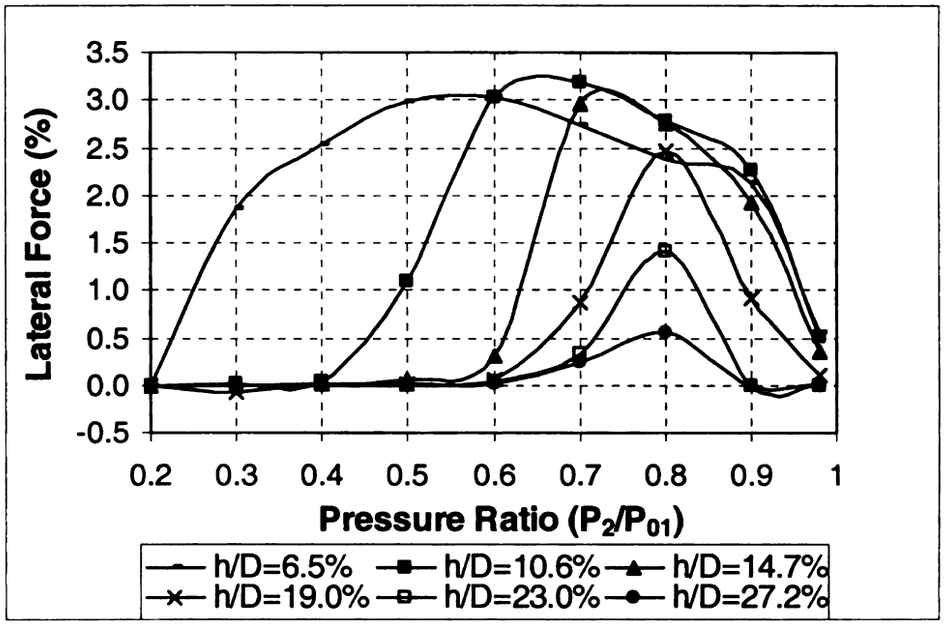

Fig. 4.10 Variation lateral force

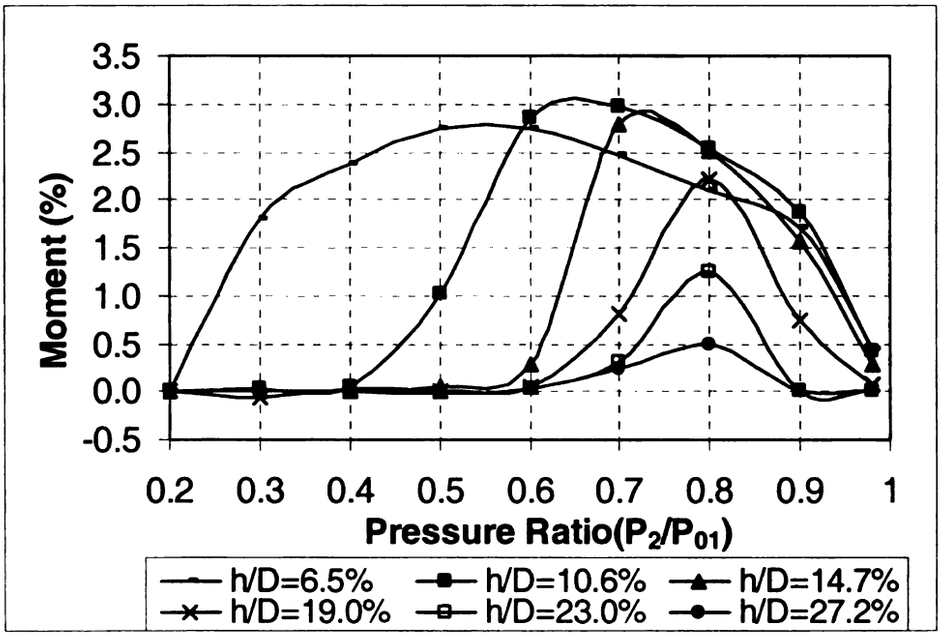

Fig. 4.11 Moment caused by vertical force

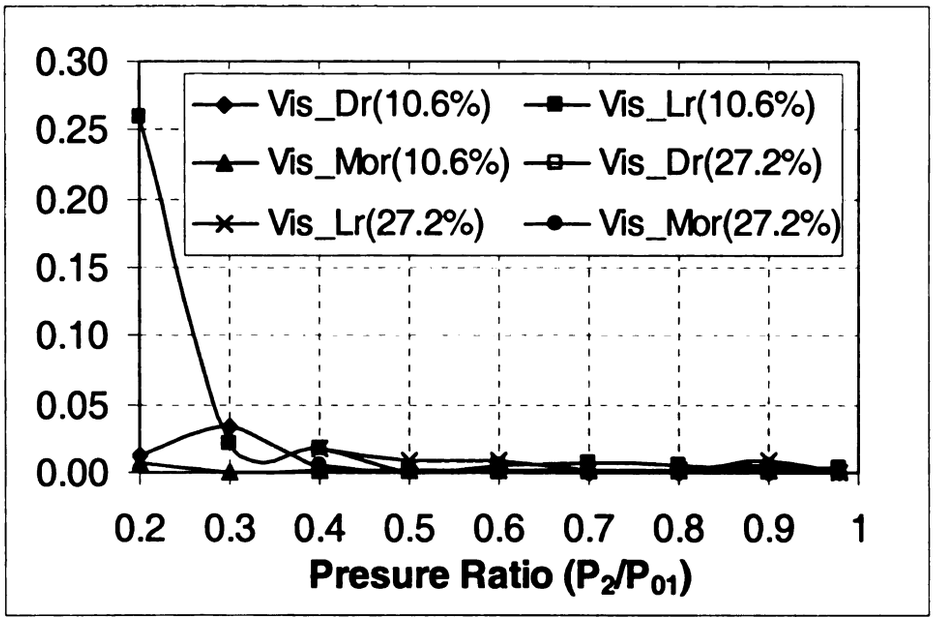

Fig. 4.12 Ratio of viscous to total forces and moment

With the fact the amplitude of dimensionless lift and moment are about the same, the equation (3) can be simplified to $Mo \approx L \bullet (l_r - 1)$ with the counterclockwise direction. lr is the ratio between stem length and plug radius. Normally lr is much bigger than 1, which means the lift defined the amplitude of total moment and the direction.

The forces and moment mentioned above are total forces and moment including both friction and pressure difference. Fig. 4.12 shows that the viscous force and moment is only a little fraction. At small pressure ratio, the viscous lift accounts a little bit more. For example, at 10.6% opening, the viscous lift ratio is about quarter of total lift. This is because the total force is very small at small pressure ratio.

Understanding fluid mechanism at steady state

All parameters we mentioned above are shown in Fig. 4.12 for 10.6% opening situation. The dimensionless lift and moment are 1/3 of their original value to show other curves clearly. Average Mach number is obtained at the same plane of the average tangential velocity component ratio obtained.

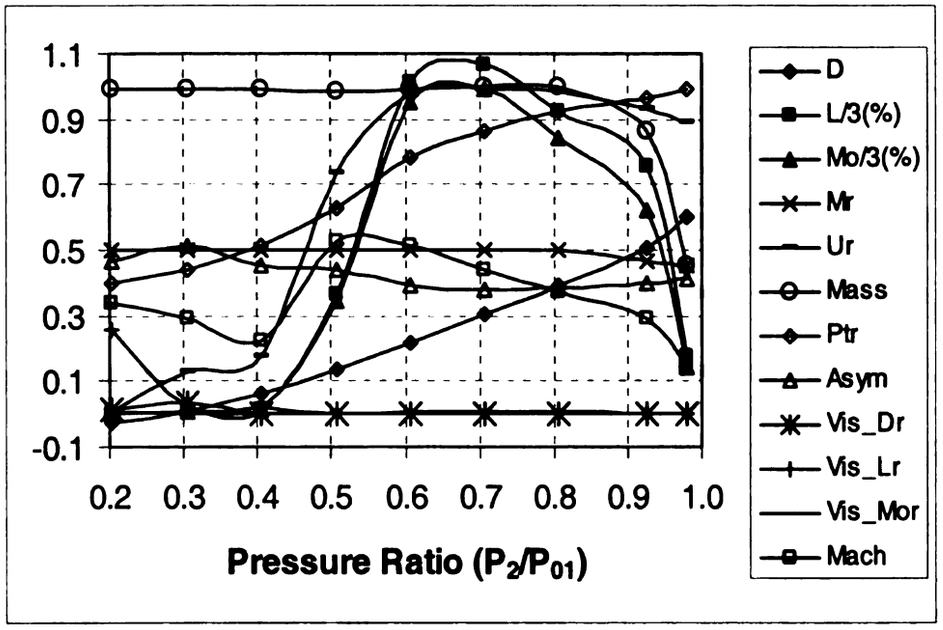

Fig. 4.13 Variation of parameters at different ratio at fixed opening of 10.6%

As shown in Fig.4.2 and 4.8, there is huge pressure distribution between two sides in Pattern (c) comparing with others. Pattern (b) and (d) are less asymmetric, while pattern (a) and (e) are very symmetric. By comparing the lift and moment amplitude in Fig. 4.13, it is very clear that it is the flow asymmetry that makes the pressure distribution along the vale surface asymmetric and finally causes big amplitude lift and moment. This is confirmed by Fig. 4.13 in a more qualitative way. Two key parameters determine the lift and moment amplitude, flow asymmetry and pressure difference. The Mach number represents the pressure difference, because according to thermodynamics compressible

flow theory and Fig. 4.8, at same inlet pressure, pressure decreases as Mach number increasing. That means with Mach number increasing, the average pressure in the plug attachment side decreases, and more pressure difference occurs between two sides. Also another important factor, asymmetry ratio, means how much difference of acting area of two sides of the flow. The more the ratio is, the bigger the area difference is. The force is pressure times area, so some how, the trend of lift and moment changing is defined by Mach number timing asymmetry ratio as shown in Fig 4.13. In high pressure ratio, the asymmetry ratio decreases a little bit, while Mach number increase quickly. This causes the steep slope of lift and moment as pressure ratio is higher than 0.9. Then asymmetric ratio starts to decrease, while Mach number increase slowly, the lift increasing speed slows down until reaches the peak value in between the pressure ratio of highest Mach number and Lowest asymmetry ratio. Then it drops quickly as Mach number drops and flow becomes more symmetric.

4.2.5 Fluid structure interaction mechanism

It is far from enough to only understand the steady state flow mechanism. In reality, plug vibrates driven by the forces and moment, which affect the fluid forces also. To understand the interaction mechanism, displacement is added in both vertical and lateral directions on valve plug.

Interestingly for subsonic flow, symmetric geometry causes asymmetric flow while asymmetric geometry causes symmetric flow. When the plug moves from its balanced position, the flow pattern changes from (c) to (a) immediately and keeps the pattern. This means that in large pressure ratio, the asymmetric flow pattern does not have strong stability, it always has tendency to become symmetric. For sonic or supersonic flow, the

flow pattern (c) is very stable. There is no result showing that it changes pattern due to geometry asymmetry.

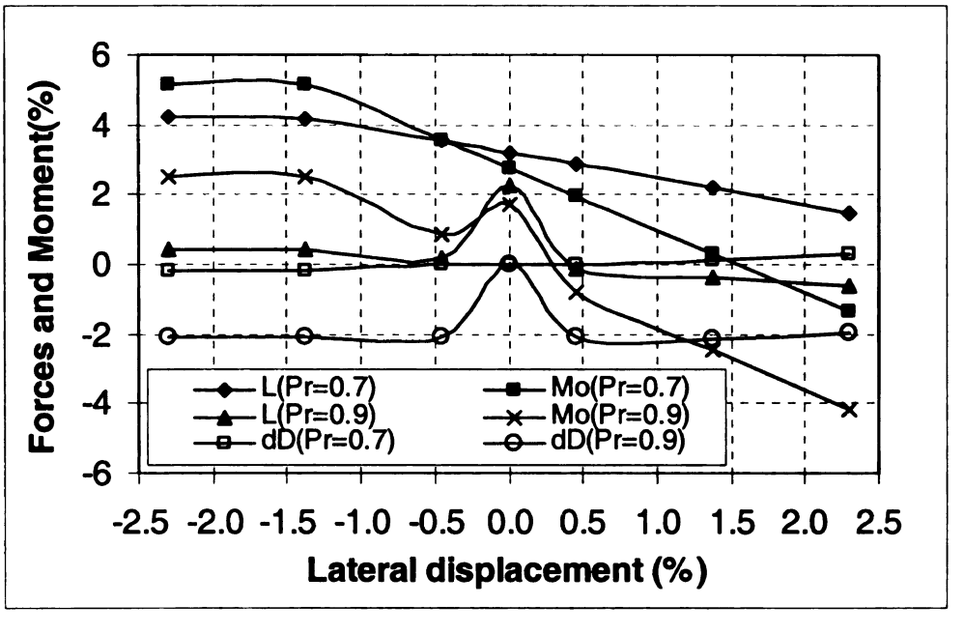

Fig. 4.14 Forces and moment changing due to lateral displacement on plug

By looking at the forces and moment change due to plug displacement, it is clear that the plug lateral vibration is due to hydraulic forces and it also affects the vertical force, which can cause or strengthen the vertical vibration. The data in Fig. 4.14 are obtained when opening ratio is 10.6%. Driven by lift, the plug moves to positive direction, then the excitation amplitude drops. It reaches some maximum displacement position, forced by the combination of stem bending force and dropping hydraulic force. Then it moves back. It reaches some point in other side, and come back again.

This is a typical self-excited vibration mechanism. For subsonic flow, the excitation looks like a part of sin wave, while for supersonic flow is linear by simple assuming that plug vibrates within in –0.5% to +0.5%. The vibration center point is defined as x=0 point. Then the excitation for supersonic flow can be expressed as y=kx, while subsonic

y=ksinx. By assuming, the vibration is perfect harmonically, x=sint, then the two excitation basically can be expressed in time, as part of sin wave as shown in Fig. 4.15. By using Fourier series, the periodic excitation can be expressed as infinite series of sin or cos wave. If there is a frequency matches the plug natural frequency, resonance happens, which can cause huge amplitude lateral vibration.

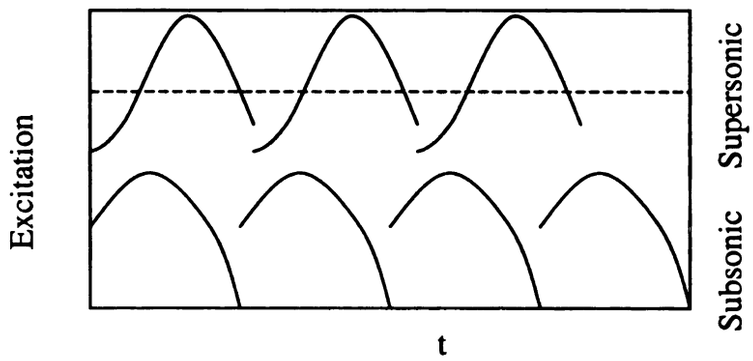

Fig. 4.15 Excitation under lateral vibration

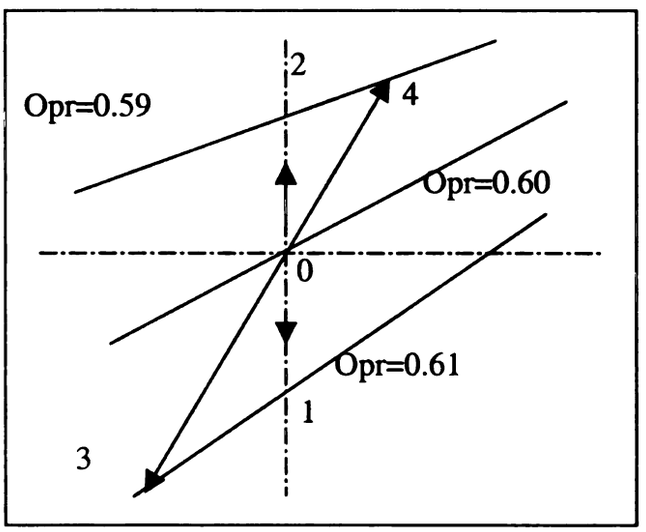

Fig. 4.16 Self-excitation mechanism in vertical direction

Plug lateral movement not only has effect on lateral excitation, but also has strong effect on vertical excitation when flow is subsonic as shown in Fig. 4.16 in the same way and at about same amplitude. That means the excitation can be expressed as same equation as lateral subsonic excitation. Also, resonance may occur. When flow is

supersonic, the lateral force has very little influence on drag. So in this way, the worst situation for the valve probably happens in large pressure ratio, when both lateral and vertical vibration resonate simultaneously.

The vertical vibration can be analyzed by using the same way as lateral vibration. Fig.5.7 shows clearly how the vertical displacement affects the drag. At pressure ratio about 0.8, there is little difference between the drag in different opening. As the pressure ratio departure to less, the difference becomes larger and larger due to different curve slopes. The smaller the opening is, the steeper the curve is. To explain it clearly, enlarged sketch is shown in Fig. 4.16. For example, if at balanced position opening ratio is 0.6, when the plug moves toward larger openings, such as 0.59, instead of reduce the value, the vertical force becomes bigger, pushes the plug further until stem spring force push it back. When the plug moves to small opening, as drag drops, same thing happens. In reality it is even worse because the pressure ratio changes with opening. So instead of oscillation in the cycle of 1-0-2, the drag oscillates within bigger cycle of 2-0-4. This is typical self-excitation mechanism. For pressure ratio larger than 0.8, reverse process happens which means it is impossible to form the self-excitation mechanism. In reality, the valve is operated either at large pressure ratio with large opening or small pressure ratio with small opening. So, based on above analysis, the self-excited vibration can only happens in small opening situation, which is confirmed by former Soviet Union researchers.

The vertical force has strong influence on plug lateral vibration in the blank area between two nearest lines in Fig 4.16. For example, if the plug vibrates between the opening ratio 6.5% and 10.6%. At pressure ratio of 0.4, the lift changes from 0 to 2.5. Of

course, no plug can vibrates with such large amplitude in reality. This example is just to show how the lift changes. The influence of pressure ratio changing due to vertical vibration make the problem more complicated

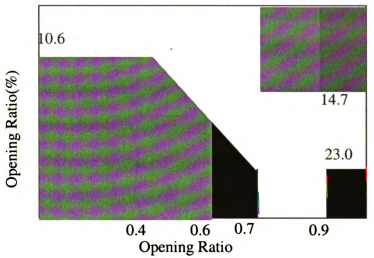

Fig. 4.17 Sketch of valve safe operation area

Based on all above analysis, all areas may cause problem are superposed in following Fig. 4.17. In the darker area, possibility that the valve has serious problem is less. It is hard to accept such a narrow safe operation area. So the design should be improved to reduce lateral and vertical vibration excitation mechanism.

4.3 Analysis on improving design

Reducing the lift and moment acting on valve at balanced position is very important to reduce vibration, because they are the driven excitation of valve vibration. The key to improve design, in terms of reduce lateral force and moment, is making the flow pattern symmetric. As we analysis before, the asymmetric flow attachment on plug side is one important cause of flow asymmetry. Also, we know that the longer the flow attach the

plug side, more possible that it cause unbalanced force. So the main idea to improve the valve design is to make the flow attach the seat side and separates earlier in plug side

4.3.1 Possible improved designs

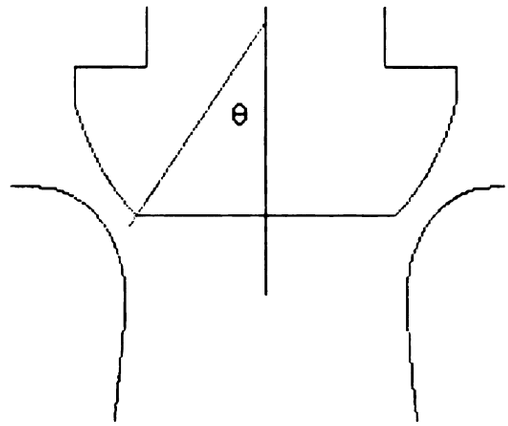

Fig. 4.18 Flat cut design

As we know that stall happens in a position where the wall curvature changes sharply, a simple improved design came out by cutting center part of plug at the angle θ shown in Fig. 4.18. To show the influence of cut angle on lateral force clearly, the value in Fig. 4.19a is the absolute ratio of lateral force for cutting edge valve and maximum lateral force for original valve (L_{omax}). Similar with original design, lift changes with pressure ratio. But the range of pressure ratio with large amplitude of lateral force decreases as θ increases. This is due to the decreasing of asymmetric flow pattern region and interaction area between plug and fluid. For original valve, asymmetric flow pattern occurs when pressure ratio is higher than 0.5. For 44.9° cutting design, only symmetric flow patterns can occur. In Fig. 4.19b, the absolute ratio of maximum lift and original valve maximum lift is plotted with different cut angle. From θ=0° to about 30°, the maximum lateral force (L_{max}) decreases slowly. From θ=30° to about 40°, lateral force decreased dramatically. After 40°, there is little force remaining, under such situation and only symmetric flow

patterns happen, pattern (a) at large pressure ratio and pattern (c) at small pressure ratio. This design is called flat cut.

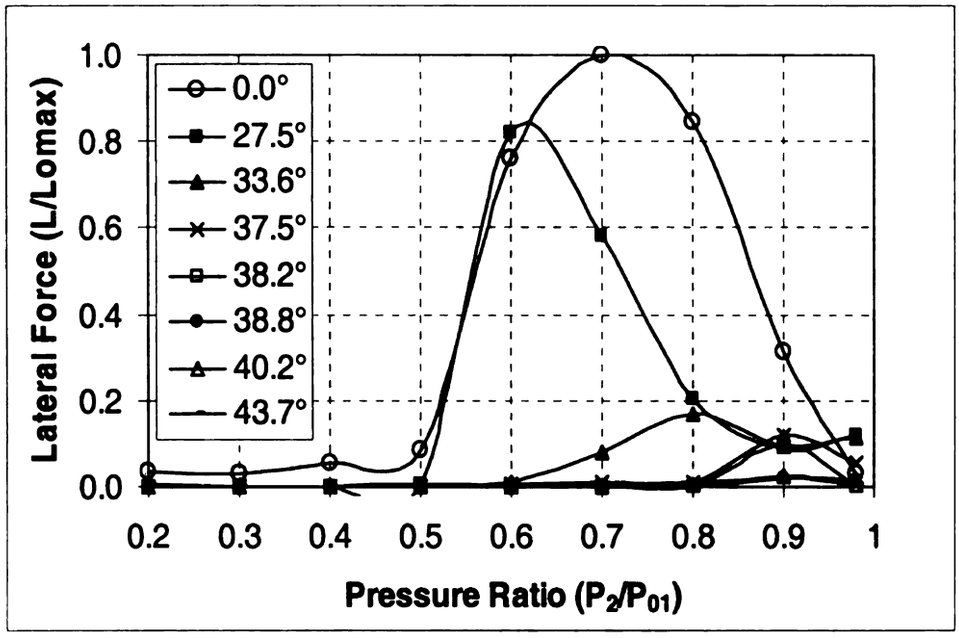

a. Variation of lateral force with pressure ratio at different cut angle

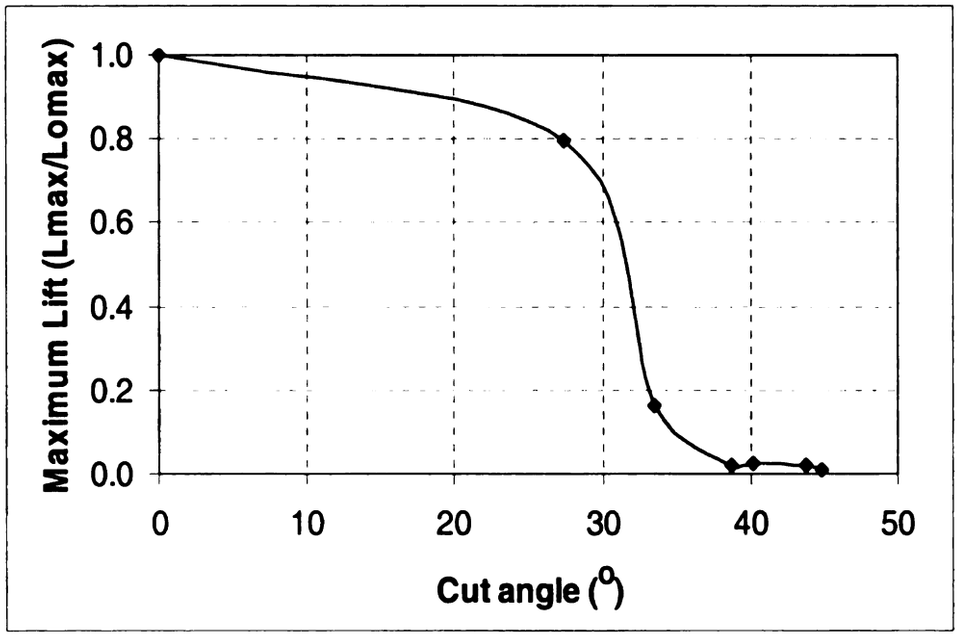

b. Variation of maximum lateral force with cut angle

Fig. 4.19 Variation of lateral force under different cut angle at 10.6% opening

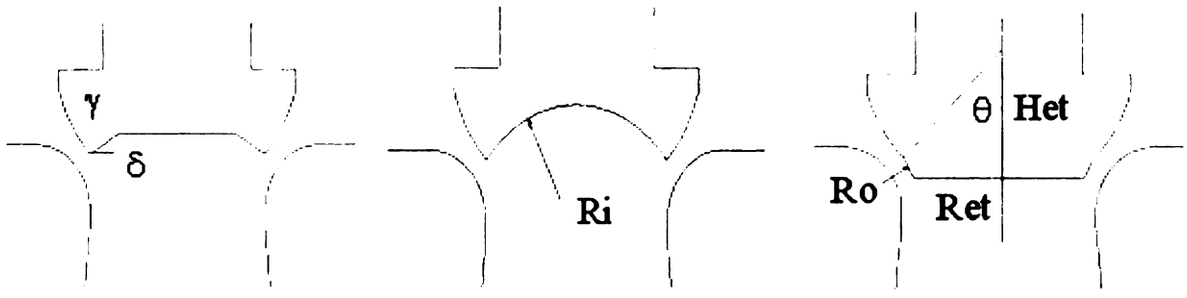

a. Arc cut b. Dish bottom c. Guiding

Fig. 4.20 Three other improved designs

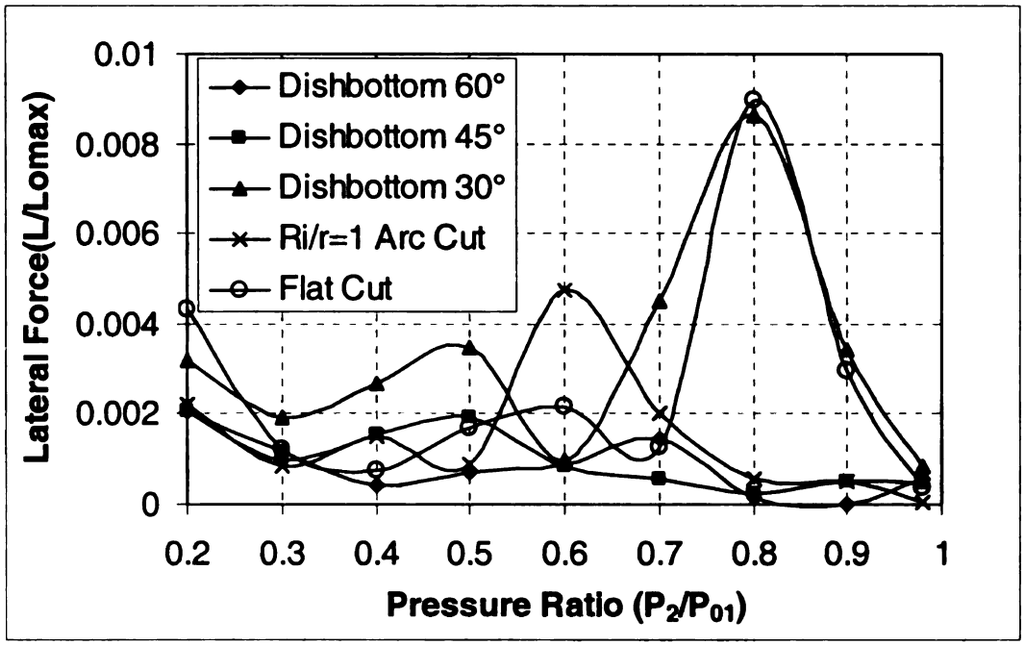

Fig. 4.21 Comparison of lateral force at Opr=10.6% for different designs

Five other improved designs were simulated. The cut angle θ is 45°. For arc cut, Ri/r=1, for dish bottom, δ=60°, 45° and 30°, h/r=0.15. The lateral force ratio of between improved designs and maximum value of original design (L_{omax}) is shown in Fig. 4.21 for different designs. Both arc cut and dish bottom design are better than flat cut. For arc cut, when Ri/r is 1, the lateral force reduced to half of flat cut design (Ri/r=∞). In this way, reduce Ri can further reduce lateral force. For dish bottom design, the lateral force decreases as δ increases. From δ=30° to 45°, the lateral force has a big decrease, after

45°, there is no big drop in lateral force. For example, when δ=60°, the maximum lateral force reduced to about 1/5 of flat cut design. Plug corner angle γ is defined as the angle between tangential direction of plug side profile with cutting edge as shown in Fig. 4.20. In this case, the corner angle is reduced in this way, flat cut, dish bottom 30°, arc cut (which is 45°) or dish bottom 45° and 60°. This is just the way that lateral force reduces. So in our view, making the corner angle sharper is an efficient way to reduce lateral force at constant cut angle. The dish bottom design is better than arc cut design if the corner angle is same.

Compared with above improved designs, the guiding design as shown in Fig. 4.20c is more "active". The curvature of plug not only can cause separation happen in plug side by the sharp corner, but also can guide flow attaching the seat side. Thus lateral force and moment can be reduced. It basically is welding an extended part on the flat cut plug. Four parameters defined the plug curvature, cutting angle θ, extending height ratio Het/r, extending radius ratio Ret/r and the extending radius Rc. Because of so many parameters, two of them are fixed, the cutting angle θ=45°, and the extending radius Rc equals the seat side cure radius. Under opening ratio of 10.6%, two different combinations, H_{et}/r=0.65+R_{et}/r=0.68 and H_{et}/r=0.75+R_{et}/r=0.59, are tested and result is shown in Fig. 4.22. To show all the curves clearly, the value of second combination is 1/6 of actual value. Compared with original design, both designs can reduce the lateral dramatically. The peak lateral force, such as under pressure ratio of 0.7 is caused by asymmetric separation after the flat cut part. Separation is sensitive to extension curvature. For example, the peak value of second combination is 15% of original design but is about 13 times of first combination. A well guided design, such as the first combination, can

reduce the force to the same level of flat cut design or maybe even better. More simulations need to be done to optimize guide valve design due to so many parameters defining the curvature.

According to above discussion about improved designs, the flat cut and dish bottom designs are preferred because they can reduce excitations dramatically and also easier to be manufactured than the guiding design.

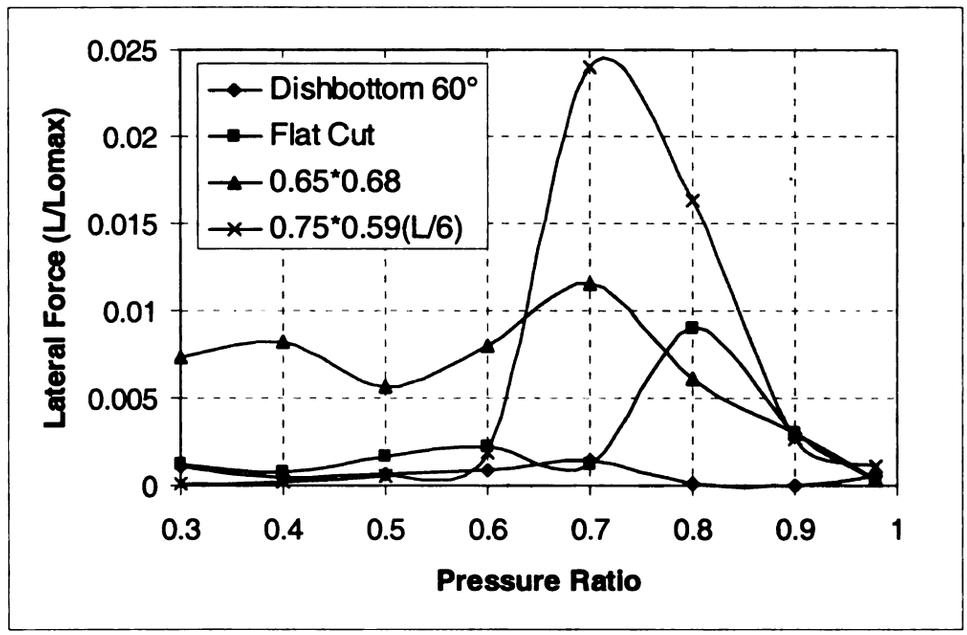

Fig. 4.22 Comparison between improved designs at 10.6% opening

4.3.2 Other tested designs

As shown in Fig. 4.23, four other designs were also simulated. The plug radius was increased two times to be design (a), one half time and being cut to be design (c). A semisphere was welded on the flat cut is design (b). Design (d) is a simple guiding design. The CFD results under 10.6% opening are shown in Fig. 4.23. All designs are better than original valve in terms of lateral force, especially at large pressure ratio. But

still dish bottom (60°) design is better than them at large pressure ratio as shown in Fig. 4.24.

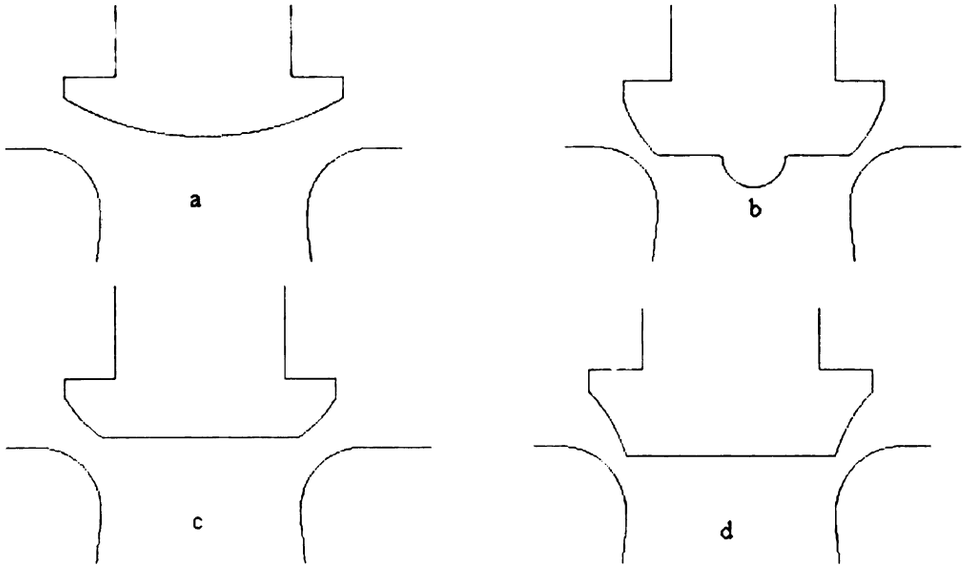

Fig. 4.23 Several other designs

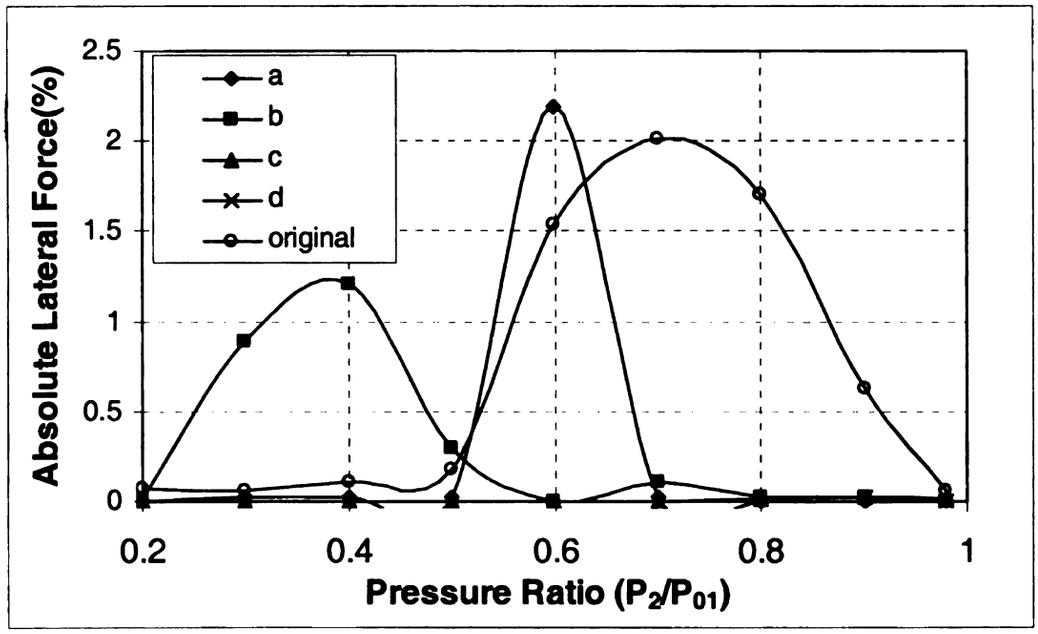

Fig. 4.24 Comparison with original design at 10.6% opening

4.3.3 Discuss on an improved design

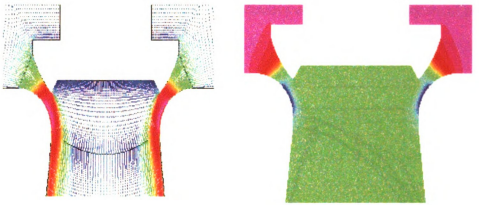

a. Pattern (a) for improved design

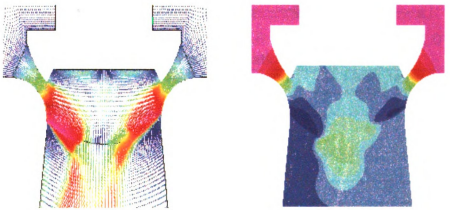

b. Pattern (c) for improved design

Fig. 4.25 Flow patterns for improved valve design

Based on above analysis, the dish bottom 60° is a simple and good design. So the detail CFD results are discussed here. Only Pattern (a) and (d) happens for the new design as shown in Fig. 4.25. Under same opening, flow pattern changes from (a) to (d) at almost same pressure ratio as old design changing from pattern (c) to (d). Due to this reason, the lift and moment are reduced dramatically as shown in Fig. 4.26a. The drag of new design is almost same as old one as shown in Fig. 4.26b. To compare the difference

of them, the drag value at opening ratio of 14.7% is doubled for both old and new design. Even though there is no big difference found. Viscous effect is only a very small portion as same way as for the old design.

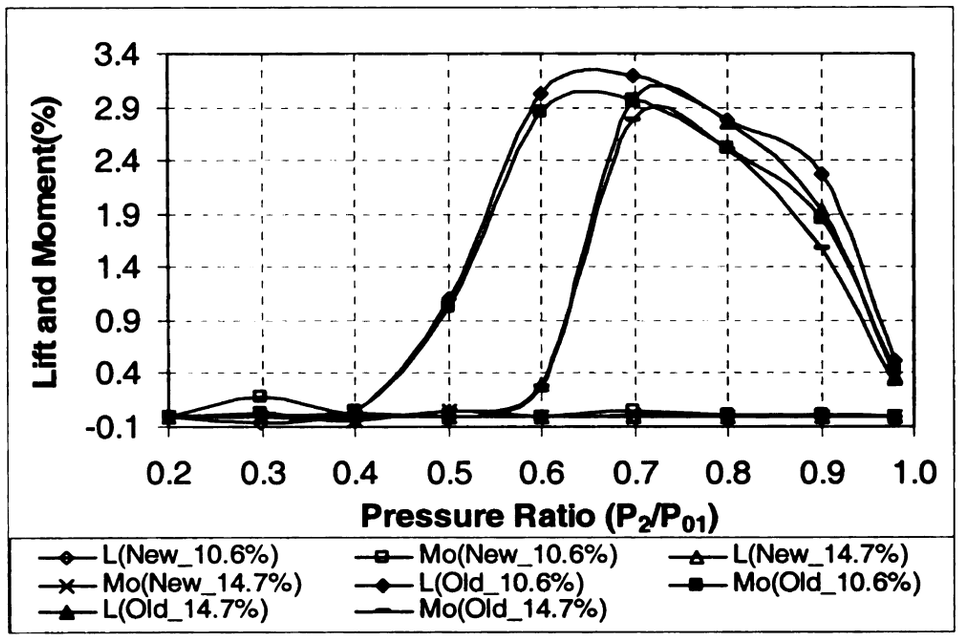

a. Lift and moment

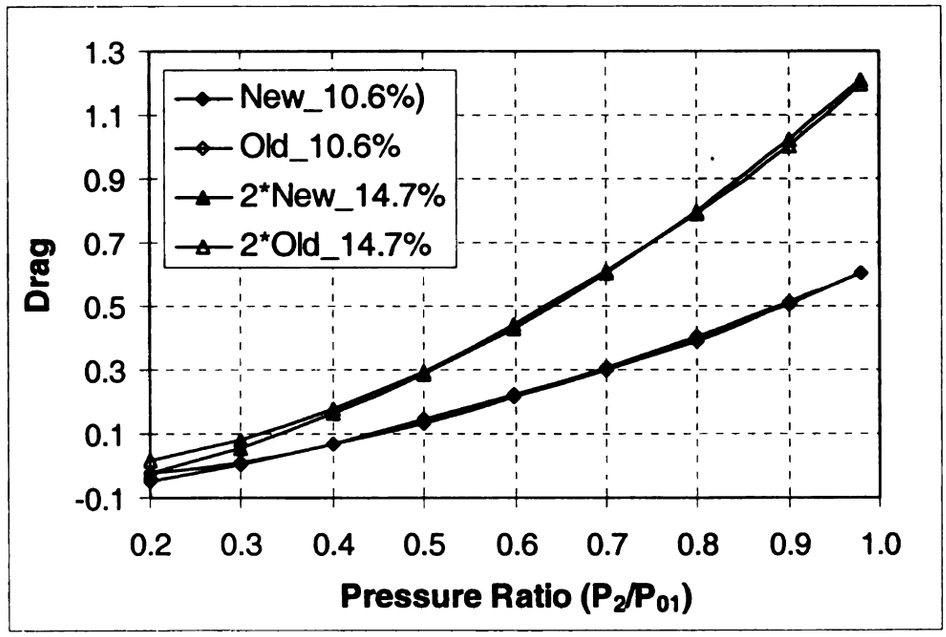

b. Drag

Fig. 4.26 Comparison of lift and moment between old and improved design

Because at the plug balanced position, the lift and moment is very small, the bending moment, which pushes the plug to one side, is eliminated. To understand the fluid structure mechanism, plug lateral displacement is added as same way of the old design under same opening and pressure ratio, Opr=10.6%, Pr=0.9. As shown in Fig. 4.27, the lateral displacement has no influence on vertical force. This eliminates the vertical vibration excitation due to lateral vibration for old design. For lateral force and moment due to vertical force, symmetric result around 0 obtained as the valve moves from one side to the other side. The moment has linear relation with lateral displacement similar to the supersonic result of the old design. Amplitude of lift changing is much less than the old design and only occurs at near center point region. At same 0.46% displacement, lateral force and moment caused by drag changes very little, while drag changes linearly. So that means the excitation due to pressure oscillation (vertical vibration) is limited.

When for some reason, such as pressure disturbance of upstream, the plug starts move to positive displacement position. The lift becomes positive and increasing. The moment becomes clock wise and increases in amplitude. Both combines together to push the valve moving further. This is a typical self-excitation mechanism, which is not found for the old design at same situation. For two reasons, it is still believed a much better design than the old one, first, the self-excitation is not strong as the amplitude of lift is very small; second, at the valve balanced position, there is no steady bending moment to cause the valve displacement.

Because the drag changing with openings remains same, the self-excitation mechanism still exits for new designs at small pressure ratio. But as shown in Fig 4.28, the difference of the lift and moment at different opening is much less than old design at

any region. So it eliminates the lateral excitation due to vertical vibration. Based on above analysis, the new design is better than current design in terms of forces, moment and fluid structure interaction.

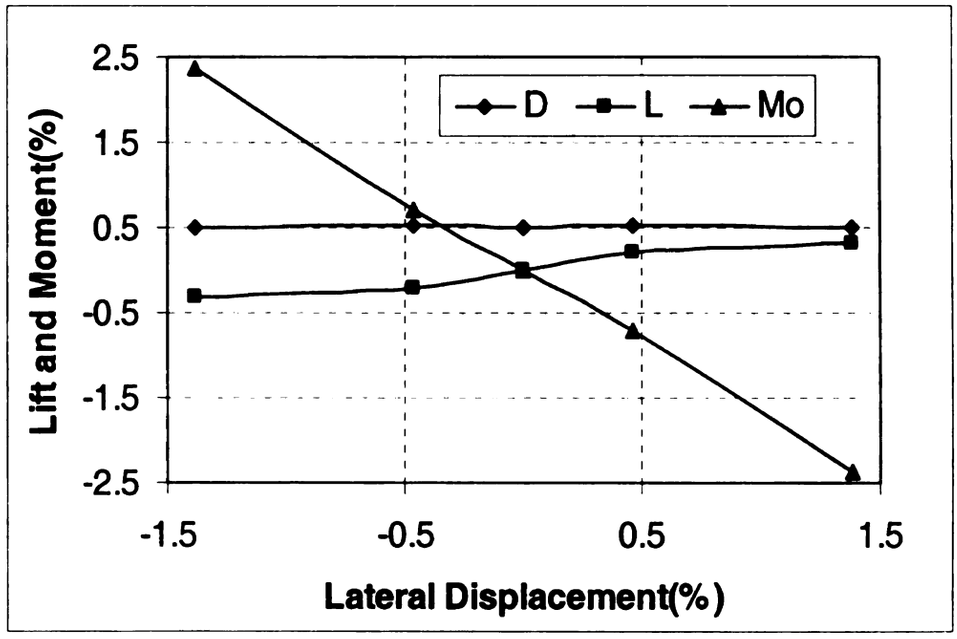

Fig. 4.27 The forces and moment changing due to lateral displacement

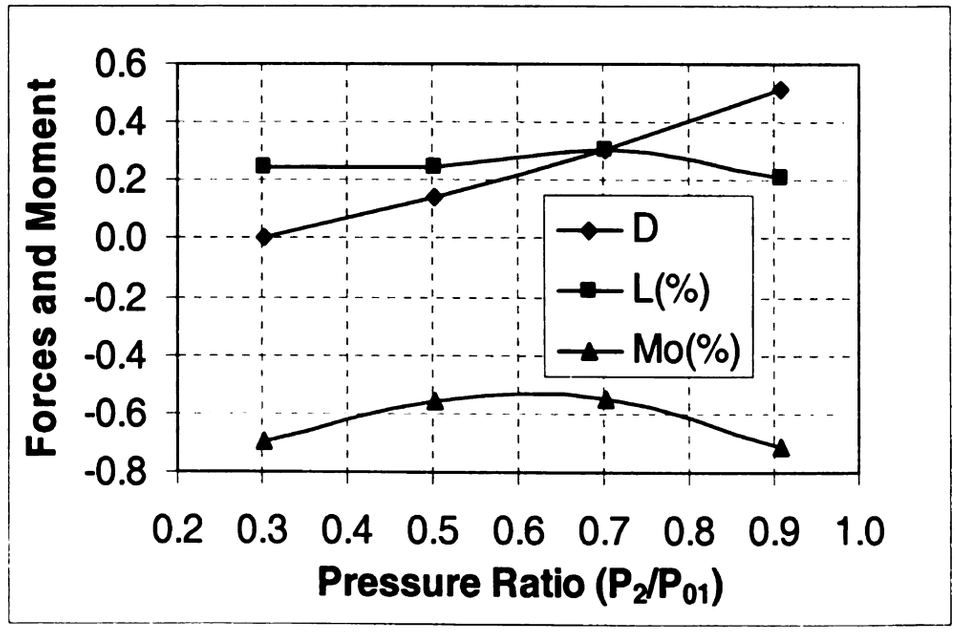

Fig. 4.28 The forces and moment changing at 10.6% opening

CHAPTER 5

3-D CFD ANALYSIS

5.1 Numerical Modeling

CFD is used to get the steady state flow field, forces and moment at balanced position of the plug for 3-D flow following the similar process as 2-D CFD analysis. Calculations were performed using TASCFLOW. CFX-BUILD was used to generate the grids. For convenience to build grid, the coordinate is moved from position shown in Fig. 2.5 in the –z direction to a position where x-y and seat throat are in same plane. According to 2-D analysis, up stream air chest has little effect on simulation results, as long as symmetric boundary conditions are used. To save time and be more general, chest is not simulated. Totally 290,124 nodes, whole grid composes four blocks as shown in Fig. 5.1, z>0, outside ring-shape block (i=41,j=81,k=31), center box-shape block (i=21,j=31,k=21); at z<0, seat ring-shape block (i=81,j=81,k=21), center box shape block (i=21,j=81,k=21). Because simulations were done for different valve openings, the throat grid (z>0) size changes to make grid density about the same. Grid density around the plug is much greater because this is the most concerned area. The flow is treated as steady state, compressible, turbulent ideal gas with high speed. For inlet boundary condition, constant total pressure and total temperature are imposed. The wall (Fig.5.1 b) is treated adiabatic smooth surface. Constant static pressure is used at valve exit. All cases were converged to maximum residence in the order of 10^{-3}. The y+ value of the valve plug surround region is about 400. Similar grid is used for improved valve design simulations.

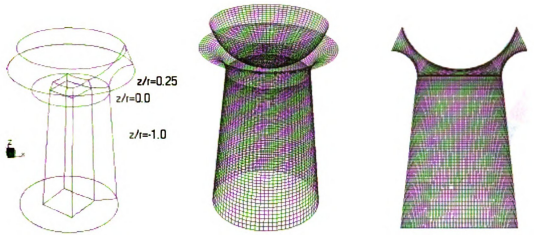

a. Grid blocks b. Valve inner surface c. Cross section grid

Fig. 5.1 Computational grid

5.2 Flow Patterns

According the simulation result, three flow patterns happen. At large opening (h/D>20%), due to large volume flow rate, the valve is full of flow. A little region of separation happens at plug center. Separation may happen in down stream seat side near exit, which has very little effect on the plug. This pattern can be considered as large mass flow rate pattern (a) or (e). For convenience, it is called pattern (e) as shown in Fig. 5.2.

When opening ratio is less than 20%, at large pressure ratio, flow passes through the valve asymmetrically as shown in Fig. 5.3. As shown in x=0 and y=0 cross-section velocity field, stall happens earlier in left side (+x and +y direction) of plug and right side (-x and –y direction) of seat. At z/r=0 plane, secondary flow happens. Two vortexes are symmetric about +45° line counting form +x with displacement from seat center line. Velocity field at z/r=-1 plane clearly shows that flow attaches the quarter phase of +x to +y seat and separates from other part. This is a typical 3-D pattern (c) flow. Pressure field is plotted in both fringe and contour forms. After the valve throat, the average pressure on

+x+y phase of plug is bigger than on opposite part. This finally can cause force, moment and torque acting on plug.

x=0 plane y=0 plane

Fig. 5.2 3-D flow pattern (e) at pressure ratio of 0.9 and 23.1% opening

x=0 plane y=0 plane z/r=0 plane z/r=-1 plane

a. Velocity Field

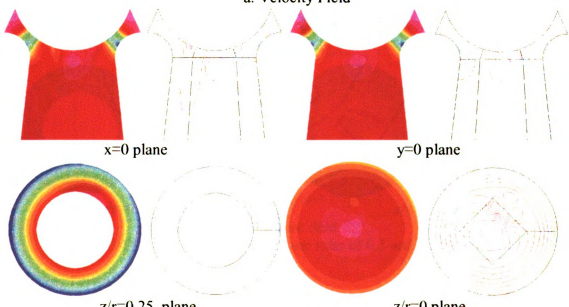

x=0 plane y=0 plane

z/r=0.25 plane z/r=0 plane

b. Pressure field

Fig. 5.3 3-D flow pattern (c) at pressure ratio of 0.9 and 10.6% opening

As pressure ratio decreasing, the flow pattern changes form (c) to (e). As shown in Fig. 5.4, free jet flow pattern (e) is almost symmetric around axis z. Secondary flow happens

in the center of z/r=0 plane. Main flow is at the center and separates from seat as shown in z/r=-1 plane. The pressure distribution around plug is also quite z-axis symmetric. The trend that flow changes form pattern (a) to (e) agrees with 2-D result under small opening situation. Pattern (a) is not found in 3-D simulation results.

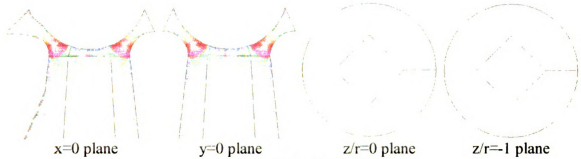

a. Velocity Field

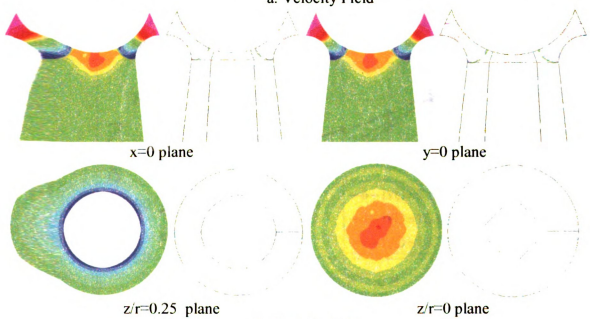

b. Pressure field

Fig. 5.4 3-D flow pattern (e) at pressure ratio of 0.5 and 10.6% opening

5.3 Force, Torque and Moment

The percentage of dimensionless drag, $D = \frac{D_t}{\pi P_{01} r_0^2}$, is shown in Fig. 5.5. Dt is the absolute drag; P_{01} is the inlet total pressure; r_0 is the radius of the plug. Because the grids do not include upstream plug surface, the drag here means vertical force acted by the

passing fluid. Drag increases as pressure ratio increases, which agrees with 2-D result. The drag difference between different opening ratios is larger at smaller pressure ratio. At about pressure ratio about 0.9, drag at different opening has the least difference. It is observed that the peak unbalanced lateral force, moment and torque occur under such pressure ratio. In 2-D simulation result, drag has least difference at pressure ratio of about 0.8. Under such situation, peak lateral force and moment also occur, especially for big opening situation. This may because the flow is about to be sonic under such pressure ratio. This is confirmed by the calculation results of mass flow rate variation with pressure ratio both in 2-D and 3-D situation.

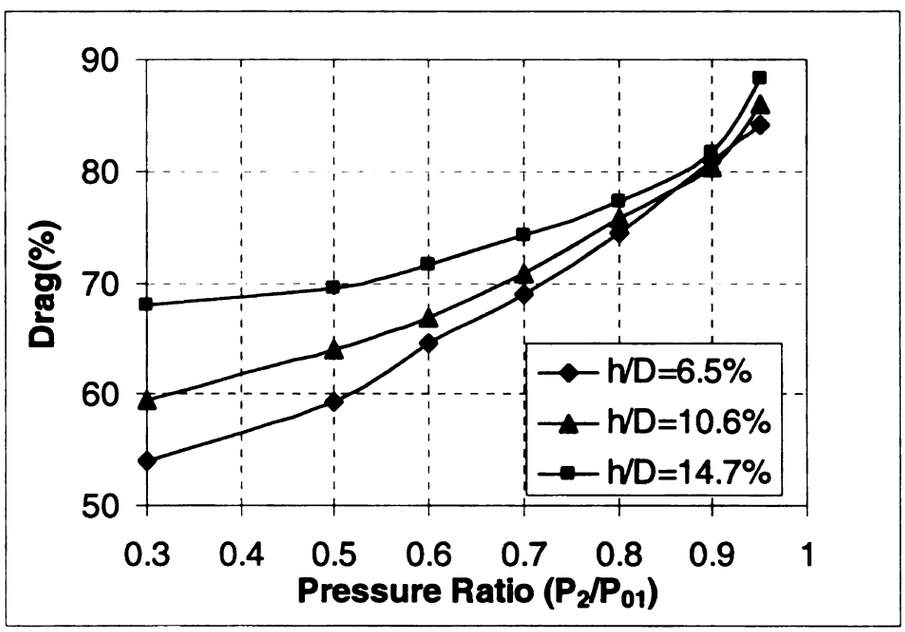

Fig. 5.5 Drag variation with pressure ratio

Under pressure ratio of 0.9, plug opening affects drag value as shown in Fig. 5.6. From almost closed situation, drag decreases until opening reaches about 10%, then starts increasing. This trend agrees with the experiment result of Schuder and Moussa's unpublished computation data. According to some failure report, this is also the opening

when valve failure frequently occurs. In Schuder's paper, large drag oscillation at this turning point was found. We suspect that some properties in this turning point cause large drag oscillation, which finally may cause large amplitude vertical vibration.

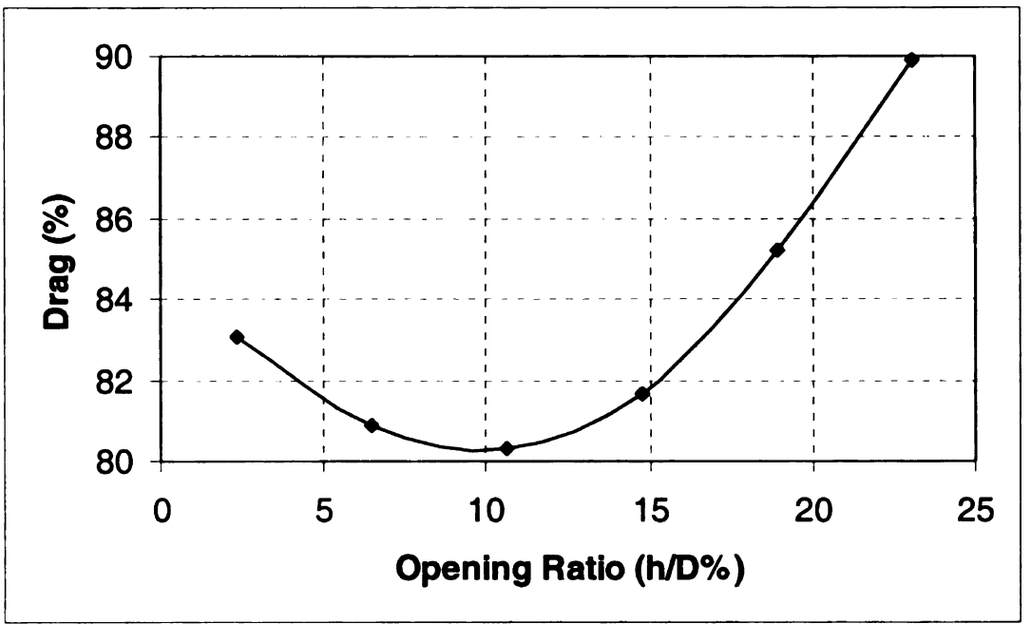

Fig. 5.6 Drag variation with valve opening changing Pr=0.9

Dimensionless lateral force, $L = \frac{L_t}{\pi P_{01} r_0^2}$, and moment, $M_O = \frac{Mot}{\pi P_{01} r_0^3}$, are defined similar with dimensionless drag. Lt is the absolute lateral force and Mot is the absolute moment caused by drag. Torque is caused by lateral force around plug center, non-dimensionlized as $T_L = \frac{T_{Lt}}{\pi P_{01} r_0^3}$. T_{Lt} means total torque acting on plug. Absolute values of dimensionless lift, moment and torque at three openings and different pressure ratios are plotted in Fig. 5.7. Lateral force and moment have similar variation trend with pressure ratio changing at one fixed opening. At small opening situation, only one peak occurs at pressure ratio of about 0.9. As opening becomes larger, another peak starts to occur at small pressure ratio region. This peak has less amplitude and moves toward the 0.9

pressure ratio peak, which has maximum values, as opening increases. In 2-D large opening situation, the maximum values occur at pressure ration about 0.8. Torque is caused by friction. It is much less than lateral force and moment at large pressure ratio.

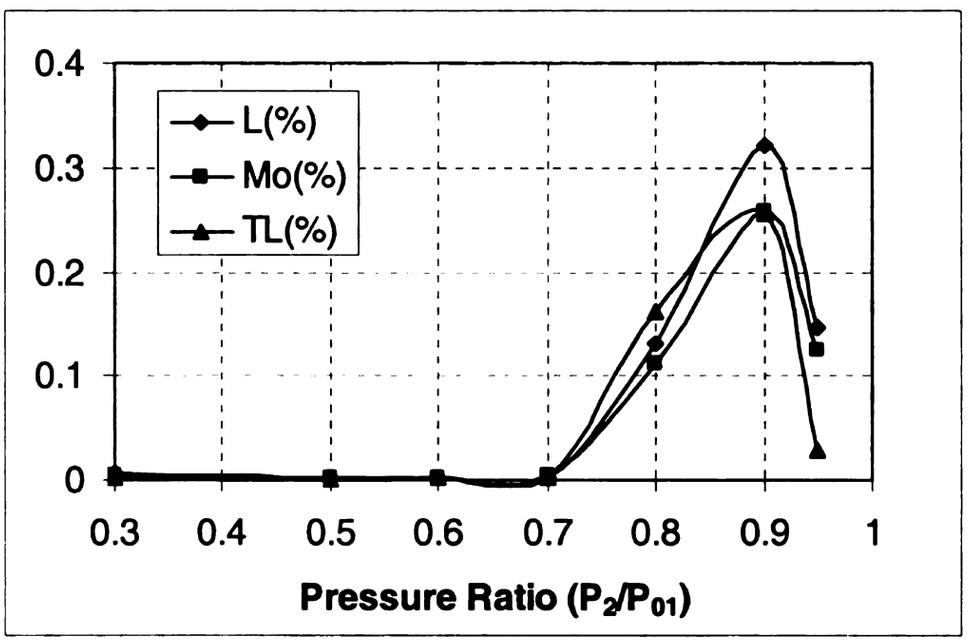

a. Valve opening ratio h/D=6.5%

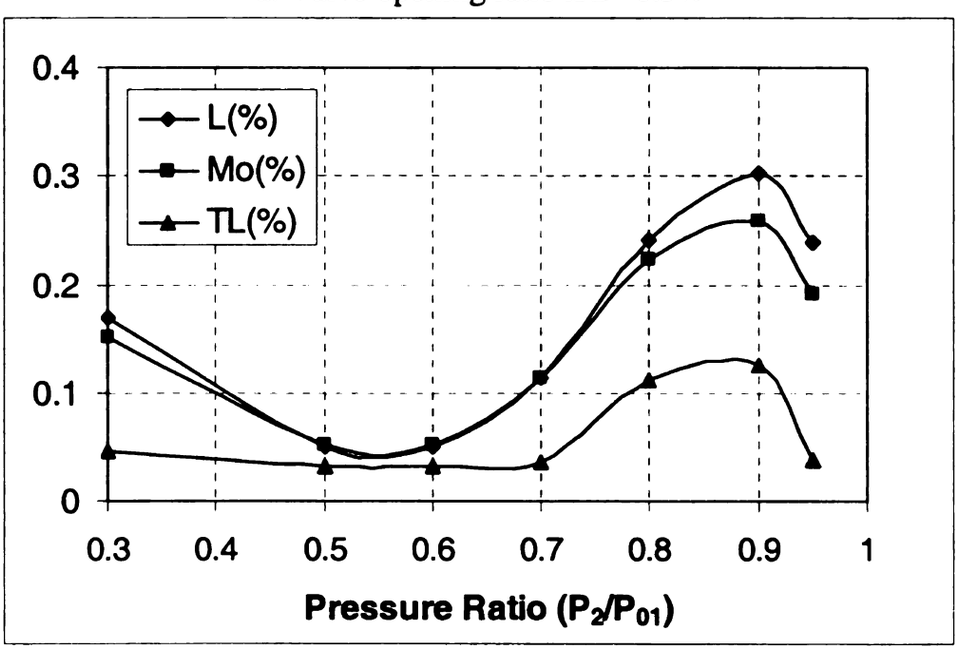

b. Valve opening ratio h/D=10.6%

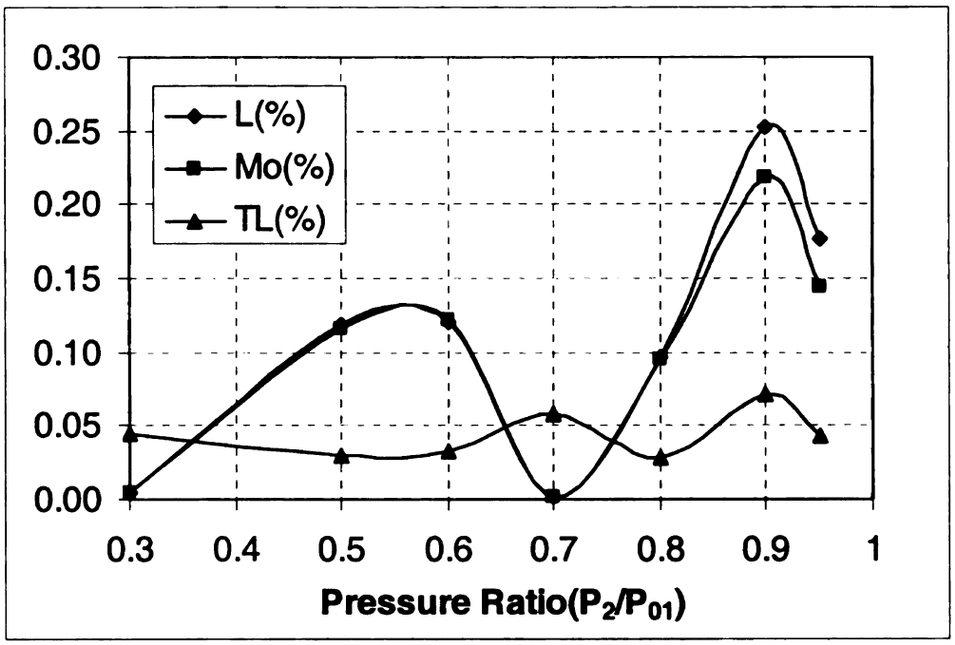

c. Valve opening ratio h/D=14.7%

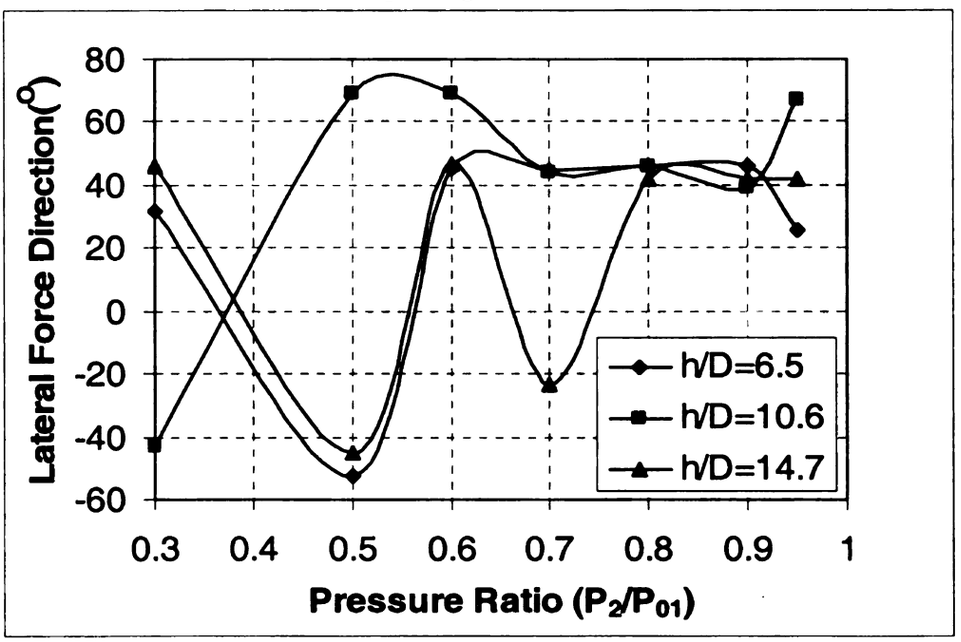

d. Direction of lateral force

Fig. 5.7 Absolute values of lift, moment and torque

According to CFD result, lateral force and moment are always in one direction. The lateral force direction at different valve opening and pressure ratio is shown in Fig. 5.7d. It randomly point to an angle in the range of –60° to 80° counting from +x direction. Torque normally changes from clockwise to anticlockwise at pressure ratio between 0.5 and 0.7.

More results at pressure ratio of 0.9 and different openings are shown in Fig. 5.8. Force, moment and torque have similar trend. They increase dramatically from very small opening to 5% opening. Then it declines slowly. After 15% opening, it decrease quickly. At opening ratio between 5% and 15%, they remain high value, which may cause large amplitude vibration. In reality, due to big loss, it is uncommon to have a large pressure ratio of about 0.9 at small valve opening. This is the reason it is believed that the most dangerous opening is between 10% and 15%. Some valve failures under such openings were reported. From here we know that to avoid valve operating at the position and pressure ratio, which can cause peak value force and moments, is an important way to reduce the possibility of valve failure.

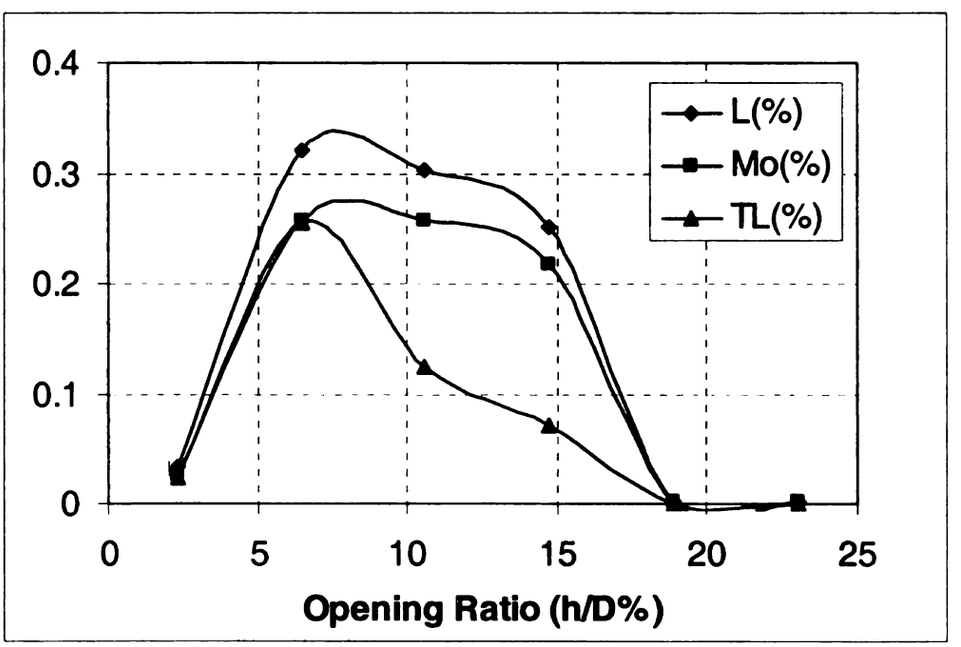

Fig. 5.8 Maximum excitations at different opening when Pr=0.9

The forces and moment mentioned above are total force, moment and torque caused by both friction and pressure difference. Fig. 5.9 shows the ratio of viscous effect with total absolute values at 14.7% opening. Compared with pressure difference, viscous

effect is very small, maximum 2%. Due to the smaller absolute value, at small pressure ratio, the viscous effects account a little bit more than at high pressure ratio. These agree with 2-D simulation results. Torque ratio is not shown here because it is 100% caused by friction.

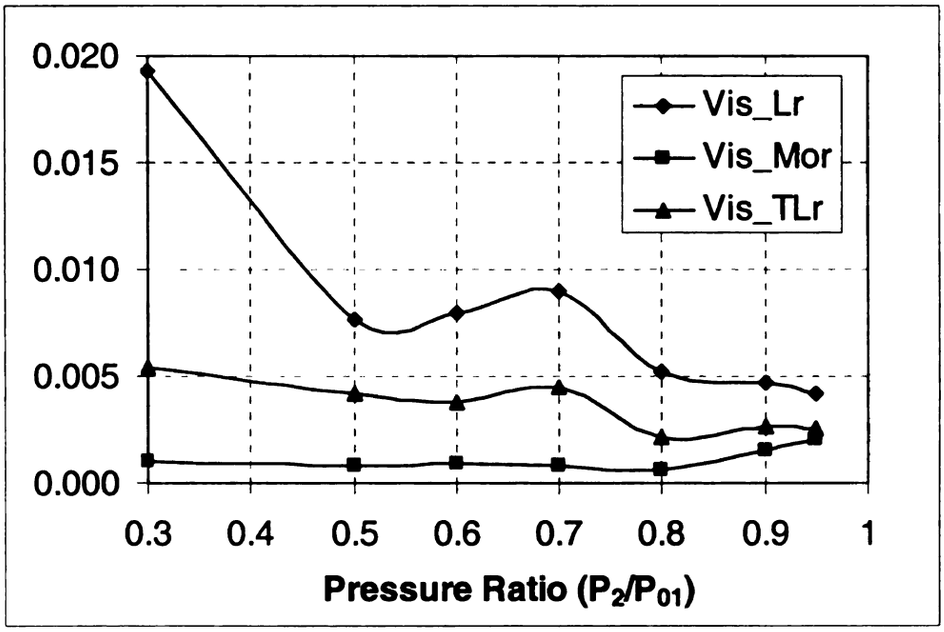

Fig. 5.9 Viscous effect at 14.7% opening

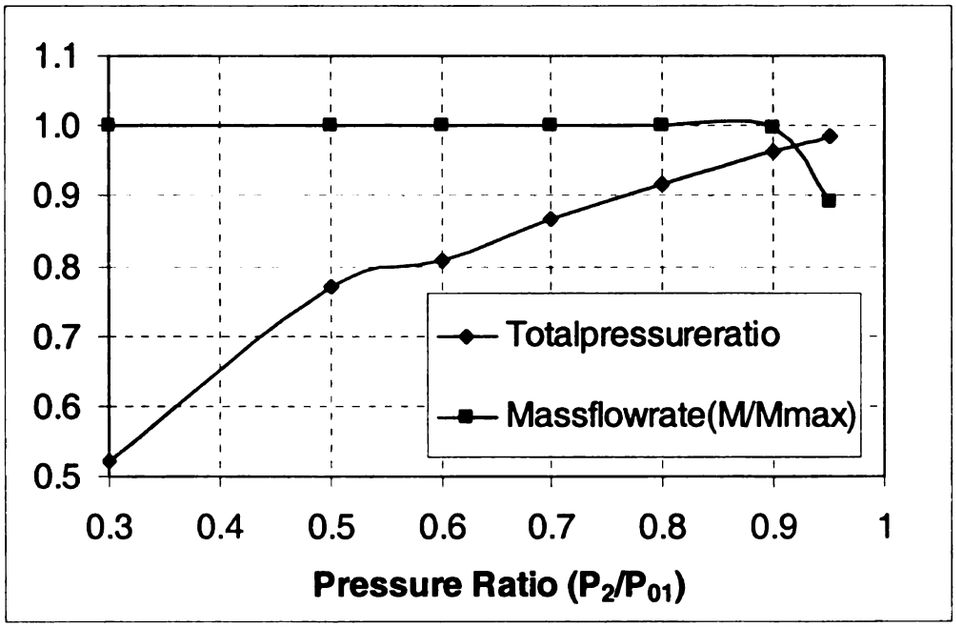

Fig. 5.10 Total pressure ratio and mass flow rate variation at 14.7% opening

Fig. 5.10 shows how mass flow rate and total pressure ratio change with the pressure ratio at 14.7% valve opening. Because the valve exit area is much larger than valve throat area, the flow can be choked at large pressure ratio of 0.9. Total pressure ratio drops as pressure ratio decreases.

5.4 3-D Simulation Results For Improved Designs

Similar with 2-D analysis, three symmetric flow patterns are captured for dish bottom improved design (θ=45°, δ=60° and h/r=0.15). As shown in Fig. 5.11, pattern (a) happens in about same region of pressure ratio and opening for original design pattern (c). Accoring to velocity field in different view, after valve throat, stall happens in the plug side after the sharp conner. In seat side, no stall happens and flow attaches to the circumferential seat wall. Both velocity field and pressure field are pretty z-axis symmetric. No secondary flow is captured at down stream.

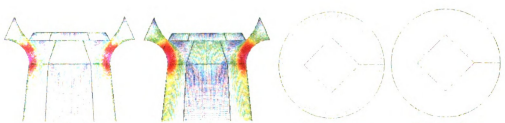

a. Velocity field

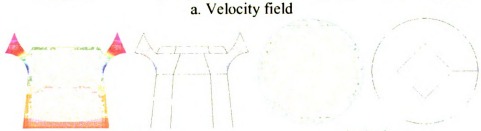

b. Pressure field

Fig. 5.11 Pattern (a) at Pr=0.9 and Opr=10.6% for dish bottom design

At small pressure ratio, flow becomes free jet flow as shown in Fig. 5.12. Due to the curvature of plug, flow joins further downstream than pattern (c) in original valve design.

The cross section pressure and velocity field is more symmetric than 2-D result. For original design flow pattern (e), secondary flow happens in z/r=0 plane, while here no secondary flow is captured.

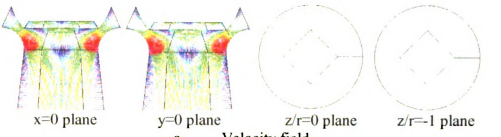

a. Velocity field

b. Pressure field

Fig. 5.12 Pattern (e) at Pr=0.5 and Opr=10.6% for dish bottom design

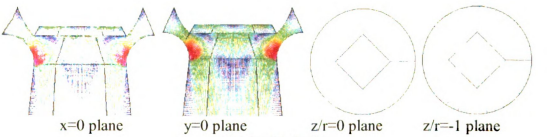

a. Velocity field

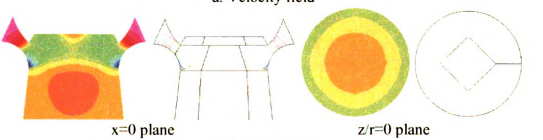

b. Pressure field

Fig. 5.13 Pattern (d) at Pr=0.5 and h/D=10.6% for dish bottom design

There is an intermediate flow pattern (d) occurs between pattern (c) and (e) as shown in Fig. 5.13. It is also z-axis symmetric. In 2-D dish bottom and 3-D original design

simulations, this pattern is not captured. In this pattern, at down stream, the free jet shape is like a ring, not like the joined circular free jet in pattern (e).

The velocity fields are plotted in Fig. 5.14 for flat cut design. Similar flow patterns occur in similar region as dish bottom design in most cases. But at small opening and pressure ratio, an asymmetric flow pattern (c') happens as shown in Fig. 5.15. Strong secondary flow happens in z/r=0 plane. In dish bottom design under same situation, the flow is in pattern (e). For this reason, dish bottom is thought a better design than flat cut.

Pattern (a) (Pr=0.9) Pattern(d)(Pr=0.7) Pattern (e)(Pr=0.5)

Fig. 5.14 Flow patterns for flat cut design at Opr=10.6%

x=0 plane y=0 plane z/r=0 plane z/r=-1 plane

a. Velocity field

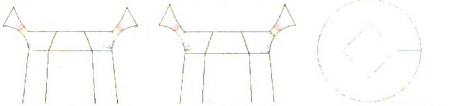

x=0 plane y=0 plane z/r=0 plane

b. Pressure field

Fig. 5.15 Flow pattern (c') at Pr=0.5 and Opr=6.5% for flat cut

The CFD results (%) of excitations are plotted in Fig. 5.16. To show them clearly, the values of moment for flat cut design at pressure ratio of 0.5 and 0.3 are 10 percent of actual value. Most values are less than 0.002% except some points at small pressure ratio.

Dish bottom design has better performance especially at small pressure ratio. At large pressure ratio, there is no big difference between them.

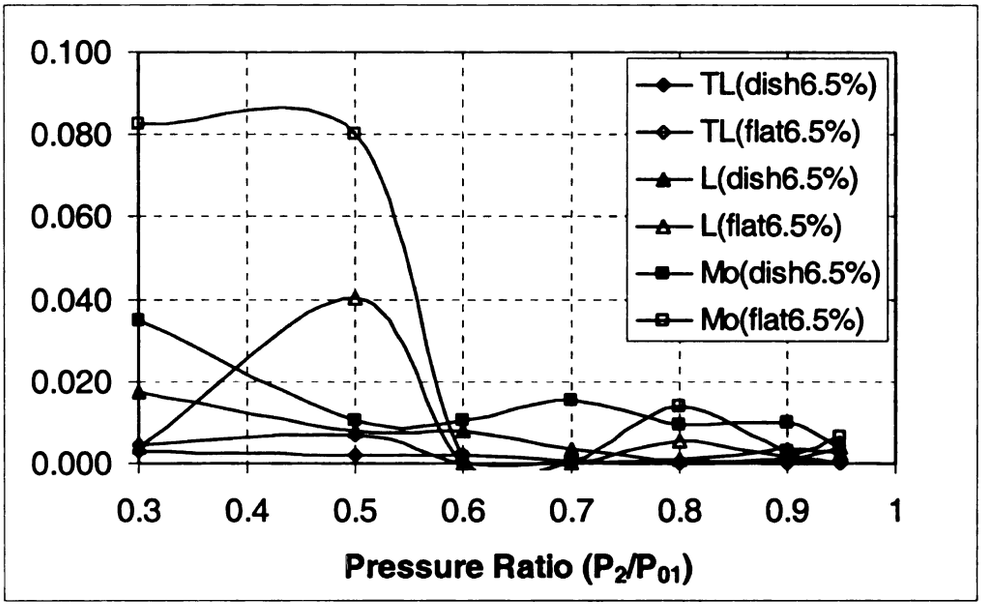

a. h/D=6.5%

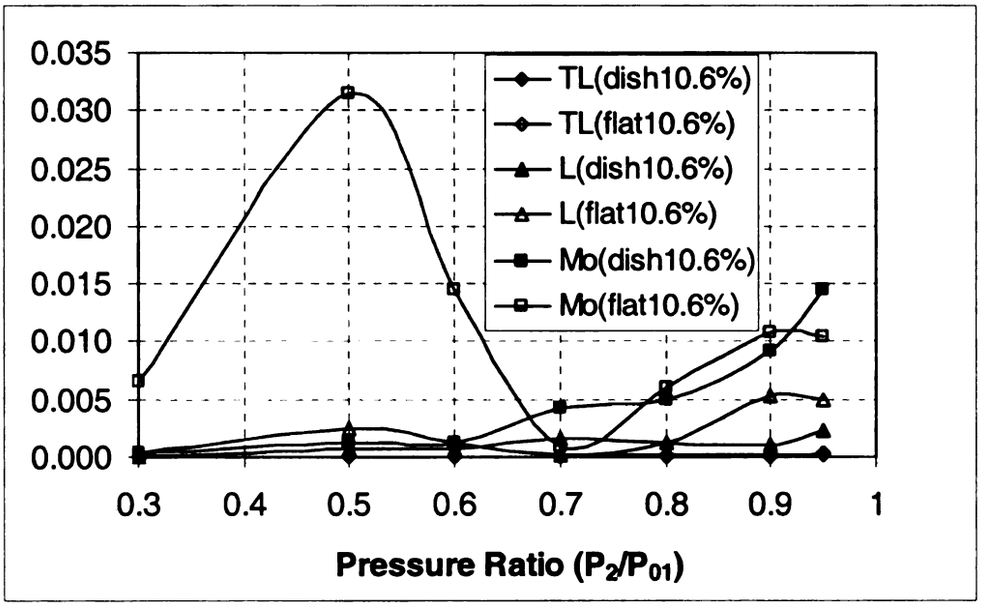

b. h/D=10.6%

Fig. 5.16 Lateral force, moment and torque for improved designs

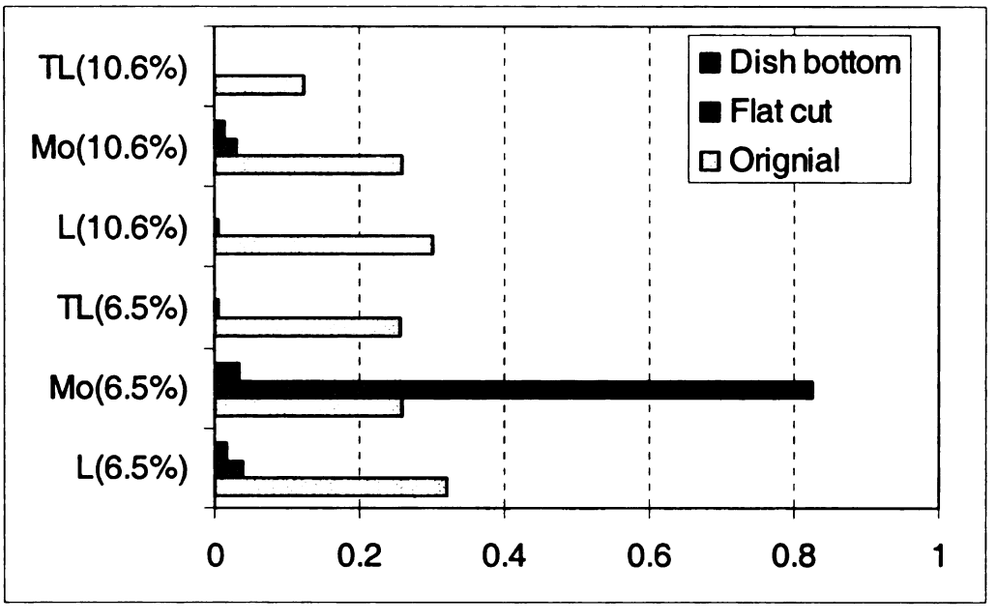

a. Maximum lateral force, moment and torque

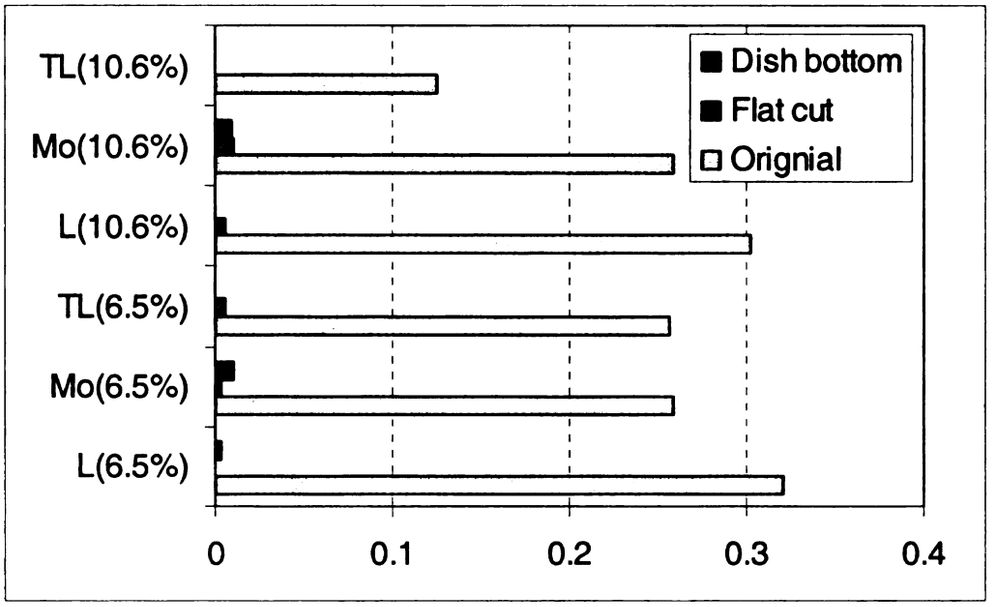

b. Lateral force, moment and torque at pressure ratio of 0.9

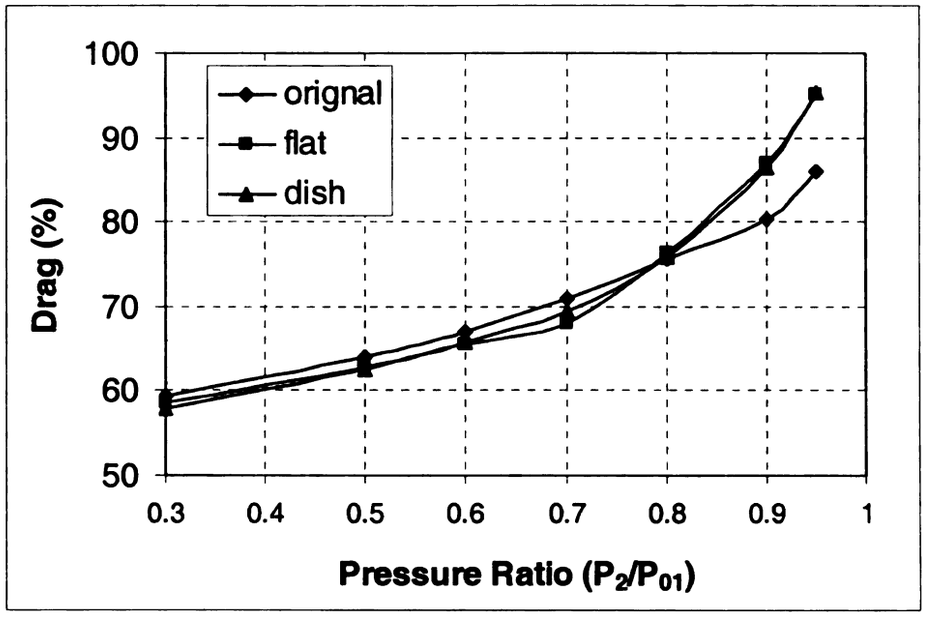

c. Vertical Force

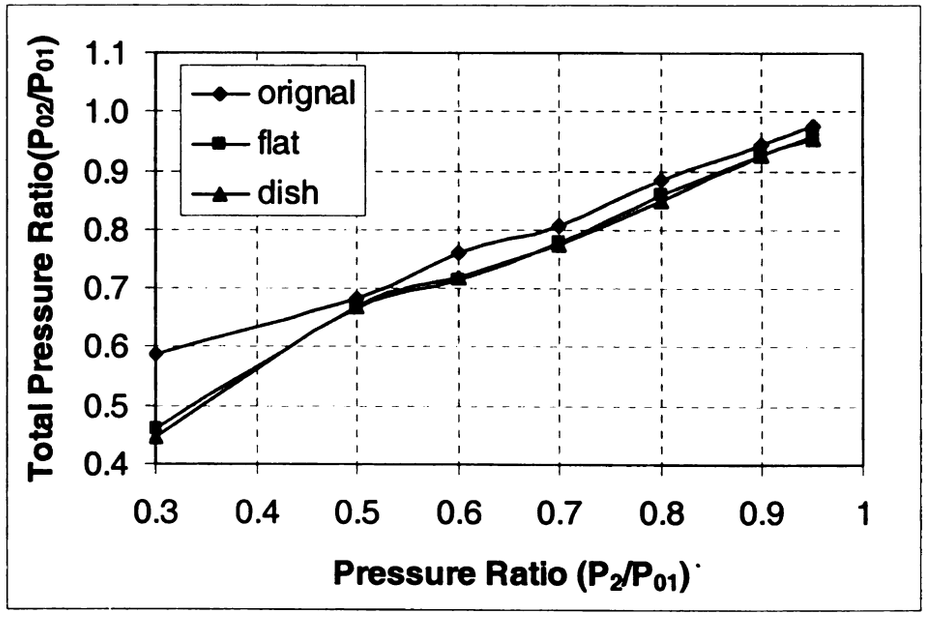

d. Total pressure ratio at h/D=10.6%

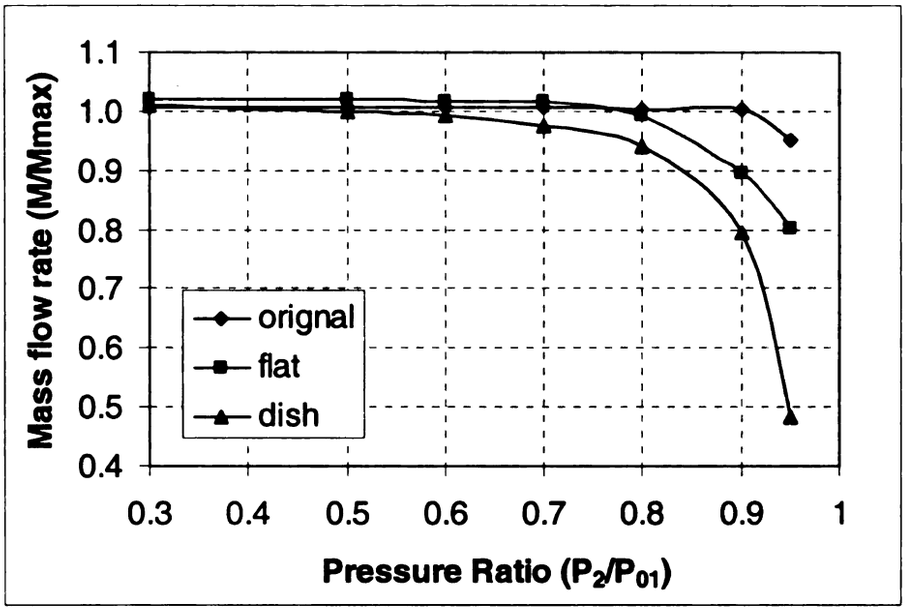

e. Mass flow rate at Opr=10.6%

Fig. 5.17 Comparison between original and improved designs

To compare the performance of original and improved designs, the absolute values of excitations, total pressure ratio and mass flow rate ratio are plotted in Fig. 5.17. It shows that the maximum excitation values at different pressure ratios for improved designs are much less than original design, except for flat cut design maximum moment at 6.5%. Only at small pressure ratio, big amplitude of moment of flat cut designs occurs, which is due to flow pattern (c'). The values at pressure ratio of 0.9 are plotted in Fig. 5.17b. It shows that at large pressure ratio, the improved designs are much better than original design in terms of reducing fluid induced excitations.

The trends of drag changing with pressure ratio are similar as shown in Fig. 5.17c. Two improved designs have almost same amplitude of drag under same condition. At pressure ratio larger than 0.8, drag of original design is smaller. At pressure ration smaller than 0.8, it is a little bit larger than improved designs.

The total pressure ratio of original valve is larger than improved designs, especially at small pressure ratio. The ratio of mass flow rate and maximum mass flow rate of original design is shown in Fig. 5.17e. At large pressure ratio, the original valve can by pass more mass flow than flat cut design, which can by pass more than dish bottom design.

CHAPTER 6

EXPERIMENTAL INVESTIGATION

6.1 Equipment Setup

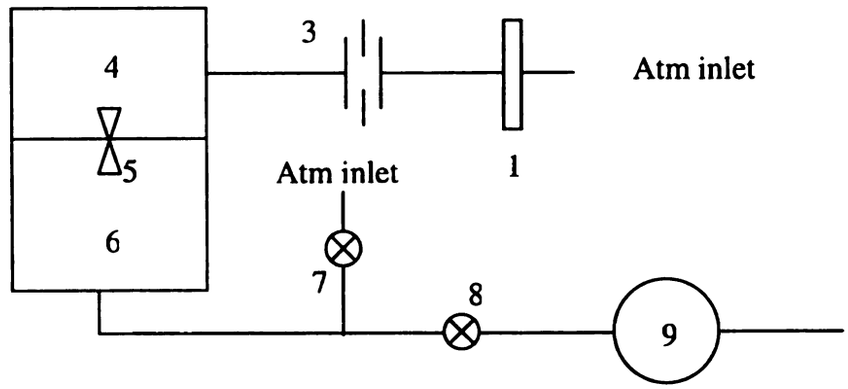

a. Schematic experiment system

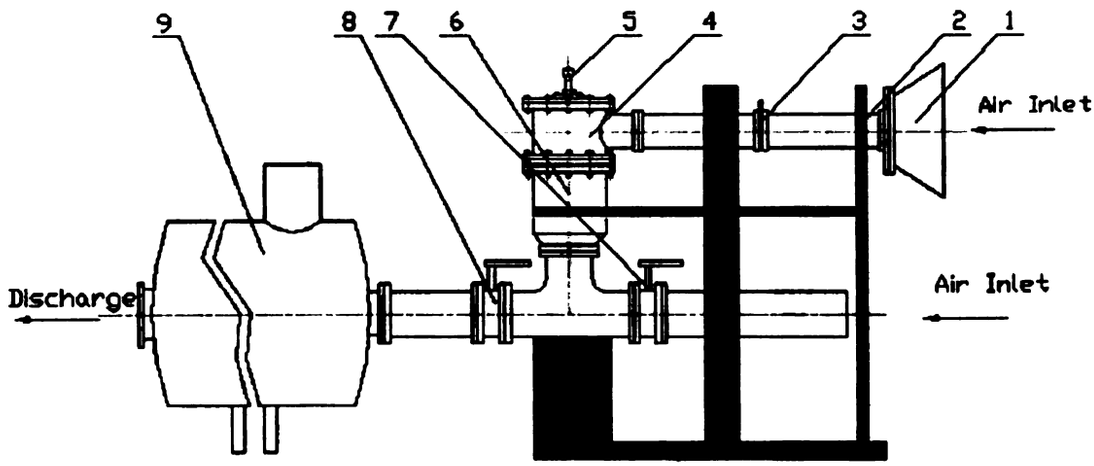

1. inlet silencer 2. support structure 3. orifice 4. inlet chest 5. test valve 6. outlet chest 7. bypass valve 8. throttle valve 9. vacuum pump

b. Autocad drawing of test system

Fig. 6.1 Venturi valve test System

The test system was constituted as shown in Fig. 6.1. A wind tunnel was built to test the flow patterns and instability when passing through the valve. A vacuum pump is used to build low pressure in test valve downstream to suck air through the test valve (5). The

ambient air enters the inlet pipe (1) through the orifice (3) then enters inlet chest (4). To avoid upstream and down stream influence and non-uniform inflow effect, the diameters of chests and inlet pipe are much larger than valve diameter. As a result, the pressure variation is very small and flow velocity is much reduced at inlet and outlet chests. The inlet chest and outlet chest can be considered as big tanks with constant pressure. The pressure of outlet chest is controlled by a throttle valve (8) and a bypass valve (7). The pump can be throttled to reach higher vacuum level. The by pass valve opens to increase out let chest pressure. The different combination can make full potential of the vacuum pump to reach desired pressure ratio. Some pictures of the system are shown in Fig. 6.2.

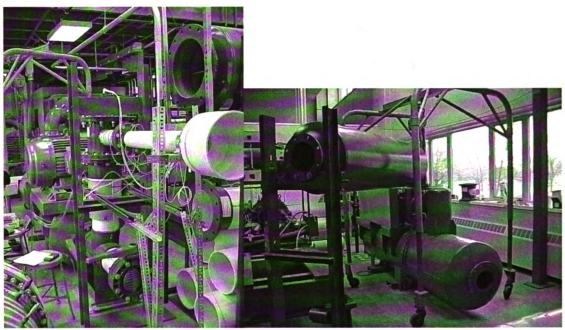

a. View from inlet pipe side b. View from vacuum pump side

Fig. 6.2 Pictures of the experiment system

6.1.1 Vacuum pump

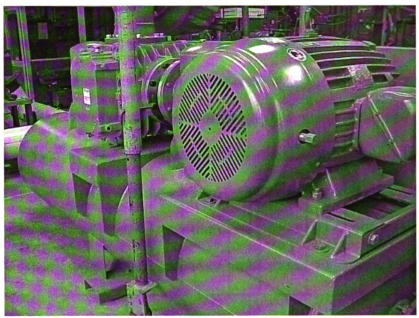

Fig. 6.3 Picture of vacuum pump

The ROOTS RAM™ Whispair 616 DVJ Dry Vacuum Pump is selected as shown in Fig. 6.2. It is a heavy-duty unit with an exclusive discharge jet plenum design that allows cool atmospheric air flow into the casing. This unique design permits continuous operation at vacuum levels to blank-off with a single stage unit without water injection. Standard dry vacuum pumps are limited to approximately 16" Hg vacuum because operation at higher vacuum levels can cause extreme discharge temperatures resulting in casing and impeller distortion. The Roots Whispair vacuum pump's cooling design eliminates the problems caused by high temperatures at vacuum levels beyond 16" Hg. Whispair vacuum pumps reduce noise and power loss by utilizing an exclusive wrap-around plenum and pro-prietary Whispair jet to control pressure equalization, feeding backflow in the direction of impeller movement, aiding rotation. The general statistics of the vacuum pump are shown in the table below.

Table 6.1 Pump performance table

Frame Size	Speed RPM	Maximum Free Air CFM	12" Hg Vac. CFM at BHP		16" Hg Vac. CFM at BHP		20" Hg Vac. CFM at BHP		24" Hg Vac. CFM at BHP		27"Hg Vac. CFM at BHP	
616J	1750	2367	1015	36	901	47	748	59	448	71	*	80
	2124		1310	44	1196	58	1043	72	743	86	*	97
	2437		1556	51	1443	67	1290	83	990	99	244	111
	3000		2001	63	1887	83	1734	102	1434	122	688	137

The pump is driven by a 100 HP motor at speed of 2500 RPM. It sucks the air to build vacuum in outlet chest and discharge air directly to room. At pressure ratio of 3, the vacuum pump can produce a maximum flow of about 1300 acfm and 54 acfm at a pressure ratio of about 10. Even no water needed for cooling, it can take inlet air temperature as high as 175 °F.

6.1.2 Piping system

All the pipes are in the upstream of vacuum pump. The pipes, flanges, Tees, and chests are made of PVC pipes, which are easier handle than metal and strong enough for the vacuum.

6.1.3 Valve and chests

As shown in Fig. 6.4, the chests are built here to maintain constant up stream and down stream pressure of the test valve. Their diameters are much larger than inside diameter of seat to reduce the flow velocity. The inlet chests is a Tee shape with inlet flow coming

from inlet pipe with much larger diameter than inside of pipe to reduce the influence of upstream inflow.

The ½ scale test valve seat is mounted in the center of plate separating the inlet and outlet chests. Hold in the center of inlet chest, the threaded test valve stem can be rotated to adjust valve opening. The white cables are for measurement of pressure on plug surface. They go through inside of stem pipe to data acquisition equipment. The static pressure was measured in 9 positions one the plug surface. The labels of positions are shown in Fig. 6.6. The center sensor (position 0) is designed to take both static and dynamic pressure. There are 12 static pressure positions on the seat inner surface. The white pipes go through wall of inlet chest to data acquisition equipment for static pressure measurement. 7 dynamic pressure ports are also designed at the positions of screws in Fig. 6.7. Because the valve was tested under different openings, Fig. 6.8 shows the pressure locations at different openings.

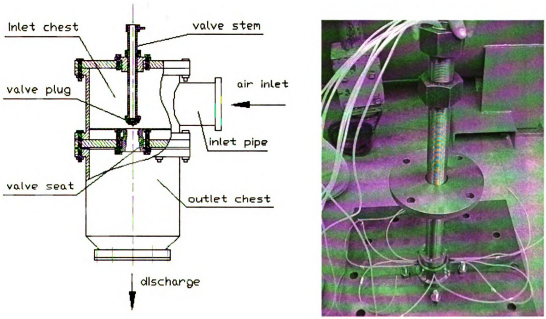

Fig. 6.4 Chests and valve

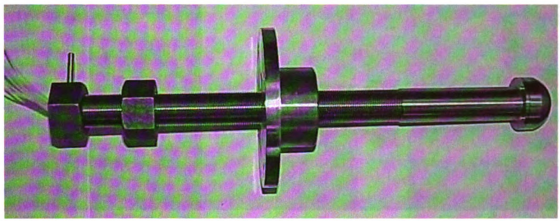

Fig. 6.5 Valve stem and plug

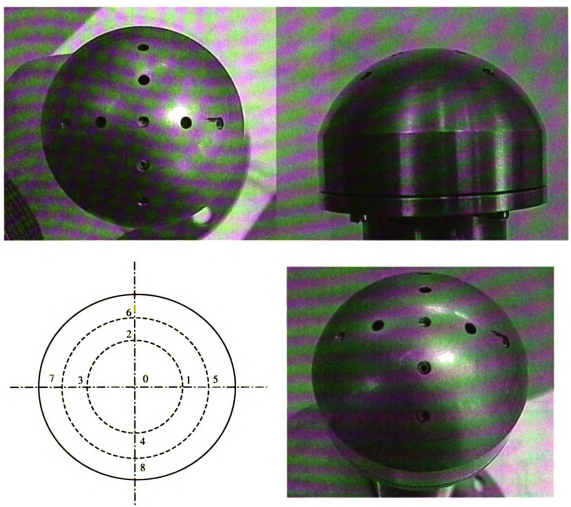

Fig. 6.6 Valve plug and pressure sensor positions

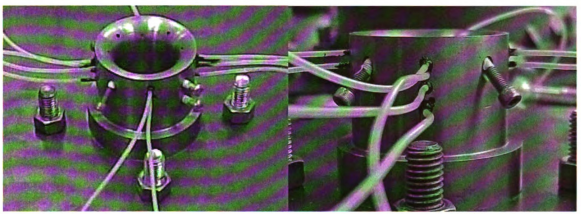

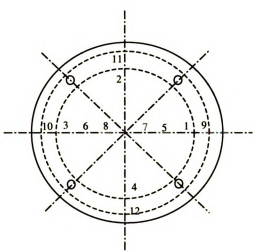

Seat

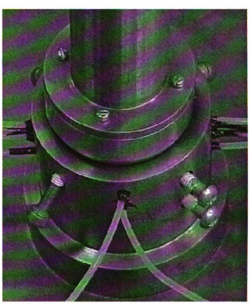

Fig. 6.7 Valve seat and pressure sensor positions

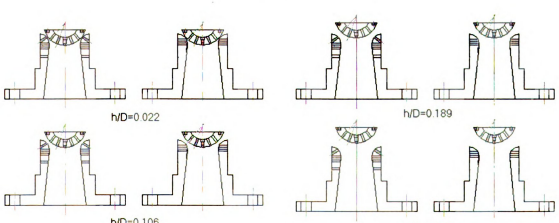

Fig. 6.8 Static pressure sensor positins at different valve opening

6.1.4 Experiment measurement system design

The major concern of this experiment is about pressure. Two kinds of pressure sensors were designed to be used, static pressure and dynamic pressure. The measurement system for pressure is shown in Fig. 6.9.

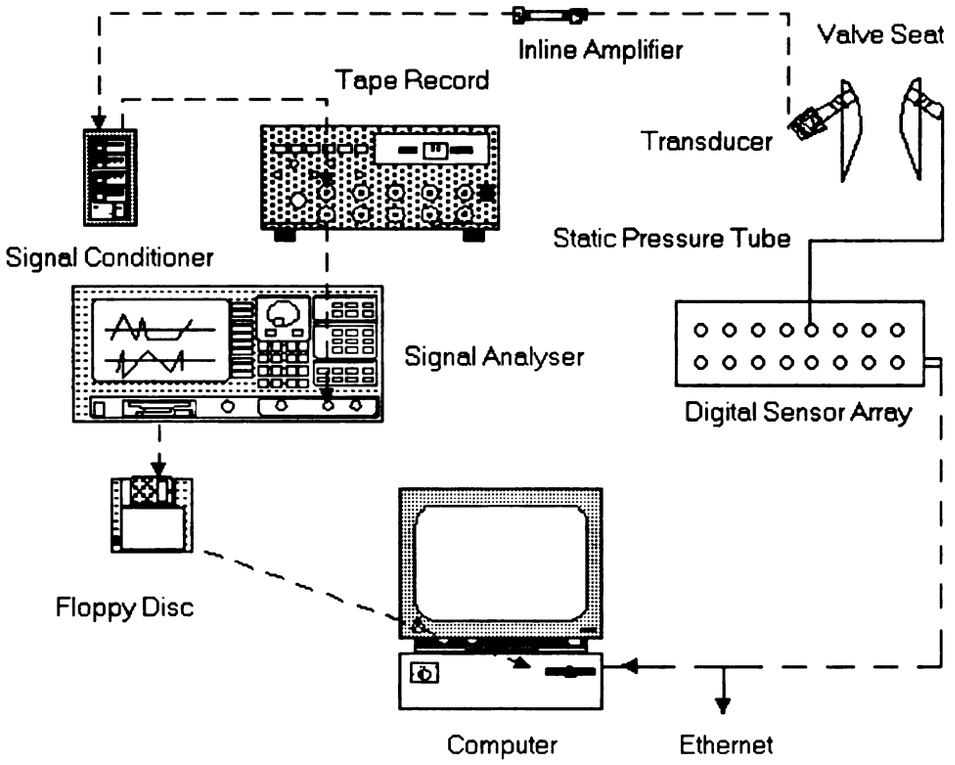

Fig. 6.9 Pressure measurement system

Besides the 21 locations in plug and seat surface, the pressure was also measured in inlet/outlet chests to get the pressure ratio ($Pr=P_{outlet}/P_{inlet}$) and inlet pipe orifice to get mass flow rate. Through the white pressure tubes, the pressure signals were transferred to digital data acquisition array, then to the computer for recording and analyzing. 2 sets of Scannivalve 3017 digital sensor arrays with 32 Channels were used. The rate of data acquisition is 200 samples/channel/sec.

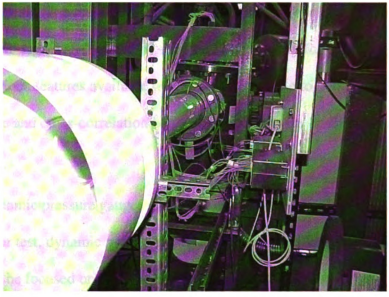

Fig. 6.10 Pictures for static pressure measurement system

7 dynamic pressure transducer installation ports were designed for PCB Model 105B02 in plug head, seat. 1 accelerometer installation surface is designed for PCB 352 A10. The system of two 4-chanell signal conditioner, one tape recorder, one signal analyzer and computer with signal processing software was made and ready to get data.

The signal from the PCB pressure transducer was conducted to an inline amplifier through a coaxial cable. The inline amplifier conditions the transducer output signal. The signal was then passed on to the signal conditioner through a 50-feet low-noise coaxial cable. Even though one inline amplifier was used for each transducer, one signal conditioner was used for all four signals. The signal conditioner powered both the inline amplifier and the PCB transducer and could also amplify the signal with fixed gain of 1, 10, 100. The amplified signals from the signal conditioner were transferred to a 4-channel digital tape recorder and stored on to a tape. The stored data on to a tape were transferred to a PC for further processing and analysis through the signal analyzer and the signal processing software. The output connectors can develop the input signals or the tape

reproduction signals. The real time signals are monitored through two-channel HP signal analyzer. The HP signal analyzer also provided the capability for on-line signal analysis through the various features available with it. It was possible to obtain the power spectrum, phase and cross-correlation between two signals for on-line monitoring of the valve.

Even the dynamic pressure gauges and data acquisition system was designed, in this first stage of our test, dynamic pressure gauges were not installed. So following discussion will be focused on static pressure data analysis.

6.2 Experiment Result and Discussion

6.2.1 Mass flow rate

The non-dimensionalized mass flow rate, maximum (choked) mass flow rate at different openings over mass flow rate at wide opening (h/D=0.734), is shown in Fig. 6.11. The opening ratio is defined as the valve lift from the closed position (h) over the valve plug diameter (D). Maximum mass flow rate increases quickly before 30% opening, then slowly to about 50% opening, and remains constant at greater openings. Thus 50% opening can be defined as the fully open position for this valve. The mass flow rate variation with changing pressure is shown in Fig. 6.12. To compare mass flows at different openings, the mass flow rate is non-dimensionalized as mass flow rate over maximum (choked) mass flow rate at the same valve opening. At small valve openings, for example h/D=0.022, the flow is choked at about Pr=0.6. At larger openings, the choke pressure ratio is larger. At wide opening, h/D=0.734, flow is choked at Pr=0.8. From this figure, the transonic region can be roughly judged, for example, at h/D=0.147 and pressure ratio between 0.65 to about 0.8, the flow is transonic and likely unstable.

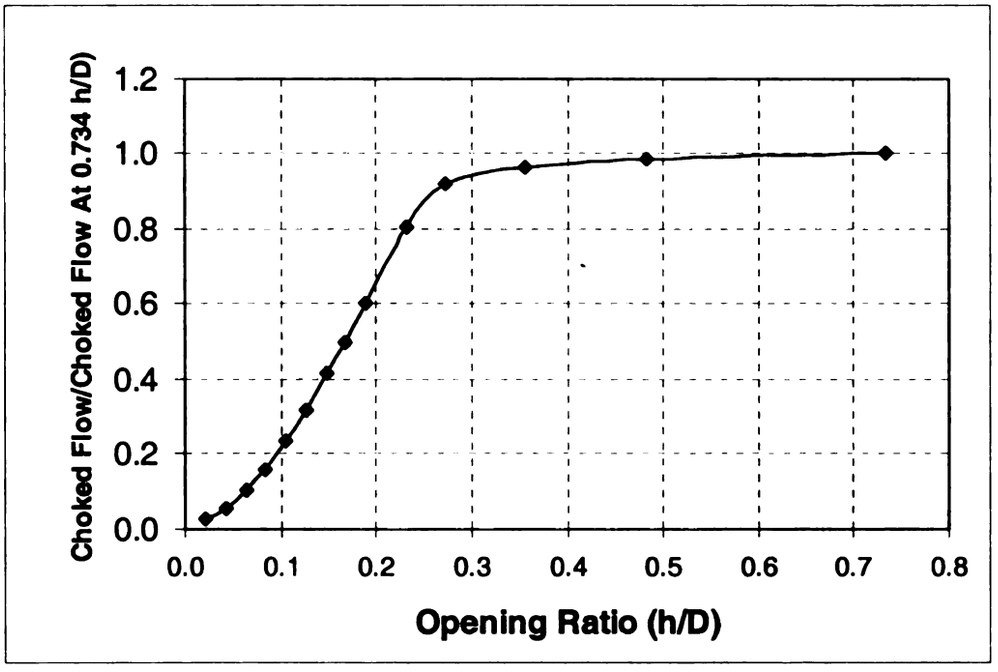

Fig. 6.11 Choked mass flow rate variation with valve opening

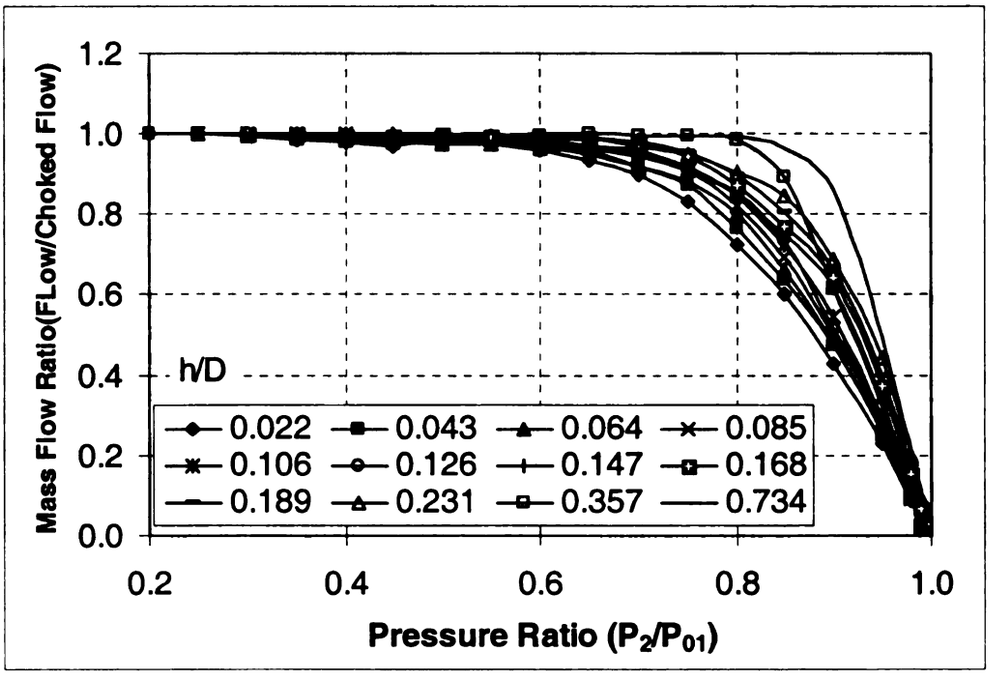

Fig. 6.12 Dimensionless mass flow rates at different openings

6.2.2 Flow regions and patterns

By considering pressure distributions, pressure oscillation frequency, and amplitude, four major flow regions, A, C, D, and E, are identified in terms of valve opening and pressure ratio, as shown in Fig. 6.13. In regions A, D, and E, one kind of pressure distribution occurs. Pressure oscillates with high frequency and small amplitude. This is due to strong turbulence. In region C, several types of pressure distribution keep changing to each other. Large amplitude of pressure oscillation occurs due to the flow pattern changing. All transition regions between C and other regions are included in region C. Thus region C is the most unstable region.

Since the flow is three-dimensional, it cannot be made visible. The flow pattern is analytically determined using the measurement results of the static pressure distribution and pressure oscillation. As mentioned before, the static pressure on the surface with which the flow is in contact is lower than that on the surface with which the flow is not in contact. Also, the pressure on the surface over which the flow is steadily in contact varies randomly, with larger amounts of variation than in the regions where flow is separated. These trends were proved to be true by the experimental results of Araki. The flow patterns and corresponding pressure distribution are roughly drawn in Fig. 6.14. The pressure in Fig. 6.14 is gauge pressure (psi). The two cross sections where sensors are located are perpendicular to each other for each pattern in the figure. Even the "visualized" flow patterns are not very accurate due to the complicated flow and difficulty of judgment from limited numbers of sensors, but they can still help to understand the flow phenomena.

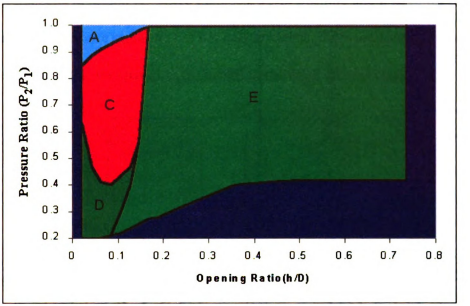

Fig. 6.13 Flow regions

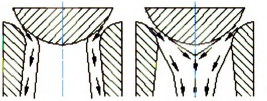

Pattern A

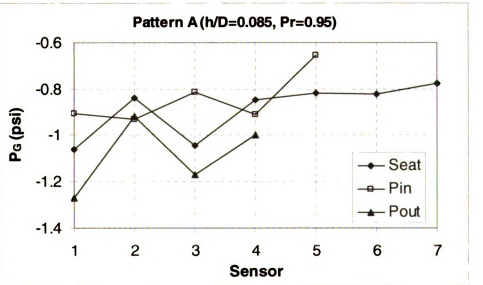

Fig. 6.14 Pattern A and corresponding pressure distribution

Pattern A happens in region A, where there is a small opening and a large pressure ratio. Pattern A is almost symmetric but not axisymmetric. Flow attaches to the seat in one cross section, while it expands to the center in the other cross section.

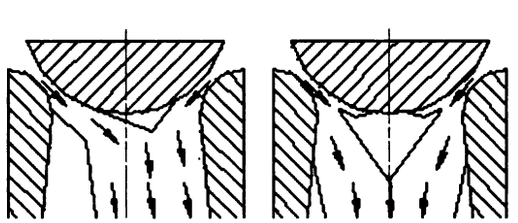

Pattern C

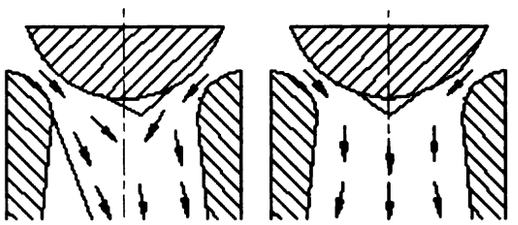

Pattern C'

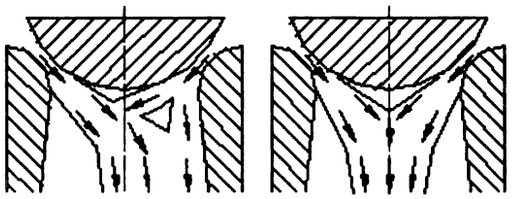

Pattern C_0

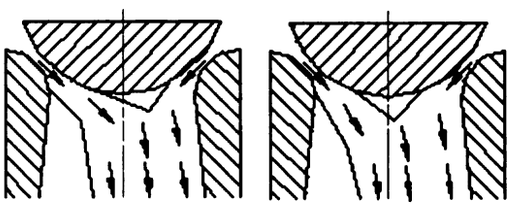

Pattern C_1

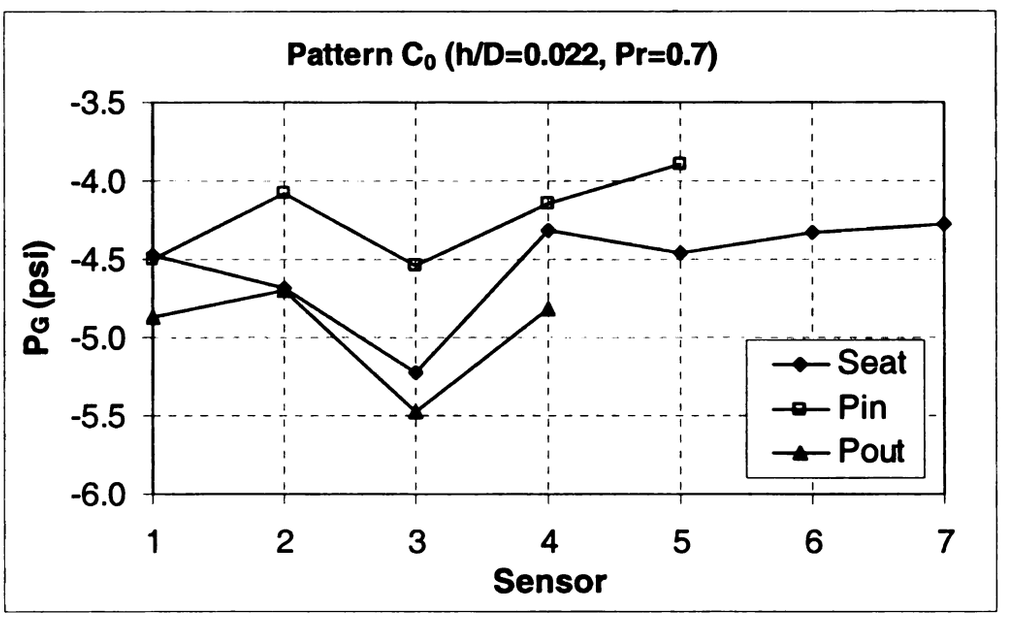

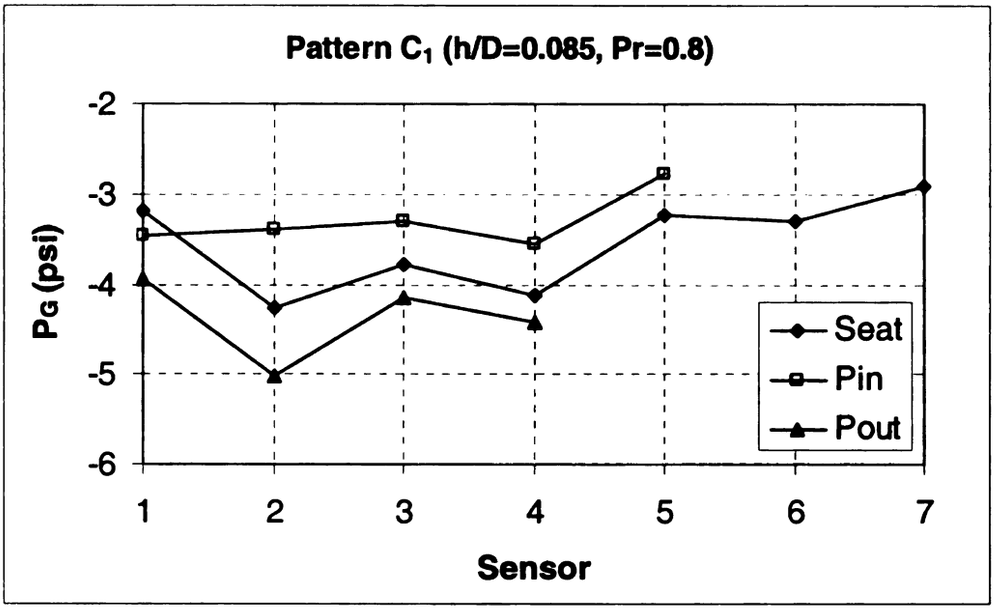
Pattern C_1 (h/D=0.085, Pr=0.8)
-2
-3
-4
-5
-6
P_G (psi)
1
2
3
4
5
6
7
Sensor
Seat
Pin
Pout

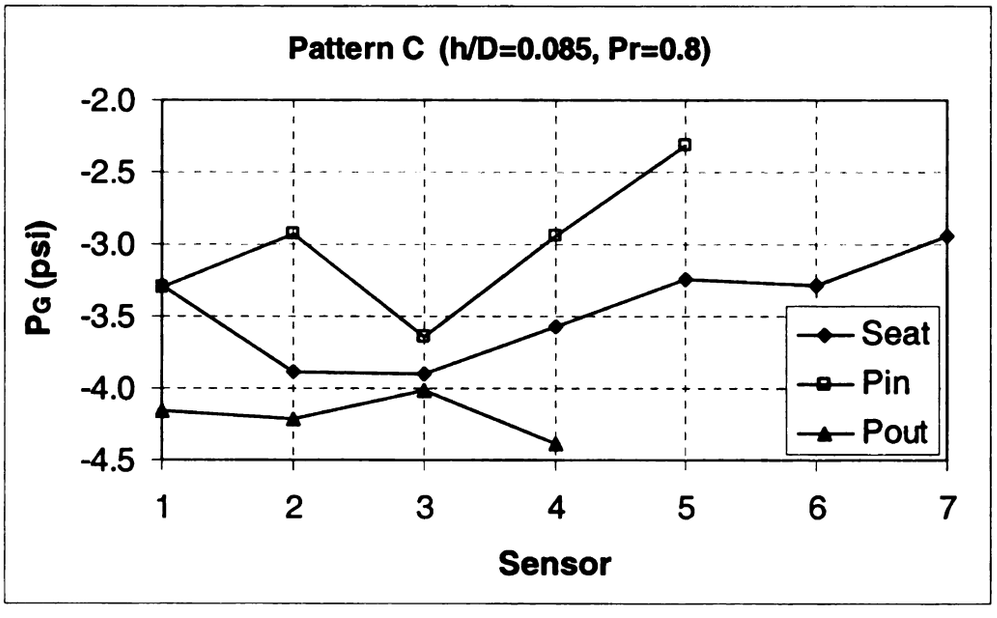
Pattern C (h/D=0.085, Pr=0.8)
-2.0
-2.5
-3.0
-3.5
-4.0
-4.5
P_G (psi)
1
2
3
4
5
6
7
Sensor
Seat
Pin
Pout

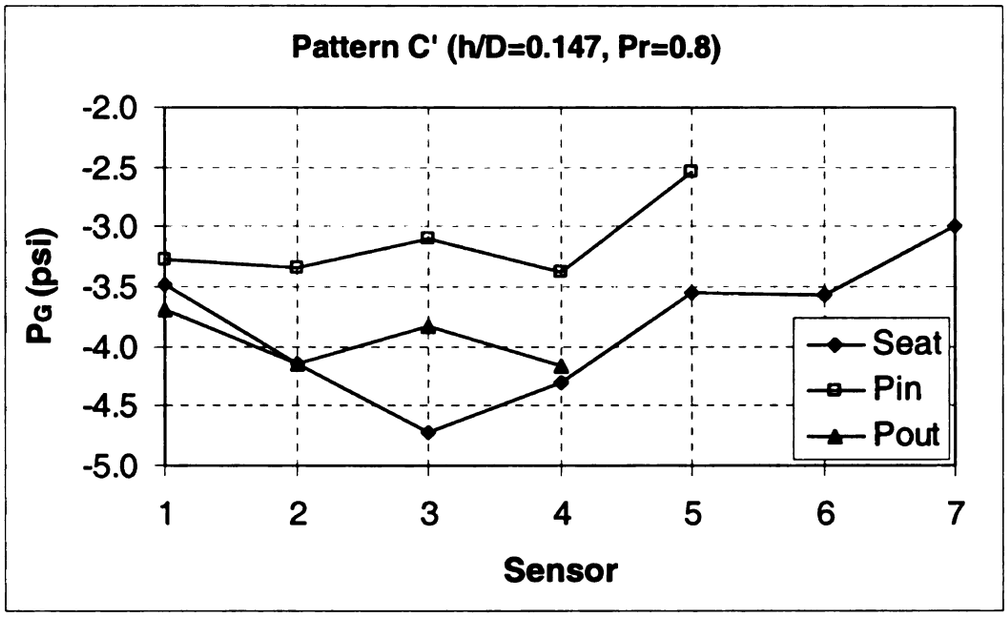

Fig. 6.15 Pattern C and corresponding pressure distribution

Region D is located in the lower left part of the chart. Pattern D as shown in Fig. 6.13 happens. It is almost axisymmetric free jet due to supersonic result from small opening and pressure ratio. After valve throat, flow expands and joins together. The direction is not straight down, thus touch the seat in some place down stream.

Flow in region E is axisymmetric. Due to large mass flow rate at large opening, flow is full of or almost (with some separation at downstream seat side) full of the valve. Separation occurs in the center of plug.

Flow in region C is most unstable. A lot of reported failures occur in this region. For pattern C, flow attaches to one side of the seat and separates from the other and joins together near the plug center in one cross section. In the other cross section, flow attaches to the seat sides and the two streams join farther from the plug center. Part of the flow also attaches to the plug center. The 'hollow' region actually is full of flow shown in the other cross section and a vortex. This is a very unstable flow pattern. It can change to three other patterns: C_0, C_1, and C'. At a small opening (h/D<0.064), the flow pattern

keeps changing between C_0, C_1, and sometimes C. At somewhat larger opening, it keeps changing between C and C_1. At opening ratios larger than about 0.106 h/D, the flow pattern oscillates between patterns C and C'. As the transient regions between different regions are also included in region C, at the boundary of the region, some intermediate flow patterns happen. By comparing Fig. 6.11 and Fig. 6.12, it was found that flow in upper part of region C is transonic.

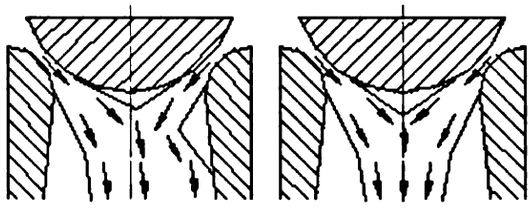

Pattern D

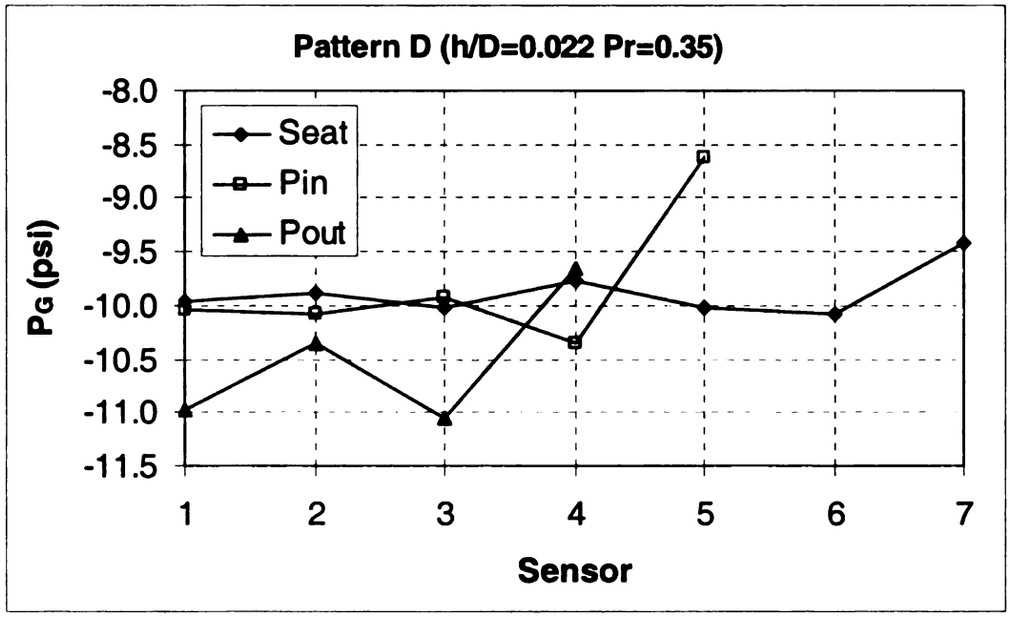

Fig. 6.16 Pattern D and corresponding pressure distribution

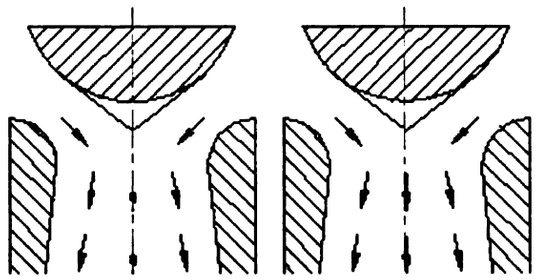

Pattern E

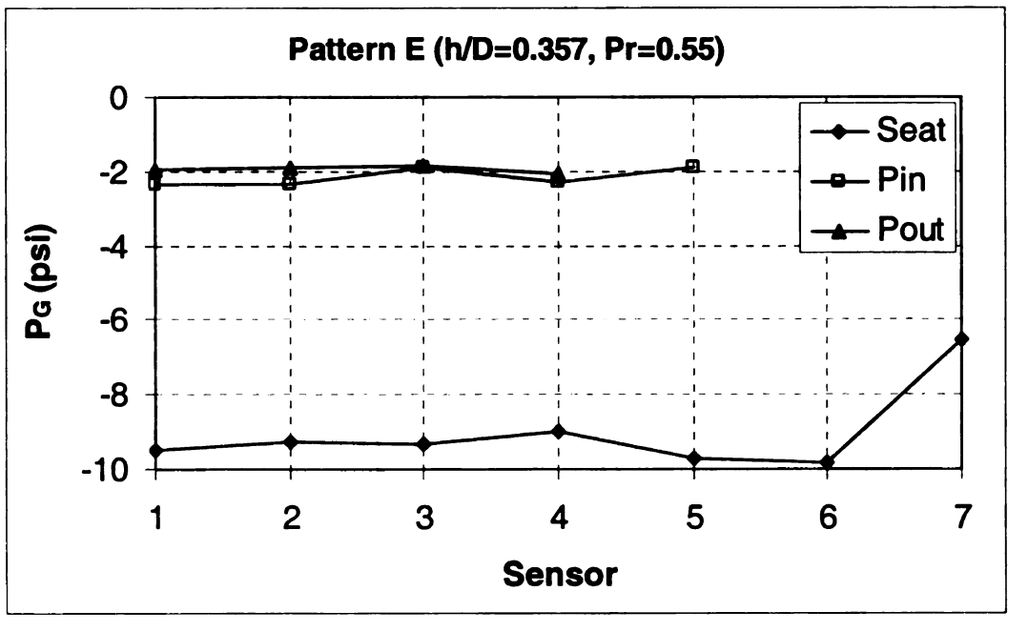

Fig. 6.17 Pattern E and corresponding pressure distribution

6.2.3 Flow asymmetry

An asymmetric pressure distribution can cause forces resulting in plug vibration. Thus time-averaged pressure differences between opposite pressure sensors are calculated. In Fig. 10, Aveseat ΔP means time-averaged $(|P_1-P_3|+|P_2-P_4|)_{seat}/2$. Here P_1, P_3, P_2, and P_4 are measured static pressures from the sensors 1, 2, 3, and 4 in the seat as shown in Fig. 6.7. Avein ΔP means time-averaged $(|P_1-P_3|+|P_2-P_4|)_{plug}/2$; Aveout ΔP means time-averaged $(|P_5-P_7|+|P_6-P_8|)_{plug}/2$. P_1, P_3, P_2, P_4, P_5, P_6, P_7, and P_8 are measured static pressures from the sensors 1, 2, 3, 4, 5, 6, 7, and 8 in the plug as shown in Fig. 6.6.

Aveplug ΔP means (Aveout ΔP+Avein ΔP)/2. The pressure difference is nondimensionalized by the inlet chest pressure P_1.

Pressure difference variations with pressure ratio at different valve openings are shown in Fig. 10. At small openings, the plug side pressure difference has similar trends and similar amplitudes to the seat side. The peak value occurs at some place near the pressure ratio of 0.5 located in region C at most cases (at very small opening, such as h/D=0.022, the peak pressure happens in region D). At a middle opening (h/D=0.168), the seat side pressure difference is higher than that on the plug side. At large openings, which are located in region E, the plug side pressure difference is very small at large pressure ratio, similar to all other openings. Then, as pressure ratio is decreased, the plug side pressure difference increases and reaches a constant value at a pressure ratio of about 0.7. At this opening, flow diffuses in the seat passage after the throat. At pressure ratios between 0.65 and 0.85, asymmetric flow happens in the passage after the throat, making the seat side pressure difference much larger.

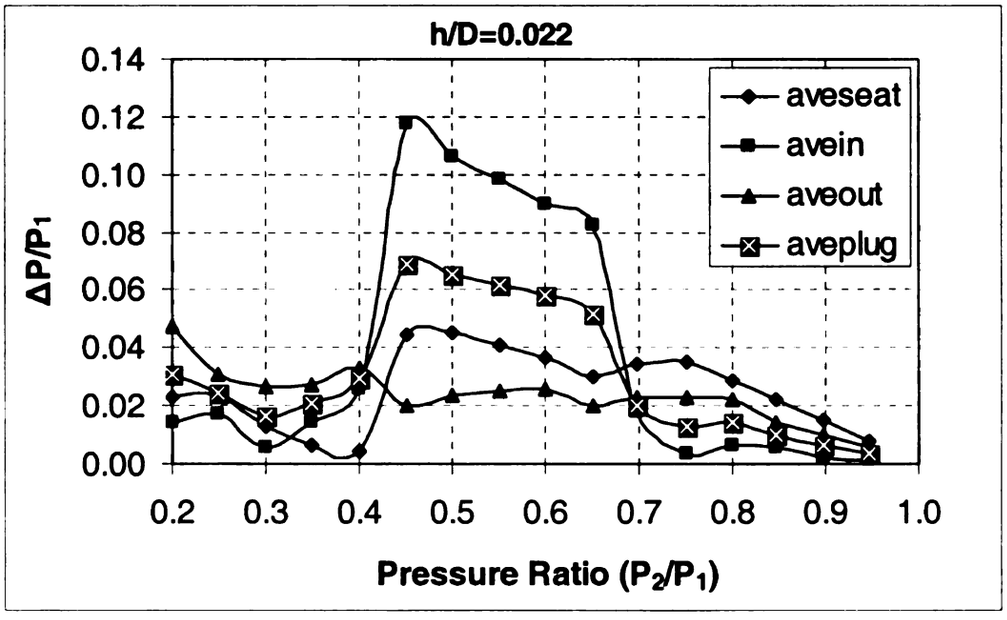

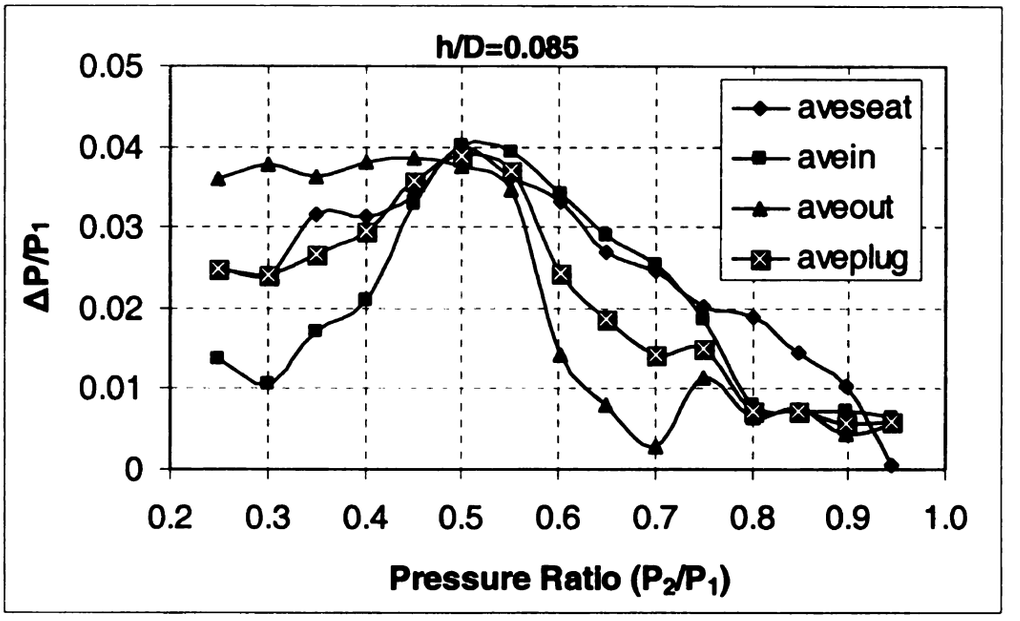

a. Changing from region A to C to D with decreasing pressure ratio

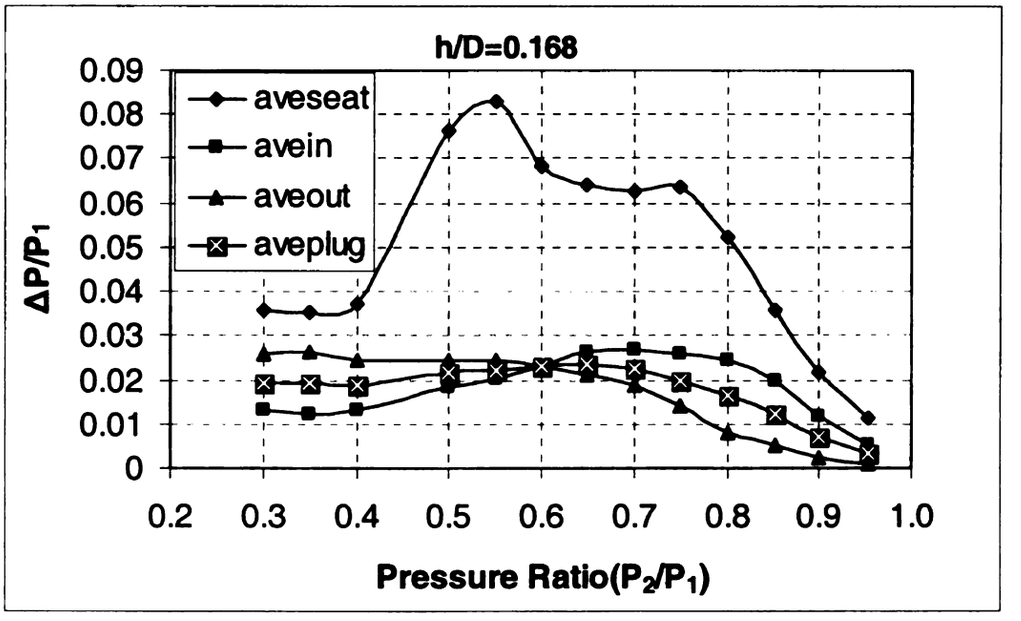

b. Changing from region C to E with decreasing pressure ratio

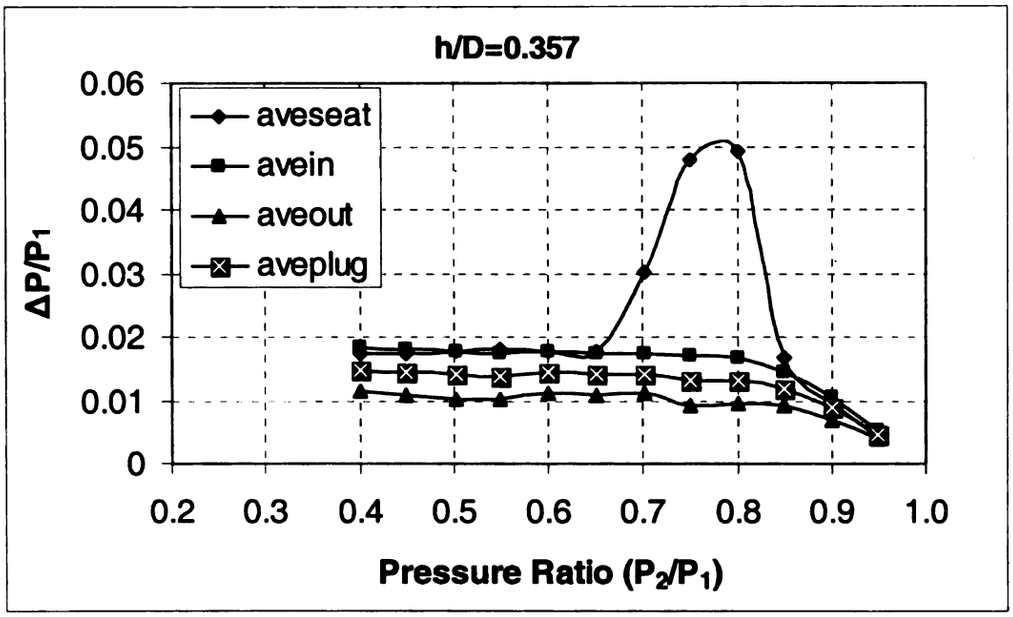

c. Region E

Fig. 6.18 Pressure difference variation with pressure ratio at different openings

The maximum average pressure difference across the plug surface (aveDp_plug), its corresponding pressure ratio (Pr_plug), and maximum average pressure difference across the seat surface (aveDp_seat) are shown in Fig. 6.19 for different valve openings. As the valve plug travels to the fully open position, the maximum pressure difference in the plug side decreases. The seat side pressure difference increases and reaches its peak value at about 0.23 h/D opening, then drops down. Because the pressure difference in the plug side causes hydraulic forces on the plug, for venturi valve, smaller openings mean more possibility of valve failure when upstream pressure is constant. Compared with Fig. 8, the pressure curve shows that the maximum pressure difference happens in the lower part of region C in most cases except the very small opening situation such as h/D=0.02. Under very small opening situation, the maximum pressure difference happens in region D.

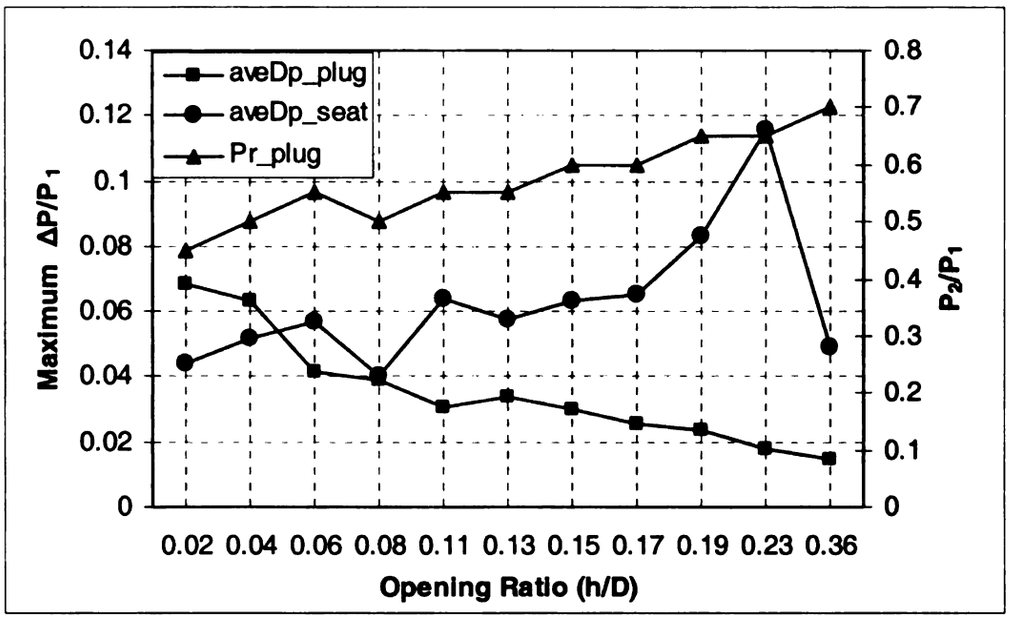

Fig. 6.19 Maximum pressure difference and corresponding pressure ratio

6.2.4 Flow instability

Pressure oscillation on the plug surface at 0.085 h/D opening is shown in Fig. 6.20. The numbers from 0 to 8 are the sensor numbers on the plug surface as shown in Fig. 6.6. For example, the curve 0 shows the absolute gauge pressure (psi) oscillation at the plug center. The x-axis is time. At large pressure ratio, Pr=0.95, pressure oscillation is random around some average mean value with small amplitude. This is in region A. Flow is typically turbulent. At pressure ratio of 0.9, it is clearly shown that the flow pattern jumps from A to C_0 then quickly to C_1. At pressure ratio of 0.8, flow pattern A disappears, while patterns C_0, C_1, and C keep changing to each other with large amplitude and low frequency. Decreasing pressure ratio further, the pattern changing frequency becomes higher until the pressure ratio reaches 0.4, below which the flow becomes pattern D, supersonic free jet flow. The trend is the same for any other valve opening except the very large opening (h/D>0.168). At very large openings, only pattern E occurs, as shown in Fig. 6.21. Pressure oscillation is due to turbulence with small amplitude.

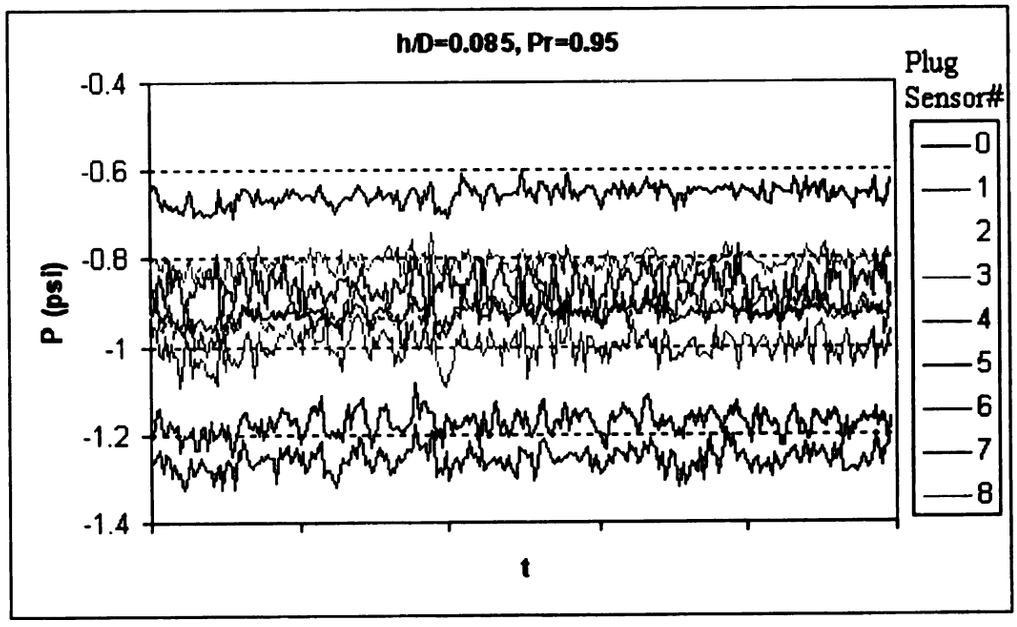
h/D=0.085, Pr=0.95
Plug Sensor#
0
1
2
3
4
5
6
7
8
-0.4
-0.6
-0.8
-1
-1.2
-1.4
P (psi)
t

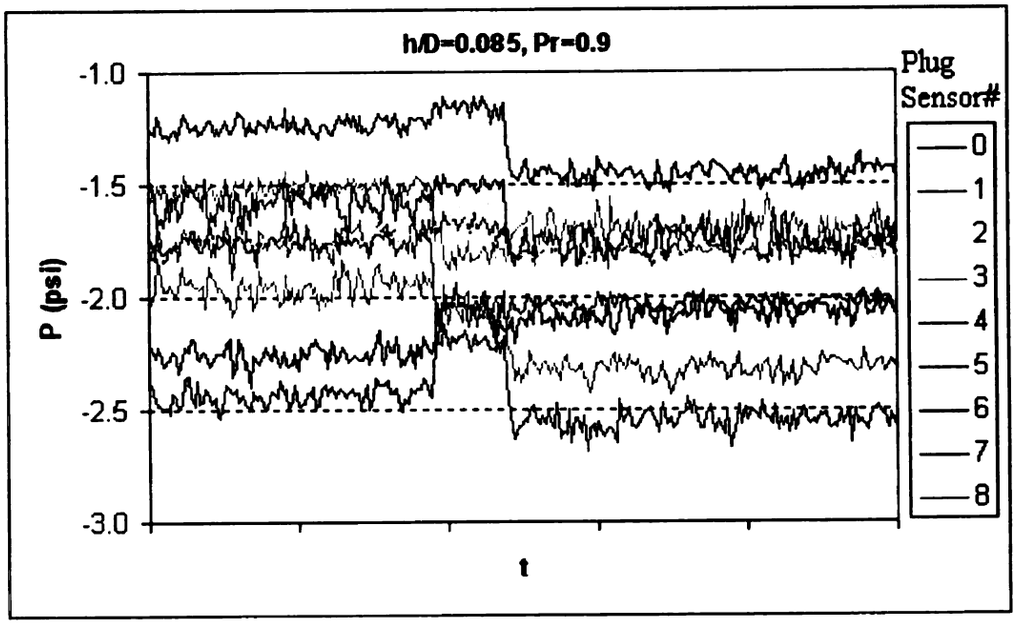
h/D=0.085, Pr=0.9
Plug Sensor#
0
1
2
3
4
5
6
7
8
-1.0
-1.5
-2.0
-2.5
-3.0
P (psi)
t

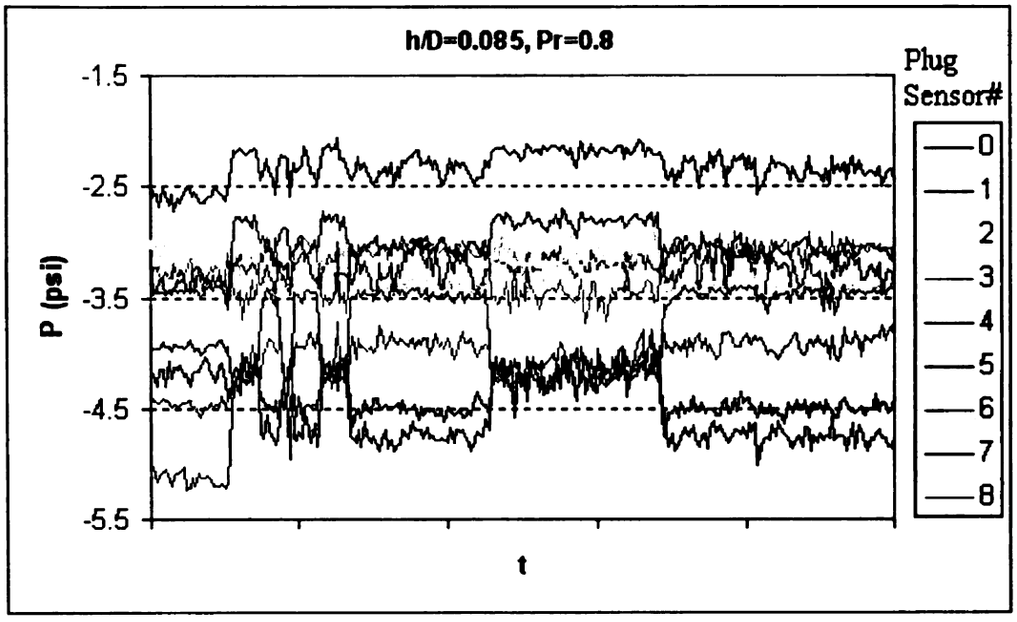
h/D=0.085, Pr=0.8
Plug Sensor#
-1.5
-2.5
-3.5
-4.5
-5.5
P (psi)
t
0
1
2
3
4
5
6
7
8

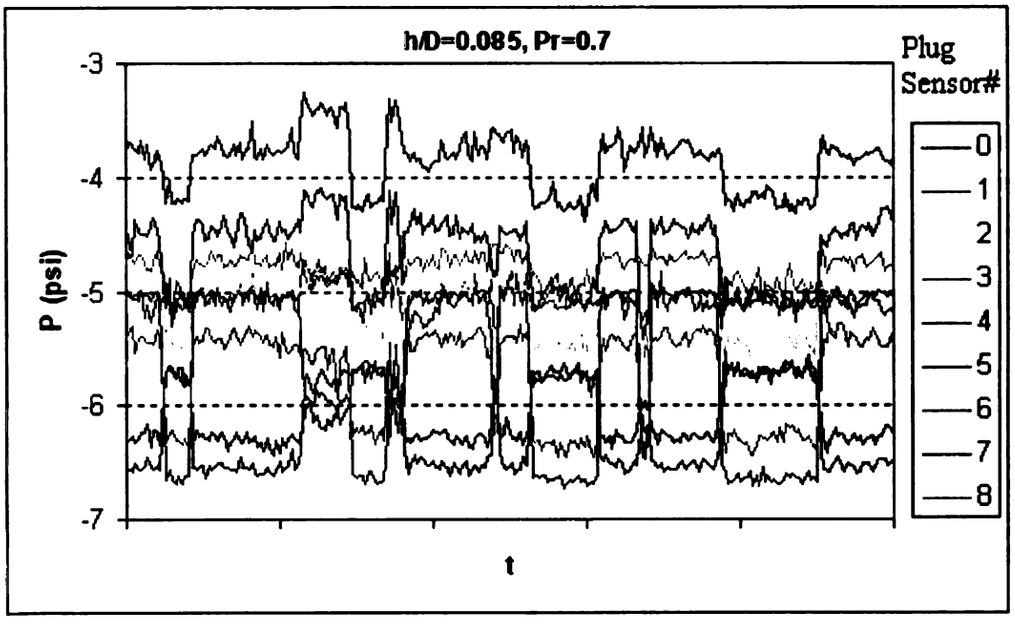
h/D=0.085, Pr=0.7
Plug Sensor#
-3
-4
-5
-6
-7
P (psi)
t
0
1
2
3
4
5
6
7
8

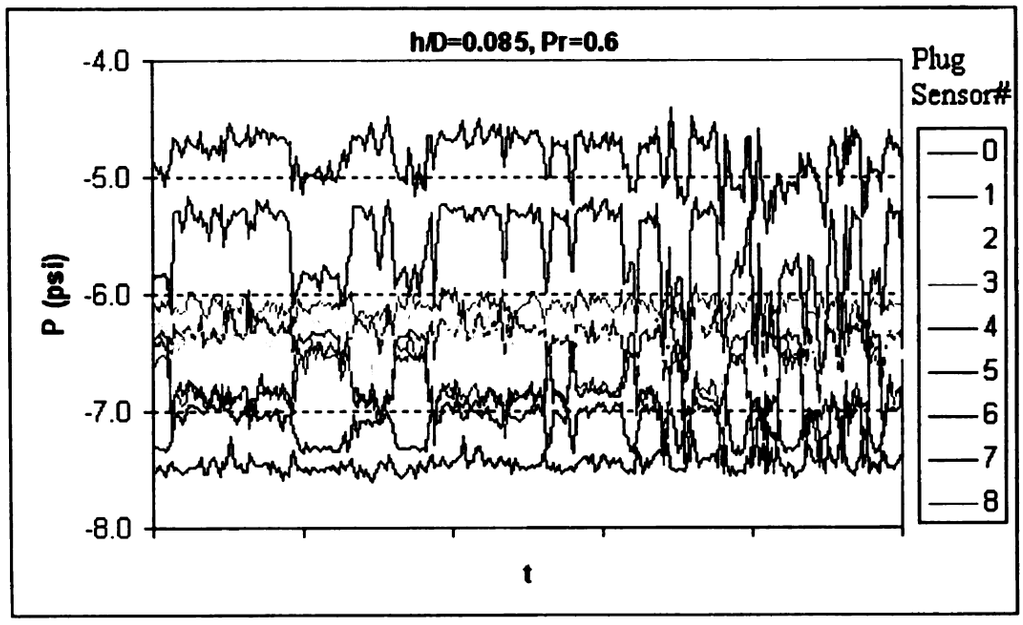
h/D=0.085, Pr=0.6
-4.0
-5.0
-6.0
-7.0
-8.0
P (psi)
t
Plug Sensor#
0
1
2
3
4
5
6
7
8

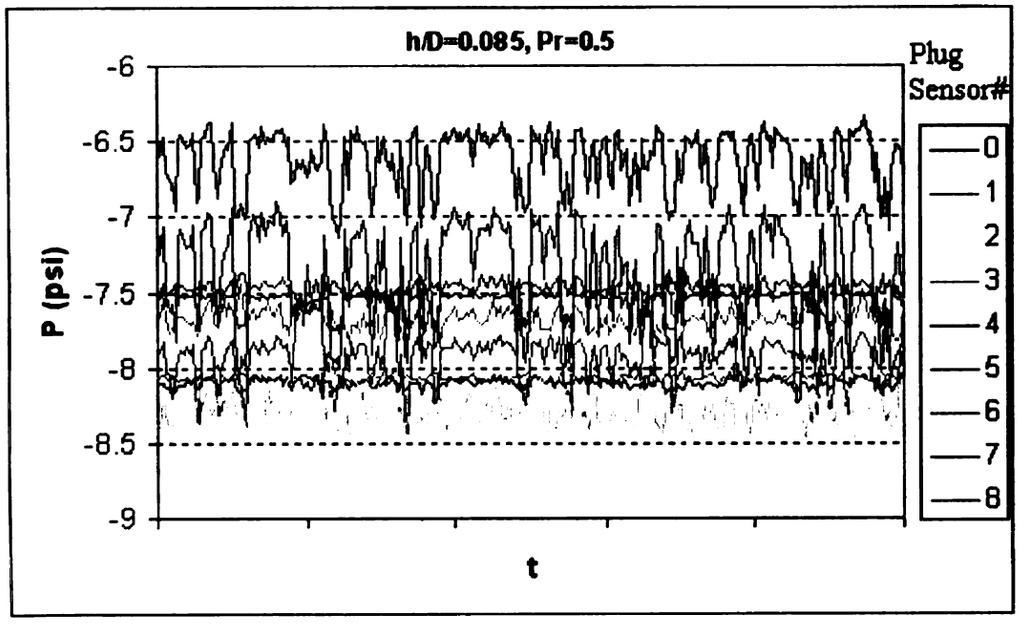
h/D=0.085, Pr=0.5
-6
-6.5
-7
-7.5
-8
-8.5
-9
P (psi)
t
Plug Sensor#
0
1
2
3
4
5
6
7
8

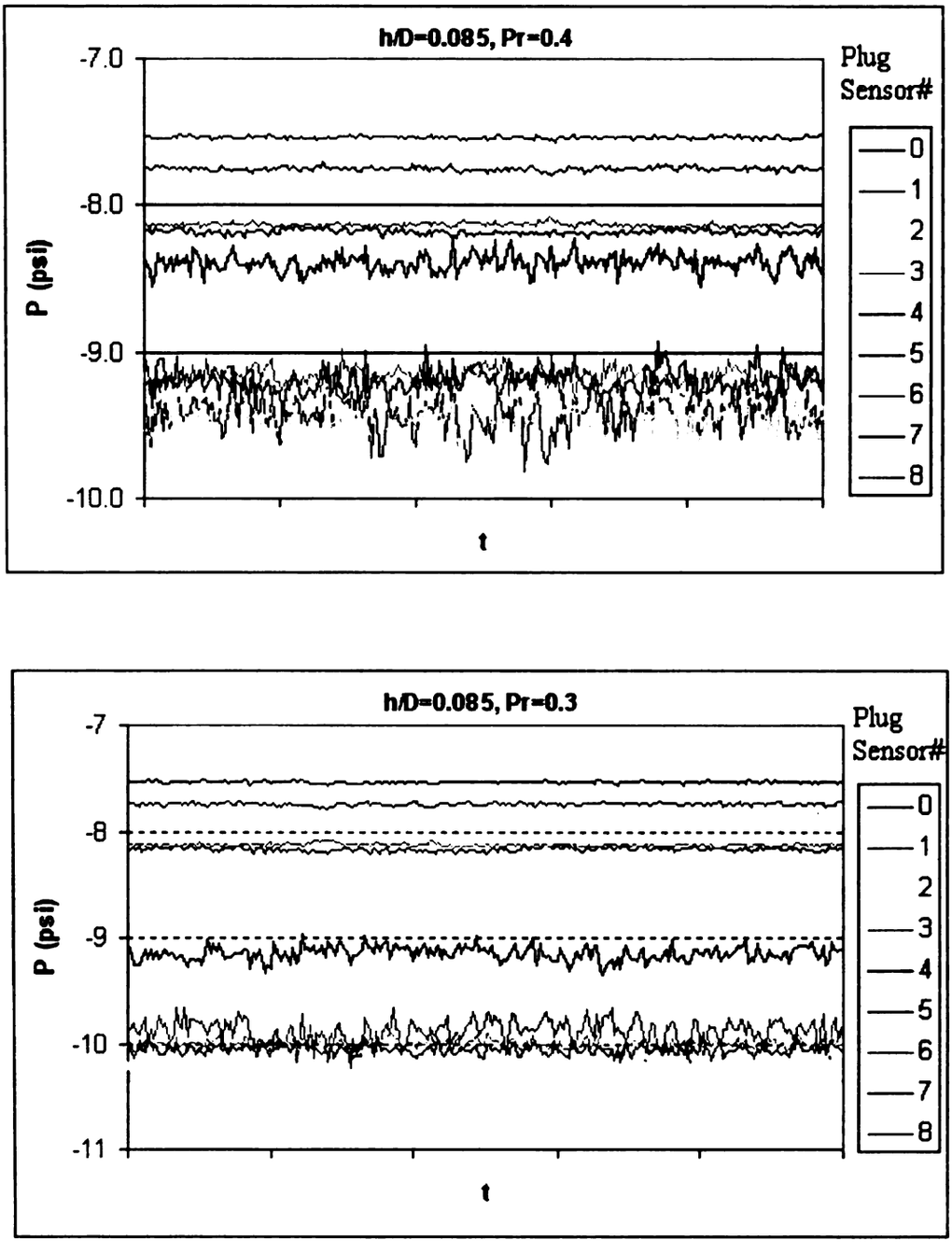

Fig. 6.20 Pressure oscillation at different pressure ratios and 0.085 h/D opening

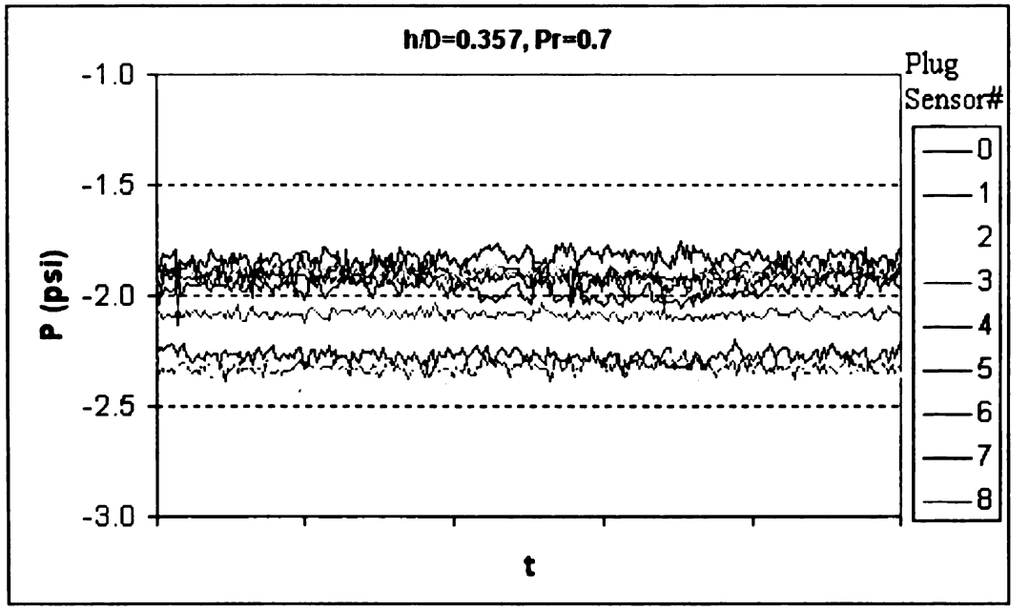

Fig. 6.21 Pressure oscillation at pr=0.7 under 0.375 h/D opening

To compare the pressure oscillation amplitude, the maximum peak-to-peak value of oscillation ΔP is calculated. It is also nondimensionalized by the inlet chest pressure P_1. Pressure oscillation maximum peak-to-peak values at different positions on the plug surfaces at three openings are shown in Fig. 6.22. The numbers from 0 to 8 are the sensor numbers on the plug surface, as shown in Fig. 6.6. At small or large openings, a large amplitude pressure oscillation happens in the region near the plug center, while at middle openings, it occurs on the whole surface. The center pressure oscillation mainly causes vertical force oscillation, and the pressure oscillation of the upstream side surface of the plug mainly causes lateral force oscillation. So, for a real valve, large amplitude of vertical vibration will happen at small openings, whereas large amplitude of both lateral and vertical vibration will happen at middle openings. This may be a reason that the recent reported valve failure happened at the opening ratio of 0.147 h/D.

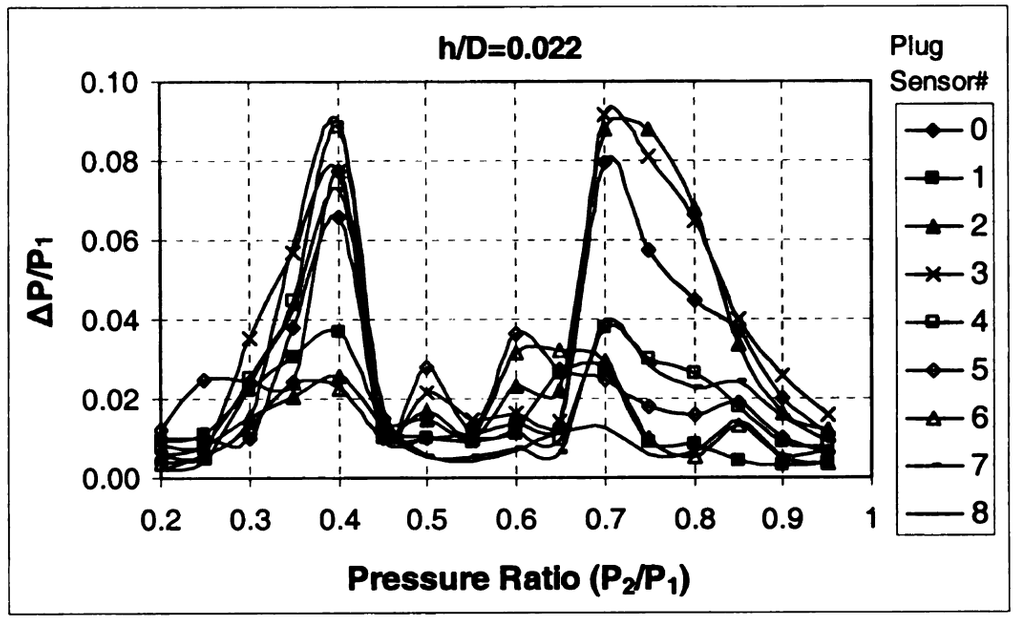

a. At small valve opening

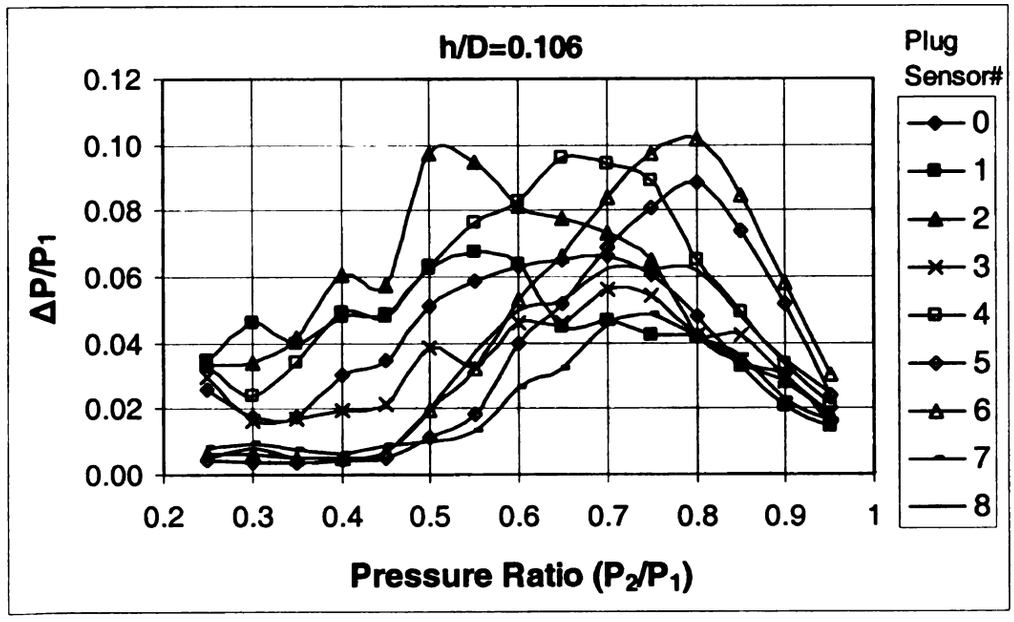

b. At middle valve opening

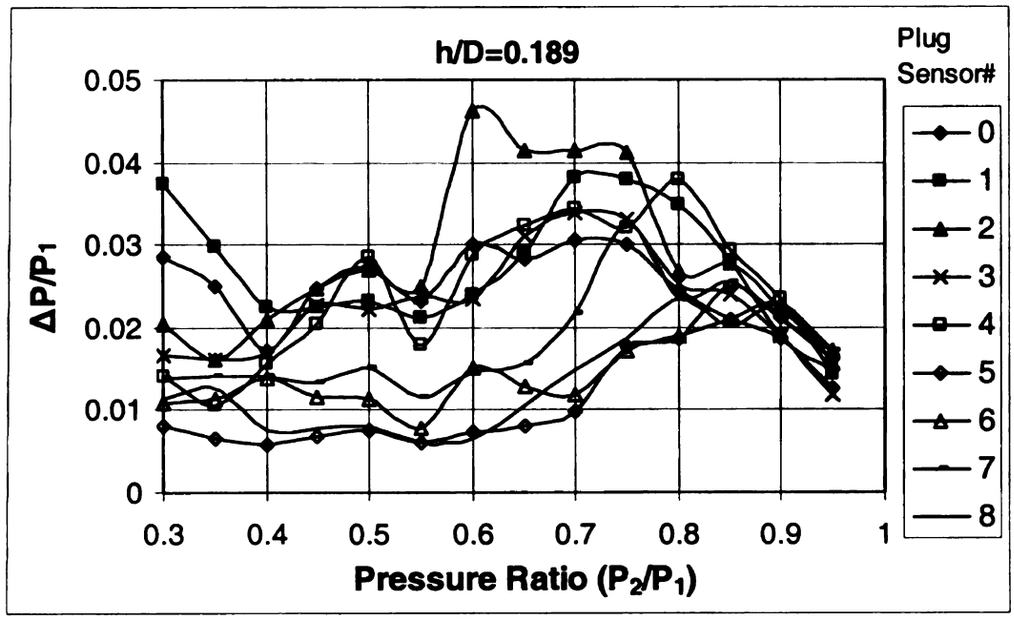

c. At large valve opening

Fig. 6.22 Peak-to-peak value of pressure oscillation

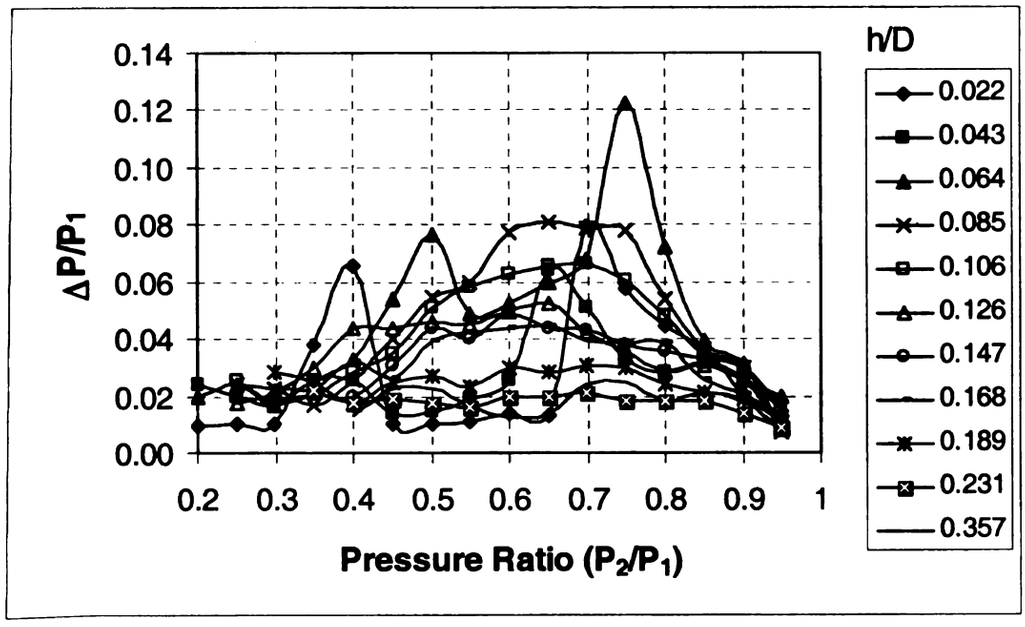

Fig. 6.23 Peak-to-peak value of pressure oscillation at plug center

Fig. 6.23 shows the pressure oscillation, $\Delta P/ P_1$, of the plug center at different openings. At small openings, there are two peaks. As the opening increases, the two peaks move toward each other. They join together, becoming one flat peak for 0.085 h/D opening. Then the curve becomes more flat with increasing valve opening.

The peak pressure oscillation (oscillation_center curve) at plug center for each opening is shown in Fig. 6.24. The corresponding pressure ratio for the peak pressure oscillation is also shown as the curve with triangle labels (Pr_peakP). maximum average pressure difference across the plug surface (aveDp_plug) is the dashed curve with square labels. It is the same curve as in Fig. 6.19. The peak value for pressure oscillation occurs at the opening of h/D=0.064, then it decreases with increasing valve opening. The absolute value of the pressure oscillation at the plug center is higher than the average pressure difference for the plug, which means that the pressure oscillation may be more dangerous than the asymmetric pressure distribution. The pressure ratio at which the maximum pressure oscillation occurs is about 0.7. At this pressure ratio, flow is mostly transonic, which agrees with the theory mentioned above. The pressure ratio line is located in the middle part of region C.

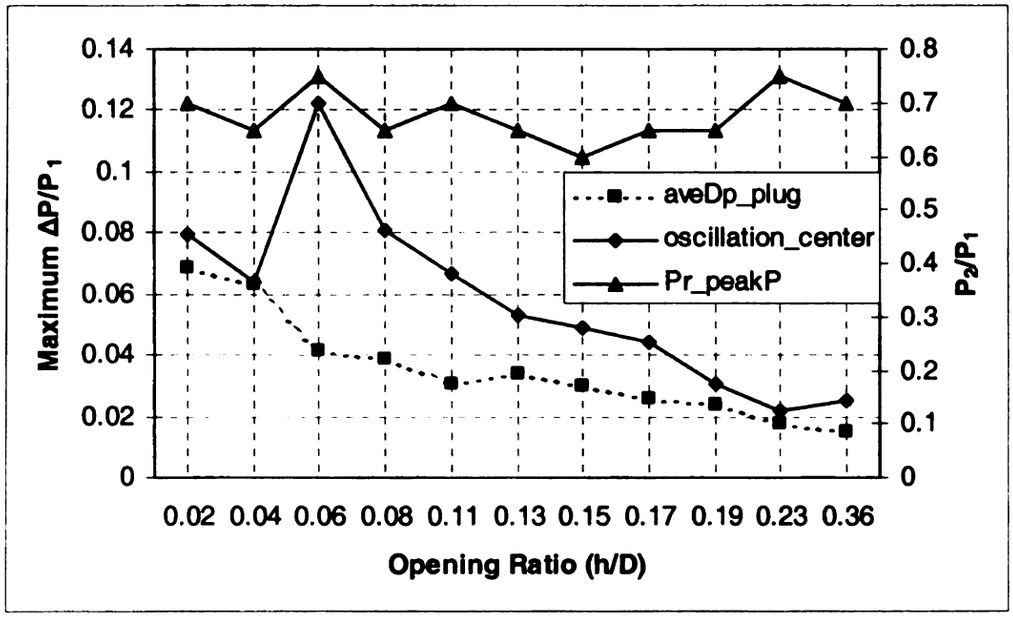

Fig. 6.24 Peak value of pressure oscillation with opening changing

6.2.5 Superposition of pressure oscillation and difference

Based on the above analysis, the pressure oscillation and difference amplitude are superposed in Fig. 6.25. Region C is a dangerous region for valve operation in terms of flow asymmetry and instability. In the upper part of region C (around Pr=0.7), flow is quite unstable due to the flow pattern changing. This is because in such a situation, the flow is transonic, which is fluctuating, and fighting for the plug attachment as mentioned above in the discussion of theory. At the lower part of region C (around Pr=0.5), the flow is more asymmetric. This is the result of asymmetric flow expansion. The lower left part (red) of Region C is highly dangerous.

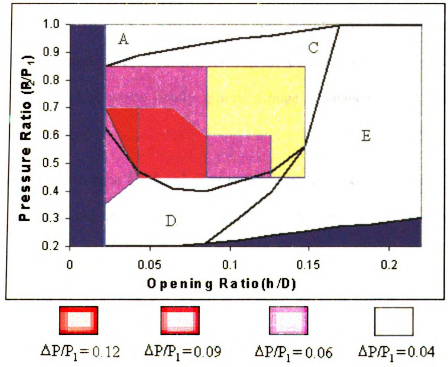

Fig. 6.25 Superposition of pressure oscillation and difference

CHAPTER 7

CONCLUSION

This study confirmed that asymmetric unstable flow is the root cause of valve problems resulting in large amplitude of unsteady forces, moments and torque. The valve plug can be broken in a very short time by the large amplitude of the excitations, or in long-term operation by small amplitude of the excitations.

An analytical and numerical study on turbine governor valve was performed to clarify the fluid/plug interaction mechanism. Large adverse pressure gradient due to diffusion or shock waves cause stalls when flow is diffused through valve as internal flow. Stalls in both valve plug and seat side are not axilly symmetric. This causes asymmetric flow patterns for current design. The asymmetric flow pattern for current design causes asymmetric pressure distribution along plug, which finally generates huge unbalanced force and moment at valve natural position.

The interaction between fluid and plug is the excitation mechanism that causes plug vibration. Vertical and lateral vibration affect each other and make the valve operation situation even worse.

The key point to improving the design is to make the flow pattern symmetric for any situation. Changing the valve plug curvature is proved to be a simple way to improve the valve design by both theory and numerical method. Making the plug curvature sharper than seat side is one way to make flow separate in plug side earlier than in seat side to push the flow attach seat side and reduce its influence on valve plug. Several improved designs were studied. They are better than current design in terms of reduced excitations

of valve vibration, especially in large pressure ratio situation. The dish bottom design is recommended because it can make flow more symmetric and reduce the excitations significantly at any pressure ratio according to the validation by CFD data. It is also easy to be manufactured.

Flow asymmetry and instability of a ½-scale venturi valve for a steam turbine was determined from tests at different valve openings and pressure ratios. The results showed that asymmetric and unstable flow occurs in the valve, which can result in plug vibration causing valve failure. Regions with large amplitude of pressure oscillation and difference were identified for the current valve design.

BIBLIOGRAPHY

Araki, T; Okamoto, Y; Ootomo, F, "Fluid Induced Vibration of Steam Control Valves",Toshiba Review, Vol. 36, issue 7, ISSN 0372-0462, Tokyo Shibaura Electric Co., Kawasaki, Japan, pp.648-656, 1981

Becker, J. V., "Characteristics of Wing Sections at Transonic Speeds", NACA-University Conference on Aerodynamics, 1948

Eguchi, Tsuyoshi; Hirota, Kazuo; Honjo, Masanobu; Magoshi, Ryotaro, "Study of Self-Excited Vibration of Governing Valves for Large Steam Turbines", Mitsubishi Heavy Industries, Ltd, 1982

Emmons, H. W., "The Theoretical Flow of a Frictionless, Adiabatic, Perfect Gas Inside of a Two-Dimensional Hyperbolic Nozzle", NACA Tech. Note, No. 1003, 1946

Mattingly, J.D., "Elements of Gas Turbine Propulsion", McGraw-Hill, 1996

Hanin, R.A., O Tipah Kolebanii Reguliruyushih Klapanov Parovih Turbin, Teploenergetika, 9., p.19, 1978

Hardin, J., Krushner, F., Koester, S., "Elimination of Flow-Induced Instability From Steam Turbine Control Valves," Proceedings of the Thirty-Second Turbomachinery Symposium, Turbomachinery Laboratory, Texas A&M University, College Station, Texas, pp. 99-108, Sept. 2003

Heymann, F. J., "Some Experiments Concerning Control Valve Noise", Engineering Report, Westinghouse Electric Corp, Lester, Pennsylvania

Heymann, F. J. and Staiano, M. A., "Steam Control Valve Noise", Engineering Report, Westinghouse Electric Corp, Lester, Pennsylvania

Kline, S. J., Abbott, D. E., and Fox, R. W., "optimum Design of Straight walled diffusers", ASME Journal of Basic Engineering, 1959

Kline, S. J., "On the Nature of Stall", ASME Journal of Basic Engineering, vol. 81, series D, no. 3, September 1959

Kuo, Y. H., "On the Stability of Two-Dimensional Smooth Transonic Flows in Local Supersonic Velocities", NACA Tech. Memo, No. 1215, 195

Liepmann, H. W., Ashkenas, H., and Cole, J. D., "Experiments in Transonic Flow", U.S. Air Force Technical Report, No. 5667, 1948

Moussa, Z. M., "Current Status of the RDC Steam Turbine Valve Study", Internal report of Elliott Company, 1976

Schuder, Charles B., "Understanding Fluid Forces in Control Valves", Intrumentaional Technology, Journal of the Instrument Society of America, May 1971

Shapiro, A. H., "The Dynamics and Thermodynamics of Compressible Fluid Flow", Vol. 2, The Ronald Pres Company, 1954

Weaver, D.S., "Flow Induced Vibrations in Valves Operating at Small Opening", IAHR Symposium Proceedings, B13, Karlsruhe, Germany, 1979

Widell, Karl-Erik, "Governing Valve Vibrations in A Large Steam Turbine", IAHR Symposium Proceedings, B14, Karlsruhe, Germany, 1979

White, F.M., "Fluid Mechanics", McGraw-Hill Inc., Third Edition, 1994

Zarjankin, A.; Simonov, B., "New Control Valves, Their Parameters and Service Experience in the Turbines", Joint- Stock Company for the Development of New Technologies in Energetics, ENTEK, Co. Ltd., Russia

Zhang, D.; Engeda, A., "Venturi valves for a steam turbine and improved design considerations", Journal of Power and Energy, Vol. 217 Part A, 2003

Zhang, D., Engeda, A.; Hardin, J.; Aungier, R. " Experimental Study of Steam Turbine Control Valves ", Submitted to Journal of Power and Energy (#C07903)

Ziada,S., Buehlmann,E.T.; Bolleter,U., "Flow impingement as an excitation source in control valves". Journal of Fluids and Structures 3, 529-549, 1989